NAWI Graz
Natural Sciences

TU Graz

Lukas Patscheider, BSc

Geological-geotechnical characterization and process analysis of the mass movement in the Seres Valley near Campill (South Tyrol, Italy)

MASTER'S THESIS

to achieve the university degree of

Master of Science

Master's degree program

Geosciences

submitted to

Graz University of Technology

Supervisor

Univ.-Prof. Dipl.-Ing. Dr.techn. Roman Marte

Institute of Soil Mechanics, Foundation Engineering and Numerical Geotechnics

Univ.-Prof. B.A. M.Sc. Ph.D. Daniel Scott Kieffer

BSc MSc Ing. Volker Reinprecht

Institute of Applied Geosciences

Dr. rer. nat. Volkmar Mair

Amt für Geologie und Baustoffprüfung, Provinz Bozen

Graz, May 2026

Affidavit

I declare that I have authored this thesis independently, that I have not used other than the declared sources/resources, and that I have explicitly indicated all material which has been quoted either literally or by content from the sources used. The text document uploaded to TUGRAZonline is identical to the present doctoral thesis.

Date | Signature

Acknowledgement

I would like to express my sincere gratitude to all those who supported me during the preparation of this Master's thesis.

First, I would like to express my sincere gratitude to Prof. Dr. Roman Marte for his friendly and considerate supervision, as well as for the professional discussions throughout the development of this work.

My sincere thanks also go to Volker Reinprecht for his professional and valuable suggestions, particularly regarding the geomorphological aspects of this study.

At this point, I would like to thank the Office for Geology and Building Materials Testing of South Tyrol for their support. The idea for this thesis emerged from conversations with Volkmar Mair in late summer 2024 and I am especially grateful for his immediate willingness to provide all relevant materials (aerial photos, videos and geospatial data) and support from various employees of the office.

I would like to express my special thanks to Daniel Constantini, who was my main contact at the provincial office. Thank you for always being there to offer help and advice and for valuable input on many of my questions. In particular, I greatly appreciated your introduction to the geology of the Dolomites!

I would also like to thank Corrado Morelli for supervising the geological conditions, as well as Ulrich Obojes to put the laboratory at my disposal and giving advice.

Finally, I would like to thank Michael Jesacher for providing his original diploma thesis, Thomas Fontana from the ALTO DRONES company for his hints with the point cloud handling and Markus Kaspar for carrying out the laboratory tests at TU Graz.

I am especially grateful to my family, who have supported me throughout all stages of my life and have always believed in me. Thank you for your patience, encouragement and for inspiring my curiosity from an early age. You have shown me how rewarding it is to develop an enthusiasm for exploring topics - I will always carry this curiosity with me, thank you!

Kurzfassung

Gravitative Massenbewegungen zählen zu den bedeutendsten geomorphologischen Naturgefahren im alpinen Raum und stellen eine große Herausforderung für deren Bewohner dar. Sie werden maßgeblich durch das Zusammenwirken geologischer, geomorphologischer sowie hydro-meteorologischer Faktoren kontrolliert. Die vorliegende Arbeit untersucht Ursachen und Auslöser, die zu dem kaskadenartigem Massenbewegungsereignis vom 17. Juni 2024 im Serestal bei Campill (Gadertal, Westliche Dolomiten) führten.

Die Studie kombiniert geologische und geomorphologische Geländekartierungen, strukturgeologische Analysen, Geomorphic Change Detection (GCD), laborbasierte geotechnische und mineralogische Untersuchungen, Standsicherheitsanalysen sowie hydro-meteorologische Auswertungen, um die prädisponierenden und auslösenden Faktoren des Ereignisses zu identifizieren und ein konzeptionelles Modell (Conceptual Ground Behaviour Model, CGBM) zu entwickeln.

Die Ergebnisse zeigen, dass die Instabilität primär durch die geologische und strukturelle Situation im Anrissbereich kontrolliert wurde. Die ersten Rutschungsbewegungen entwickelten sich innerhalb der mechanisch schwachen und verwitterungsanfälligen turbiditischen Silt- und Mergelsteine der Zoppé-Formation, die von kompetenten Dolomiten der Schlern-Gruppe unterlagert werden, und somit für einen ausgeprägten Kompetenzkontrast sorgen. Strukturgeologisch befindet sich der Anrissbereich auf dem N-Schenkel einer Antiklinale, wodurch sich ein Schichthang ergibt. Auch geomorphologisch erwies sich der Anrissbereich als mobilisierungsanfällig, da er aus einer transportlimitierten Rinne bestand, die mit Regolith aus der Verwitterung der Zoppé-Fm. sowie mit kolluvialem Material einer darüberliegenden vulkanoklastischen Felswand verfüllt war. Mineralogische und geotechnische Untersuchungen weisen auf intensive Verwitterung der Zoppé-Fm. durch die Bildung von Tonmineralen hin. Die daraus entstandenen siltig-tonigen Residualböden sind durch Plastizität und geringe Permeabilität charakterisiert, wodurch Wassersättigung und Aufbau von Porenwasserdruck begünstigt werden. Hydro-meteorologische Analysen zeigen, dass das Ereignis durch die Kombination aus vorausgehender Schneeschmelze und anschließenden langanhaltenden Niederschlägen im Frühjahr 2024 ausgelöst wurde, was zu einer hohen Wassersättigung des Untergrundes vor dem Versagen führte. Mittels GCD konnte ein mobilisiertes Volumen von etwa 181.000 m³ bestimmt werden.

Das entwickelte CGBM verdeutlicht, dass Lithologie und Verwitterungsverhalten eine erstordentliche Kontrolle auf die Hanginstabilität in den Dolomiten ausüben. Feinkörnige turbiditische Formationen wie die Zoppé-Formation reagieren insbesondere auf langanhaltende Wassersättigung und kumulative Niederschläge, wodurch die Bedeutung integrierter geologischer, geotechnischer und hydro-meteorologischer Analysen für die Suszeptibilitätsbewertung alpiner Massenbewegungen im Kontext der Gefahrenzonenplanung hervorgehoben wird.

Abstract

Gravitational mass movements are among the most significant geomorphological natural hazards in alpine environments and represent a major challenge for their inhabitants. They are largely controlled by the interaction of geological, geomorphological, and hydro-meteorological factors. This thesis investigates the causes and triggers of the cascading mass movement event of June 17th, 2024, in the Seres Valley near Campill (Val Badia, Western Dolomites).

This study combines geological and geomorphological field mapping, structural analyses, Geomorphic Change Detection (GCD), laboratory geotechnical and mineralogical analyses, slope-stability analyses and hydro-meteorological evaluation in order to identify the predisposing and triggering factors of the event and to develop a Conceptual Ground Behaviour Model (CGBM).

The results demonstrate that the instability was primarily controlled by the geological and structural setting of the source area. The first sliding movements developed within the mechanically weak and weathering-susceptible turbiditic siltstone and marl layers (Zoppé-Formation) above competent dolomite (Schlern-Group), creating a pronounced competence contrast. Structurally, the source area is located on the N-limb of an anticline, where bedding dips unfavourably parallel to the slope surface (dip-slope). Also, geomorphologically the source area resulted susceptible to mobilization as it consisted of a transport-limited gully filled with regolith stemming from the weathering of the Zoppé-Fm. and colluvium from a volcanoclastic cliff above the source area. Mineralogical and geotechnical analyses indicate strong weathering of the lithologies of the Zoppé-Fm. and the formation of clay minerals. The resulting residual soils are characterized by silt and clay contents and low permeability, promoting progressive saturation and pore-water pressure build-up. Hydro-meteorological analyses indicate that the event was triggered by the combination of antecedent snow melt and subsequent prolonged precipitation during spring 2024, resulting in high ground saturation prior to failure. Through GCD the mobilized material was determined with approximately 181 000 m^3.

The developed CGBM demonstrates that lithology and weathering behaviour exert first-order controls on slope instability in the Dolomites. Fine-grained turbiditic formations such as the Zoppé-Fm respond primarily to prolonged saturation and cumulative rainfall, highlighting the importance of integrated geological, geotechnical and hydro-meteorological analyses for susceptibility assessment of alpine mass movements in the context of hazard zone planning.

Table of Contents

List of Figures

List of Tables

Abbreviations

FOS	Factor of Safety
HZP	Hazard Zone Planning
N	North
E	East
S	South
W	West
Fm.	Formation

Symbols

Small letters

c	[kN/m²]	Cohesion

Capital letters

A	[m²]	Area

Small greek letters

φ'	[°]	Effective friction angle

Capital greek letters

1 Introduction

At June 17th 2024 a mass movement developed at subalpine level at about 2000 m a.s.l. close to the village of Campill (ital. Longiarù, Province of Bolzano - South Tyrol, Italy). The mass movement involved multiple cascading processes. It started as a slope earth - debris flow (german Hangmure), probably involving prior sliding movements, from a colluvium filled gully on a slope. The first earth - debris flow propagated through the Seres valley. Through the infiltration of water from two creeks the landslide material was remobilized in form of multiple muddy debris flows through the Seres valley. The coarser debris material deposited at the end of the Seres valley where the valley gradient decreased, while a part of the mass movement continued as mud flows along the Seres creek until the village of Campill. The mass movement propagated at a velocity where it was possible to alarm the civilization. 56 houses exposed to this hazard have been evacuated for the case of further material entrainment. Damage occurred closely to the Seres creek bed at mills, bridges and mainly to the first houses of the village of Campill.

Such geohazards or gravitational mass movements are part of the natural hazards and pose serious hazards in mountainous regions like the Alps. After the definition of the United Nations Office for Disaster Risk Reduction (UNISDR) natural hazards are natural processes or phenomena that may cause loss of life, injury or other health impacts, property damage, social and economic disruption or environmental degradation (UNISDR, 2018). In numerous mountain areas worldwide, including the Alps, the occurrence of mass movements has increased over the past 20 to 30 years (Huggel et al., 2010). Recent literature supports that both fatalities (around 4.000 - 5.000 per year worldwide) and economic losses on settlements and infrastructure from mass movements remain high and show increasing trends globally, around 4 - 5 billion euros in Europe (Froude & Petley, 2018; Petrucci, 2022; Remondo et al., 2026).

Therefore, scientific investigation of the underlying geomechanical processes and their assessment form the basis for comprehensive hazard and risk assessments (Zangerl et al., 2008). Mass movement processes are primarily controlled by geological and geomorphological factors as well as by meteorological events. It is expected that climate change, mainly through changes in precipitation characteristics and temperature, will increase the hazard of mass movement (Glade et al., 2020; Remondo et al., 2026). Also, human spatial expansion into potentially endangered areas further increases the vulnerability and risk to mass movement hazards. Enhancing resilience through assessment of hazard potentials and hazard-preventive measures is therefore essential. Hazard (indication) maps, protective structures, and slope-stabilization measures require qualitative geoscientific expertise and datasets of the geological framework, the hazardous processes involved and the potential hazard scenarios (Glade et al., 2020). In specific, in the Province of Bolzano (South Tyrol) hazard zone plans are developed on communal level and are focussing around vulnerable areas (settlements) and already occurred geohazards, whereas landslide susceptibility mapping is not performed for the whole communal area (Autonomous Province of Bolzano, 2016)

In this context, different investigation methods are used to develop hazard zone plans which often pose the basis for the land-use and development plan. The most used investigation methods comprise geological and geomorphological reports and maps, Remote Sensing analyses of Orthophotos or DEMs, satellite datasets and simulations programs of different mass movement types. For certain more detailed investigated mass movements also geophysical measurements and monitoring techniques are deployed (Glade et al., 2020).

Despite extensive research on mass movement susceptibility, hazard and risk assessment in recent years there is still a great need for research to further understand the processes involved in mass movements and implement future early warning systems. Modern research is integrating satellite-based terrain analysis in the ground behavior model in combination with regional weather forecast (e.g. (Ponziani et al., 2020; Strząbała et al., 2024; Cheng et al., 2025; Kohrs et al., 2021).

Even in times of multiple modelling and simulation possibilities the first step of any modelling or hazard assessment is posed by the geoscientific field investigation. Crucial information and data about the geological conditions (lithologic properties, orientations of bedding, faults or joint sets) and geomorphological conditions (unconsolidated sediments, active or inactive mass movements, headwater and channel characteristics) as well as a general impression of the hazard potential are best gathered through field investigations.

The aim of this work is to investigate the predisposing factors (static factors like geological conditions) and triggering factors (dynamic factors like meteorological events) which lead to this mass movement event. First, an introductory part describing the relevant mass movement characteristics (e.g. Hungr et al., 2014), as well as general geological and meteorological conditions of the Dolomites is given (e.g. Gianolla et al., 2008). The event documentation describes the temporal development and the different processes involved in the mass movement event and its consequences on infrastructure. Geomorphic Change Detection (GCD) visualize and quantifies volumes of surface lowering (erosion) and surface raising (deposition).

In order to characterize the predisposing factors detailed geologic and geomorphologic field investigation and mapping was carried out. Based on the mapping, geologic profiles could be drawn through the source area of the mass movement, to better understand the influence of the geological predisposition on the development of the mass movement. Hydro- meteorological evaluations characterize the triggering factors of this mass movement. With the gathered insights a conceptual ground behavior was established, which, together with the integration of other mass movement characteristics in the Val Badia region could be incorporated into a regional ground behavior model where similar geologic conditions occur. The outcomes of this ground behavior model could be integrated in mass movement susceptibility mapping and further improvement of hazard zone plans.

1.1 Purpose, research questions and objectives

The geoscientific investigation of this mass movement event is of interest because of following reasons:

1. Detailed geologic conditions are uncertain, as there is no public available or published geologic map of the study area based on the actual stratigraphic classification of the Dolomites (Bosellini, 1996; Brandner et al., 2007). The geologic map of the Western Dolomites terminates about 1 km S of the study area. The only geologic map covering the study area was produced in 1933 (Mutschlechner, 1933), but with a partly different stratigraphic classification. An unpublished map from Jesacher (Jesacher, 1999) was available, but displays differences compared to Mutschlechner´s map. Because of the uncertain and potentially complex geologic conditions detailed geological and geomorphologic mapping and field investigations pose the prerequisite step for characterizing the geologic predisposition of this mass movement event.

2. In hazard zone planning (HZP) such far travelling and coupled processes (cascade events) like this one in Seres Valley are not foreseen, as they would require extensive investigation and modelling and therefore considerably extend the establishment times of the hazard zone plans. The HZP of the Province of Bolzano include (1) hydraulic hazards, (1) snow avalanches and (3) mass movements (Autonomous Province of Bolzano, 2016). The extent of the investigation area is subjected to establishment times and limited financial and human resources and therefore concentrated on the most vulnerable areas (settlements). Therefore, investigation limits of hazard assessment are defined as settlement areas + 300 m buffer zone (Autonomous Province of Bolzano, 2016) and consider available information from the mass movement inventory or evident potential hazardous areas. Mass movement susceptibility mapping is not performed prior to hazard zone planning. Therefore, after the actual regulations, the source area of this mass movement could not be individuated as potential hazard area in the HZP of St. Martin. In consideration of such long-travelling mass movements (cascade events) the communal HZPs reaches its limit. In this case the question rises, if such hazard scenarios should be considered in the HZPs and if yes, based on which criteria can their potential source areas be priorly identified by Remote Sensing techniques (susceptibility mapping) and which criteria should be considered during targeted field investigation.

In this context, the goal of this study is to (1) characterize the key factors (predisposing and triggering factors) which led to this mass movement and (2) to summarize the outcomes in a conceptual ground behavior model that can serve as a base for mass movement susceptibility mapping of movements of the slide and flow type in the geologic setting of the Dolomites.

The investigation is focusing on the geologic, geomorphologic, hydrogeologic and geotechnical conditions at the source area of the investigated mass movement (predisposing factors) as well as the hydro-meteorological conditions (triggering factors). Not part of the study is the investigation of the flow behavior. This is modelled/simulated by (Dey et al., 2025).

More precisely, for the geoscientific processing of this mass movement event, following questions and related chapters form the cornerstones of this work:

1. How exactly did the mass movement developed from the source area until the village of Campill? Which processes were involved? Which were the geomorphic changes?

    ➔ Event documentation (chapter 1.2)
    ➔ Geomorphic Change Detection (chapter 4.2)

2. Why did the mass movement occur at this specific location (source area)? What are the geological, geomorphological, hydrogeological and geotechnical conditions in the study area (predisposing factors)?

    ➔ Geological Model (chapter 4.1)
    ➔ Geotechnical Model (chapter 4.3)

3. What were the triggering factors for this mass movement? Are the observed conditions and processes connected to other events in the region? Is there a regional pattern regarding mass movement activity?

    ➔ Analysis of Hydrological Data (chapter 4.4)
    ➔ Conceptual Conceptual Ground Behavior Model (chapter 4.5)
    ➔ Discussion: Conceptual Ground Behavior Model in regional context (chapter 5.2)

1.2 Event Documentation

The mass movement detached S of the Peitlerkofel on the SW slope (orographic right) of the Seres valley. The source area is located between 1885 to 2030 m a.s.l. adjacent to the watershed to the Bronsara valley (locality Col Ciancidel). Before the mass movement, the source area consisted of a colluvium deposit along a 400 m long, SW - NE trending gully which is bounded by a 50 m high rock cliff in the NW. The report "Rutschung und Schlammströme Seresbach Campill, ID: 0215027700" of 2024 describes the development of this mass movement and can be found on the Italian web GIS platform for hydro-geologycal hazards (Idro-GEO; ISPRA, n.d.) . The most relevant observations of this report, together with a temporal reconstruction of the event, based on the time of the photos, is summarized as follows:

First signs of the mass movement were reported in the morning of June 17, 2024 at approximately 08:00 a.m., when continuous tree movements were observed (forest ”Bosch dal’ Ega de Vita”). Subsequent field inspection at 10:40 a.m. confirmed an active earth - debris flow with grass spots originating on the orographic right side of the Seres valley with the following characteristics (measured in QGIS):

- source area center at approx. 1970 m a.s.l. (WGS84 coordinates: 46.639983 N, 11.829089 E)
- source area length (linear): 330 m (from 2040 - 1885 m a.s.l.), Mean slope angle = 25,2°
- source area width: 30 - 60 m
- source area depth: 0 - 20 m
- Source area extent: ~ 1,6 - 2,4 ha (= 16.000 - 24.000 m^2)
- Source area estimated eroded volume: 120.000 - 200.000 m^3
- Movement velocity of earth - debris flow at 10:40 am.: ~ 1 - 2 m/min
- Deposition area (1670 m a.s.l.): d = 1,03 km (from source area center), Mean slope angle = 16,2°
- Mean slope angle from end of source area (1885 m a.s.l.) to deposition area (1670 m a.s.l.) with d = 800 m is 15°
- Campill village (1400 m.a.s.l): d = 3,1 km (from source area center), Mean slope angle = 10,4°
- Mud Flow between deposition area and Campill is 2,07 km and 7,4°

At 9.30 a.m., a first mass movement in form of an earth - debris flow, partially still with grass spots had already passed the lower bridge in the Seres valley (fig.1c) and probably deposited in the upper Seres fields, where the channel widens and gradient decreases. At that time a consistent part of the mobilized material remained deposited at the junction between the source channel (here referred to as Ciancidel channel) with the Corëtes channel and after 100 m with the Seres Valley. The mass movement developed lateral levees, causing partial obstruction of both creeks, namely Rü de Corëtes (about 80 l/s at this time) and Seres (about 220 l/s at this time). Through the infiltration of both creeks in the earth - debris flow material at the junction with the Seres valley the material was remobilized in form of muddy debris flows surges. Figure 1e shows that at 10:40 a more massive muddy debris flow with a distinct front developed along the valley carrying several trees. This resulted in an additional shift of material from the first deposition zone at the junction downwards towards the upper Seres fields. The material deposited at the upper Seres fields due to the flatter and wider channel conditions and the muddy debris flow with m-size blocks poured over part of the fields and destroyed one hut and the upper mill.

During the early afternoon, several mud flow surges developed out of the muddy debris flow material and flew through the channelized Mühlental mostly within the Seres creek bed towards the village of Campill. These surges of faster mud flows posed a direct threat to infrastructure (bridges) and settlements. Velocities of 100 m/h were reported in the afternoon. In the afternoon a decrease in coarse material transport was observed while the mud flow reached the first houses in Campill.

By 09:00 p.m., the mass movement was not moving anymore and in the Seres valley the newly established creeks started to incise the deposited material. Most of the debris flow material was deposited in the upper Seres fields, where the creek displayed a braided-anastomosing flow pattern.

On June 18, 2024 no more flow episodes were noted, the transported material definitely came to a standstill. During the field inspection around the source area on the 19th June following observations were made:

- An approx. 0,5 ha big, sliding-prone, fractured rock mass above the source area on the south was identified. This rock mass exhibits many older tension cracks, fragmented rock mass (boulders) and partly fresh terrain steps of about 10 - 20 cm, partly covered by roots under tension. These geomorphic features indicate that this area is in a metastable situation and is experiencing extremely slow sliding movements long before the event happened. The thickness of the potential mobilizable material was estimated with 7 m, which corresponds to a volume of about 30 - 40.000 m^3.

- The debris flow material shifted the Seres creek to the orographic left side of the valley and created a backwater. Some meters below this backwater the creek began to erode the foot of the earth slump - earth flow coming down from the eastern valley side (locality of Fornates; IdroGEO ID: 0210214701).

Different measures were taken to minimize the hazard:

- Bridges: Three bridges were manned with excavators to prevent blockages and secure the bridges near Miscí, Frëina and Campill. In total, 10 excavators and 6 trucks were used for transporting the material away, also at night.
- Protective barriers and trench: A diversion barrier made of concrete blocks was assembled at the bridge before Campill (Lizia street) to prevent the mud flow from spreading along the road into the village. On the forest road leading to Seres a diversion trench was quickly digged to ensure the backflow of the progressing muddy debris flows into the Seres stream (Mühlental) and secure the hamlet of Seres.
- Monitoring: Drones from the fire department were continuously monitoring the development of the mass movement. For the night spotlights were illuminating the mass movement at the upper Seres fields.
- Evacuation: With the formation of the mud flows, the houses along the Seres creek in Frëina were evaacuated. For the night between 17th and 18th June 146 people from 56 houses in Seres, Frëina and Campill, which were located closely to the stream and thus exposed at the highest risk were evacuated.
- In the following days the Seres creek bed was channelized and re-profilized to prevent the formation of new debris or mud flows. Particular attention was addressed to the erosion on the foot of the older earthflow on the orographic left side (IdroGEO ID 0210214701).

Further observations from the author of this thesis:

The debris flow deposited at the end of the Seres valley (upper Seres fields) as the valley floor gradient decreases and the valley opens leaving the muddy debris flow material space to spread over the field on the orographic left side and forming an elongated debris fan. In this area meter-scale blocks and boulders were deposited together within a matrix ranging from gravel to clay. One hut and the uppermost mill of the Mühlental were destroyed here. The muddy debris flow material began also to flow along the forest road towards the village of Seres, but the material supply diminished at that point and the deflection trench brought the material back to the Seres creek in the Mühlental valley. From this point mud flows with blocks of max. 80 cm in diameter flew along the Mühlental. Because the Seres creek incised in quaternary alluvial sediments creating the small Mühlental, the mud flows flew along the channelized stream bed causing only minor damages on some mills and the path in the Mühlental as well as bridges in Miscí and Frëina. At Frëina the streambed becomes smaller, therefore in some parts material was deposited beyond the streambed. In Campill the streambed was artificially narrowed, therefore the mud flow material with some boulders pour about 70 cm over the streambed, as deposition marks on trees and houses demonstrate, spreading into gardens, basements and first floors of the first houses of Campill.


a
b
c
d
e
f
g
h

Figure 1: Mass movement event in Seres valley at June 17th 2024. a) source area at Ciancidel channel (Roa de Corëia). b) aerial photo of source area with Corëtes channel on the right (V. Mair). c) first earth-debris flow at 9:26 a.m. at the bridge in the lower Seres valley (T. Obwegs). d) mass movement at the junction between Ciancidel channel, Corëtes channel (left) and Seres valley (Agency for Civil Protection, Province of Bolzano). e) muddy debris flow in Seres valley with prior earth flow from orographic left side (IdroGEO ID 0210214701) at the lower end of the photo (V. Mair). f) m-size blocks of the debris flow material at the end of Seres valley (above deposition zone). g) deposition zone at upper Seres fields, between lower end of the Seres valley and beginning of little Mühlental valley (V. Mair). h) mud flow surge in the Mühlental valley close to a mill (T. Obwegs). i) mud flow in the village of Campill. j) mud flow in Campill with excavators removing material from Seres creek.

1.3 Characteristics of Mass Movements and Debris Flows

Gravitational mass movements, often simplified referred to as landslides, are part of geohazards and broader natural hazards. The term gravitational mass movement refer to the downslope movement of unconsolidated material, rock and organic material driven by gravity (Highland & Bobrowsky, 2008).

Among the various approaches for classifying mass movements based on different criteria, the process-based classifications established internationally (Cruden & Varnes, 1996; Hungr et al., 2014; Varnes, 1978). This classification system is based on the material type and the primary movement type, also referred as failure mechanism or kinematics.

The movement type of mass movements can be subdivided into falls, topples, slides (rotational and translational), spreads, flows, and slope deformations (Hungr et al., 2014). A clear distinction between these types is not always possible, as transitional forms and complex movement mechanisms occur in nature. In such cases, Hungr et al. (2014) suggests the use of composite terms, while it is also essential to describe further properties like geometry (depth, length, width and volume), velocity (also referred as rate of movement) or state.

With regard to material type, the well-known classification of Varnes (Varnes, 1978) differentiates between rock, debris and earth, while the revised classification divides rock and soil and suggests using grain size classes (see table 1 from Hungr et al., 2014). Material terminology should focus on the significant or dominant material type before using transitional terms.

The unsorted material terms “debris”, “mud” and “earth” are widely used in geomorphological mass movement science. These materials developed through geomorphic processes such as weathering (residual soils), mass wasting (colluvium), glacier transport (moraine and till), volcanism or alluvial processes (Hungr et al., 2014).

Debris is a mixture of sand, gravel and boulders, often with varying proportions of silt and clay. Debris material descriptions in literature make reference to coarse clasts and matrix, whereas matrix is considered to be material finer than gravel or sand (Hungr et al., 2001; Hungr et al., 2014). After Varnes (1978) debris contains more than 20 % gravel, while earth contains maximum 20 % gravel. But this limit may have little significance with respect to mechanical behavior as for instance up to 35 % of gravel in a clayey soil has no proper influence on the friction angle or cohesion of the material (Hungr et al., 2001). Therefore, the attribution of a genetic term of the material gives valuable information regarding its composition and behavior.

Mud is a similar unsorted material, but with a sufficient silt and clay content to produce plasticity and with high moisture content. Hungr et al. (2001) proposed that the term “mud” be used for remolded mixed clay - silt soils whose matrix is significantly plastic (Plasticity Index >5 %) and whose Liquidity Index during motion is greater than 50 % (i.e., in or close to a liquid state (Hungr et al., 2014).

The term “earth” does not have established status in either geological or geotechnical material description schemes but is required as part of the established term “earth flow.” In this context, it means a cohesive, plastic, clayey soil, often mixed and remoulded, whose Liquidity Index is below 50 % (Hungr et al., 2014).

As mentioned before, supplementary geological and geomorphological terms regarding the origin of rocks (lithology) and soils/regolith (residual, colluvial [scree or talus], alluvial, lacustrine, marine, aeolian, glacial, volcanic, organic, anthropogenic fills) add valuable information regarding their composition and behavior.

Table 1: Mass movement forming material types (Hungr et al., 2014). Abbreviations: PI = Plasticity Index, LI = Liquidity Index.

Material name	**Character descriptors**	**Simplified field description**	**Corresponding soil classes**	**Laboratory indices**
Rock	Strong	Strong-broken with a hammer		UCS>25 MPa
	Weak	Weak-peeled with a knife		2<UCS<25 MPa
Clay	Stiff	Plastic, can be molded into standard thread when moist, has dry strength	GC, SC, CL, MH, CH, OL, and OH	PI > 5 %
	Soft			
	Sensitive			
Mud	Liquid	Plastic, unsorted remolded, and close to LL	CL, CH, and CM	PI > 5 % and LI > 50 %
Silt, sand, gravel, and boulders	Dry	Nonplastic (or very low plasticity), granular, sorted. Silt particles cannot be seen by eye	ML	PI < 5 %
	Saturated		SW, SP, and SM	
	Partly saturated		GW, GP, and GM	
Debris	Dry	Low plasticity, unsorted and mixed	SW-GW	PI < 5 %
	Saturated		SM-GM	
	Partly saturated		CL, CH, and CM	
Peat		Organic		
Ice		Glacier		

Table 2: Mass movement classification system modified after Varnes (1978) (29 numbered terms) and adding terms from Hungr et al. (2014)(not numbered), which divides the material in only rock and soil, but suggests using grain size terms for soil. As in nature it is not always possible to identify the dominant grain size, the Varnes (1978) classification is still mostly used. The movement type "slope deformation" was introduced by Hungr et al. (2014).

Movement type	**Rock**	**Debris**	**Earth**
Fall	1. Rock fall	2. Debris fall	3. Earth fall
Topple	4. Rock topple	5. Debris topple	6. Earth topple
Sliding (rotational)	7. Rock slump (rock rotational slide)	8. Debris slump	9. Earth slump
Sliding (translational)	10. Block slide (rock planar slide)	11. Debris slide	12. Earth slide
Additional terms by Hungr et al., 2001	Rock wedge slide Rock compound slide Rock irregular slide		
Lateral spreading	13. Rock (slope)spread	—	14. Earth spread
Flow	15. Rock creep	16. Colluvium flow	21. Dry sand flow
		17. Debris flow	22. Wet sand flow
		18. Debris avalanche	23. Quick clay flow
		19. Solifluction	24. (Rapid) Earth flow
		20. Soil creep	25. Mud flow
		Debris flood	26. Loess / Peat flow
		Debris flowslide	Clay/silt/sand/debris flowslide
Complex	27. Rock slide-debris avalanche	28. Cambering, valley bulging	29. Earth slump-earth flow
Slope Deformation	Mountain Slope Deformation Rock slope deformation		Soil slope deformation Soil creep

In addition to material type and movement type (kinematics), mass movements are further described by state of activity, distribution, style of activity, rate (velocity) and water content (see table 3; Cruden & Varnes, 1996).

Table 3: Glossary for the naming of mass movements (Cruden & Varnes, 1996)

Activity			**Description of first movement**			
State	**Distribution**	**Style**	**Rate**	**Water Content**	**Material**	**Type**
Active	Advancing	Complex	Extremely rapid	Dry	Rock	Fall
Reactivated	Retrogressive	Composite	Very rapid	Moist	Soil	Topple
Suspended	Widening	Multiple	Rapid	Wet	Earth	Slide
Inactive	Enlarging	Successive	Moderate	Very wet	Debris	Spread
Dormant	Confined	Single	Slow			Flow
Abandoned	Diminishing		Very slow			
Stabilized	Moving		Extremely slow			
Relict						

The eight activity states defined by Cruden and Varnes (Cruden & Varnes, 1996) can be grouped into three principal categories: active, inactive, and relict (table 3 and 4). An active mass movement is one that is currently moving. This includes both mass movements showing continuous movement and those that have been reactivated after a period of inactivity (Classes 1 and 2), regardless of the rate of displacement.

The term inactive refers to mass movements that are not moving at the present time. This category includes mass movements that (i) have not moved during the last 12 months (inactive), (ii) have moved within the last annual cycle but are not currently moving (suspended), or (iii) are not currently active but may be reactivated by changes in controlling factors (dormant) (Classes 3, 4, and 5).

The third category comprises mass movements that are no longer expected to be reactivated under present conditions. These include mass movements that (i) are no longer affected by the original controlling factors (abandoned), (ii) have been rendered stable by remedial measures (stabilized), or (iii) were formed under different geomorphological or climatic conditions (relict) (Classes 6, 7, and 8). Such mass movements have reached a condition in which movement has ceased, and there is no evidence indicating that movement will resume.

Table 4: Activity classes after Cruden & Varnes (1996).

Class	Activity state	Description
1	Active	mass movement that is currently in motion
2	Reactivated	mass movement that, after a period of inactivity, is active again
3	Inactive	mass movement that has not moved within the last 12 months
4	Suspended	mass movement that moved during the last annual cycle but is currently inactive
5	Dormant	inactive mass movement that can be reactivated by changed controlling factors
6	Abandoned	inactive mass movement that is no longer influenced by its original controlling factors
7	Stabilized	inactive mass movement whose movement has been reduced or ceased by remedial measures
8	Relict	inactive mass movement formed under different geomorphic or climatic conditions

The **rate (velocity)** of mass movements is divided into seven classes, ranging from several meters per second to a few millimeters per year (table 5; Cruden & Varnes, 1996). Depending on the movement velocity, different mitigation measures can be applied to reduce the associated hazard potential (Hungr et al., 2014).

Table 5: Mass movement velocity scale after Cruden & Varnes, 1996.

Velocity class	Description	Velocity [mm/sec]	Typical velocity
7	Extremely fast	5×10^{3}	5 m/sec
6	Very fast	5×10^{1}	3 m/min
5	Fast	5×10^{-1}	1.8 m/month
4	Moderately fast	5×10^{-3}	13 m/month
3	Slow	5×10^{-5}	1.6 m/a
2	Very slow	5×10^{-7}	16 mm/a
1	Extremely slow	-	-

Indicating the geometry of the mass movement (length, width, depth and volume) is an essential attribute in mass movement description. A possible classification for slides is shown in table 6 (Rokić, 2011).

Table 6: classification after area and volume for sliding mass movements (Rokić, 2011; S.442)

Size class	Area [m²]	Volume [m³]
Very small	< 100	< 100
Small	100 - 1.000	100 - 5.000
Medium	1.000 - 10.000	5.000 - 100.000
Large	10.000 - 50.000	100.000 - 1.000.000
Very large	> 50.000	> 1.000.000

The attribute depth of sliding or failure surface is mainly restricted to the sliding type. Internationally codified depth classification is missing, but the distinction between superficial (< ~2 m), shallow- or medium (< 10 m) and deep-seated slides (> 10 m), as well as DSGSD (Deep-Seated Gravitational Slope Deformations, about > 30 - 50 m), seems to be widely applied.

1.3.1 Causes and Triggering Factors

The initiation of mass movements is controlled by a variety of factors that modify the equilibrium of a slope (Genske, 2014). These factors are subdivided in (1) predisposing, (2) triggering and (3) (movement-) controlling (Crozier, 1989). Predisposing or preparatory factors move a slope from stable equilibrium to a marginal stable, so they form the kinematic condition that a mass movement could potentially occur (susceptibility). The triggering factor(s) disturbs the force equilibrium (mechanical condition) and finally initiates the movement (failure), whereas the controlling factors influence the activity (e.g. state and velocity).

Predisposing factors or causes include topographic characteristics (e.g., slope inclination and aspect), the geological and geomorphological conditions of bedrock and unconsolidated materials (e.g. weak, weathered or jointed rocks, contrasts in stiffness or permeability, glacially steepened slopes, etc.), as well as vegetation cover and slope hydrogeological conditions. These factors determine the intrinsic susceptibility of a slope to failure (Glade & Dikau, 2002).

Triggering factors can cause instability (failure) by either decreasing the shear strength (resisting forces) or by increasing the shear stresses (driving forces). Often they are external factors that initiate failure, most notably hydrometeorological forcing (e.g., intense or prolonged rainfall, rapid snowmelt), seismic loading (earthquakes) and anthropogenic disturbances (e.g., blasting, slope steepening at the foot or loading at the top; see table 7; Glade & Dikau, 2002).

Controlling factors govern the mechanical behaviour, kinematics and evolution of the mass movement after initiation, thereby determining the activity (Glade & Dikau, 2002).

It is important to define the role of each factor, as they depend on the site-specific conditions and the failure mechanism and are relevant for planning remediation or stabilization measures.

In table 7 an overview of the role of different factors such as geology, climate, soil, vegetation, hydrology and anthropogenic influences, is given. Beneath this classification of factors, it can also be distinguished between permanent (static) and episodic (dynamic) factors.

Table 7: Overview of different preparational, triggering and controlling factors influencing mass movements in context with different characteristics (modified after Glade & Dikau (2002).

Factors Influencing Mass Movements			
Cause	**Preparatory factors**	**Triggering factors**	**Controlling factors**
Geological	Lithologic properties (strength, bedding); weathering; discontinuities (joints, faults) and orientation; tectonic disturbances; competence contrasts	Earthquakes; volcanic eruptions	Rock types; discontinuities; structural discontinuities
Climate Meteorology	Prolonged precipitation; snowmelt; temperature changes (freeze-thaw cycles)	Precipitation or hail (intensity, amount); rapid snowmelt, strong winds	Precipitation (intensity, amount)
Geomorphology / Soils	Weathering; geotechnical properties; soil type and texture; shear strength cycles; subterranean erosion (e.g., piping)	Not applicable	Saturation; strength of soils
Vegetation	Presence or absence (soil fixing vs. loosening), natural vegetation changes (e.g., wildfires, drought)	Not applicable	Vegetation
Hydrogeology	catchment area, flow paths, infiltration, thawing permafrost, enhanced weathering in joints and faults	Water content (saturation), fluctuations in GW level; rapid drawdown; pore-water pressure, base erosion, lowering friction angle + cohesion	Water content (saturation), Low permeability; lateral transport
Topography	Slope angle, aspect (exposure), height	Not applicable	Slope inclination; curvature; contour lines
Anthropogenic	Deforestation; damming; removal of slope support; artificial loading; irrigation; mining; vibration; leaking water supply	Slope incision; undercutting; surcharge	Engineering works; dams; drainage; grading

1.3.2 Mass movements of flow and slide type

Mass Movements in the study area are mainly of the slide and flow type. Therefore, these types are described with more detail in this chapter.

The sliding type of movement is characterized by downslope movement of soil or rock, which occurs prevalently along one or multiple failure surfaces or within a relatively narrow shear band where the shear strains localize. The sliding mass, isolated by a discrete failure surface, shows small internal deformation (small distortional strain). The geometry of the failure surface may by a translational or a rotational or a combination of both (Varnes, 1978; Cruden & Varnes, 1996; Hungr et al., 2014).

Rotational slides, also referred to as slumps, occur mainly in mechanically isotropic geologic conditions (weak rock or soil). The morphology is characterized by a prominent main scarp with steep to vertical displacements in the upper part and a back-tilted bench at the foot, due to the rotatory (spoon-shaped) failure surface. This type of mass movement leads to typical concave and convex geomorphological expression in the terrain. Movement velocity is usually slow to moderately slow or sometimes rapid (Cruden & Varnes, 1996; Hungr et al., 2014).

In a translational or planar slide, sliding occurs on an inclined planar failure surface. The sliding mass typically separates along a vertical tension crack (Hungr et al., 2014). This movement type is often controlled by geological discontinuities (contrasts in competence/stiffness, bedding surfaces, joints, cracks, faults and soil-bedrock contact) and can be slow (earth slide) to extremely rapid (rock slide), depending on the involved material characteristics (Varnes, 1978; Cruden & Varnes, 1996; Hungr et al., 2014).

A combination of both movements, so called compound slides, are often found in nature. Internal deformation is accommodated by multiple shear surfaces, tension cracks and minor scarps. (Varnes, 1978; Cruden & Varnes, 1996).

Flow type mass movements predominantly develop in highly water-saturated soil or debris and are characterized by rapid movement. The flow movement is similar to that of a viscous fluid and compared to the sliding type the material does not move along a defined sliding surface and the mobilized mass does not exhibit uniform displacement but variable displacement rates inside the mass. Generally, the mass can cover a long path before stopping itself and it is possible to individuate 3 zones: the eroded source area (also initiation zone), the (intermediate) transport or transfer zone and the deposition area.

Most flow processes generally exhibit a high water content (water - solid ratio of approximately 1:1 or 30 % to 70 %), however events with comparatively low water content have also been documented (Prinz & Strauß, 2018). Beneath this rapid flow movements (mud-, earth or debris flow) also very slow creeping movements are associated to the flow type. These creeping movements are not treated here.

Debris flow (german: Mure) is a wide-spread hazardous phenomenon in mountainous terrain. Debris flows are very rapid to extremely rapid surging flow of saturated debris in a steep channel. Strong entrainment of material and water from the flow path occurs (Hungr et al., 2014). It is distinct from other mass movement types in that it occurs periodically on established paths, usually gullies and drainage channels and exhibits deposition area ("debris fan"). In contrast, debris avalanches are not bound to an established path and occur on open-slope (Hungr et al., 2014). Debris flow events are often triggered by extreme rainfall events. The flow may be initiated by a slide, debris avalanche or rock fall from a steep bank, or by erosion of the steep stream bed (Hungr et al., 2014).

When material begins to move in a steep channel, the bed becomes subject to rapid undrained loading and coarse material suffers significant increase in pore pressure and can even liquefy. The bed material will become entrained in a growing surge as erosion undermines the steep banks and further debris and soil material is added to the flow. The surges travel down the channel on slopes steeper than 10–20°. The bulk of the material involved in a debris flow event usually originates from entrainment from the path, while the volume of the initiating slide is insignificant. The magnitude of debris flows therefore depends primarily on the characteristics of the channel (sediment availability) and can be estimated by different methods (Hungr et al., 2005).

As a result of channelization, a debris flow surge grows and becomes fronted either by a boulder concentration (Pierson, 1986) or a turbulent "head" (Davies, 1986). They spread out when the channel exits onto the surface of the debris (colluvial) fan, at typical slopes of 5° to 20°. The frontal boulder accumulation rapidly deposits, while the finer and more dilute material continues further downslope. Spatial gradational sorting of such materials due to the development of inverse grading or coarse surge fronts is common (Pierson, 1986).
Depending on the lithology in the catchment debris flows can transport primarily coarse debris, while in regions of sedimentary and volcanic rocks or those with highly weathered metamorphic rocks, the material may contain significant content of silt and clay and be measurably plastic (Bull, 1964). Such soil drains more slowly and remains longer in a liquid condition, leading to longer travel and lower slope angles in the deposition area. After revision of debris flow literature (e.g. (Hungr et al., 2014; Jakob & Hungr, 2005) debris flows can be specified in different categories (table 8)

Table 8: Possible debris flows specifications after different authors and categories.

Category	Classes
Grain size and texture (e.g.Hungr et al., 2014; Jakob & Hungr, 2005)	- Coarse-grained debris flow: dominated by block and gravel grain sizes - Fine-grained debris flow: dominated by sand, silt and clay - Matrix-supported: blocks and boulders embedded in a finer matrix - Clast-supported: blocks and boulders dominate with water and subordinate fine grained material
solid volume - water concentration (Costa, 1984; Pierson & Costa, 1987)	- Water floods: Low sediment concentration (<~ 5 - 10 % by volume). - Hyperconcentrated flows: Transitional flows with 10 - 40 % sediment; behave partly as fluid, partly as mass movement. - Debris flows: High sediment concentration (>~ 40-60%), with strong grain-grain interactions and non-Newtonian behavior. - Debris avalanches / granular flows: Very high solid content, little free water (> 65 %)
Genetic process (Jakob & Hungr, 2005)	- Slope-failure-initiated debris flows: Triggered by landslides, slumps, or rockfalls that liquefy. - Runoff-generated debris flows: Initiated by intense rainfall eroding channel beds and banks. - Entrainment-dominated debris flows: Start small and grow rapidly by scouring material along the flow path. - Glacial or volcanic debris flows (lahars): Triggered by meltwater, eruptions or crater-lake failures.
Entrainment (erosion) -Controlled vs Supply (transport)-Limited Flows (Jakob & Hungr, 2005)	- Supply-limited debris flows: Fixed initial volume and minimal bed erosion - Entrainment-dominated debris flows: Volume increases strongly along the path and bed erosion being the dominant sediment supply process.

For the purpose of modelling flow behaviour and runout of debris flows, rheology-based models were developed in recent years (e.g Gibson et al., 2021; Schippa, 2021; Zegers et al., 2020).

Compared to debris flows, earth flows mainly occur on gentle to moderately steep slopes and are composed predominantly of fine-grained unconsolidated material. The earth-flow mass moves as a plastic–viscous medium and is characterized by pronounced internal deformation (Highland & Bobrowsky, 2008). The movement is facilitated by a combination of sliding along multiple discrete shear surfaces and internal shear strains (Hungr et al., 2014). Depending on the lithology, the weathering behavior and channel characteristics debris flows can be composed of coarse debris, containing only small proportions of fines, or be composed of significant content of fines and be measurably plastic (Bull, 1964). Such soil drains more slowly and remains longer in a liquid condition, leading to longer travel and lower slope angles in the deposition area (Hungr et al., 2014).

Mud flows are very rapid to extremely rapid surging flows of saturated plastic soil in a channel, involving significantly greater water content relative to the source material (Plasticity Index > 5 %; Hungr et al., 2014).

1.3.3 Debris flow catchments: Supply- vs. transport-limited

Regarding the development of debris flows, their catchments are commonly classified as either supply-limited or transport-limited.

A debris flow catchment is supply-limited when debris flow occurrence and magnitude are controlled primarily by the availability of mobilizable sediment (colluvium, debris, weak rocks or channel fill), rather than by triggering mechanisms. In other words, even if triggering mechanisms (e.g. rainfall) are present, debris flows cannot occur unless sufficient loose material for entrainment is present in the catchment (Bovis & Jakob, 1999; De Haas et al., 2024).

A catchment is transport-limited when abundant sediment is available and debris flow activity is primarily controlled by the ability of flow processes to mobilize and transport that sediment. Sediment is not the limiting factor, instead, hydrologic forcing and transport capacity govern debris flow occurrence and size. In other words, a debris-flow catchment is transport-limited when sediment supply exceeds transport capacity and debris flows are limited primarily by triggering conditions (rainfall intensity, runoff or pore-pressure rise; Jakob & Hungr, 2005)

2 Site Description

2.1 Geographic Overview

The study area is located in the Autonomous Province of Bolzano - South Tyrol (Italy) in the commune of St. Martin in Thurn. St. Martin i.T. lays in the middle of Val Badia valley (German: Gadertal), which separates the Dolomites into east and west. From St. Martin i. T. the Campill Valley branches off in a southwestern direction, along whose western valley side the Peitlerkofel mountain rises (Ladin: Sas de Pütia, 2875 m a.s.l.). The Peitlerkofel forms the northwestern edge of the Western Dolomites. At the end of the Campill Valley lies the village of Campill (Ladin: Longiarü, 1400 m a.s.l.) and the valley splits into three small subalpine side valleys, e.g. Bronsara Valley and Antersasc Valley. From the alpine meadows southeast of the Peitlerkofel, the Seres creek flows for about 3 km down the small subalpine Seres Valley. At the exit of the Seres Valley, the cultivated Seres fields spread out and the Seres creek flows past some mills (Mühlental) and near the hamlets of Miscí and Seres before flowing through the small village of Frëina and the village of Campill and finally flowing into the Campill stream.

The mass movement detached south of the Peitlerkofel on the SW slope (orographically right) of the Seres valley. The source area is located at about 1970 m a.s.l. near the watershed to the Bronsara valley. Before the mass movement, the detachment area consisted of a colluvium deposit (about 1,7 ha), named Roa de Corëia, below a 50 m high rock wall.

Evidence for the occurrence of mass movements in the Campill Valley, as well as in the Dolomites around Val Badia and Val Gardena, can be found in toponyms of Ladin language. Ladin toponyms such as frëina or frena indicate mass movements of the slide and flow type or unconsolidated, sliding or falling material and can be found at the upper Seres fields and in the village of Frëina itself. The term Roa also refers to slides and flows (especially debris flows), but also refer to detachment or source area and colluvium or scree slopes (Mischì, 2021). This toponym is found in the source area of the investigated mass movement (Roa de Corëia), where it probably refers to the colluvium material below a 50 m high rock face.

The extent of the study area lays between Peitlerkofel and the village of Campill. Especially the area around the source area is of interest. Therefore, the study area (also mapping area) is of limited dimensions (1,4 km^2) and extends from the upper Seres fields W of the village of Seres until the localities of Fornates and Cialneur in the E and NE, until the Corëtes creek in the NW and the watershed between Seres valley and Bronsara valley at the Ciancidel huts in the S.

The W part of the study area is within a Natura 2000 protected habitat site and buffer zone of UNESCO Site Puez-Geisler. The forest around the source area is regarded as a protection forest composed of alpine larch, pine and spruce forest.

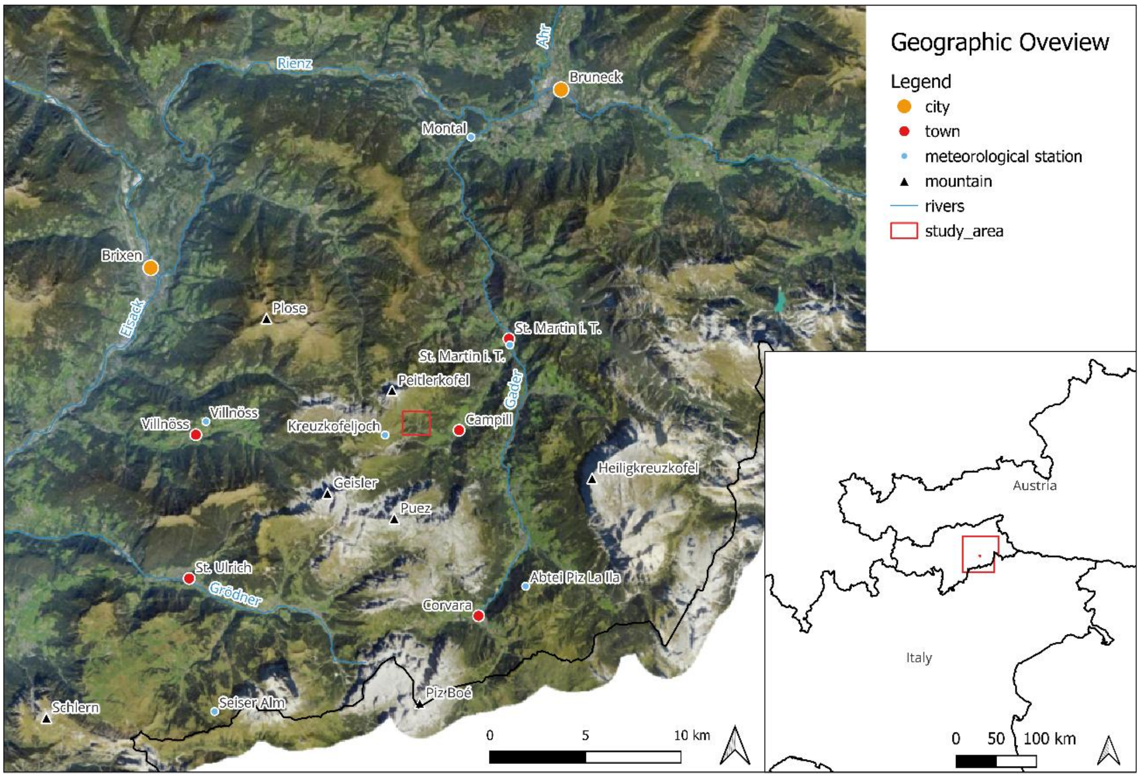

Figure 2: Geographic Overview of SE South Tyrol with the study area and the relevant meteorological stations. Background: Orthophoto 2023 (Province of Bolzano).

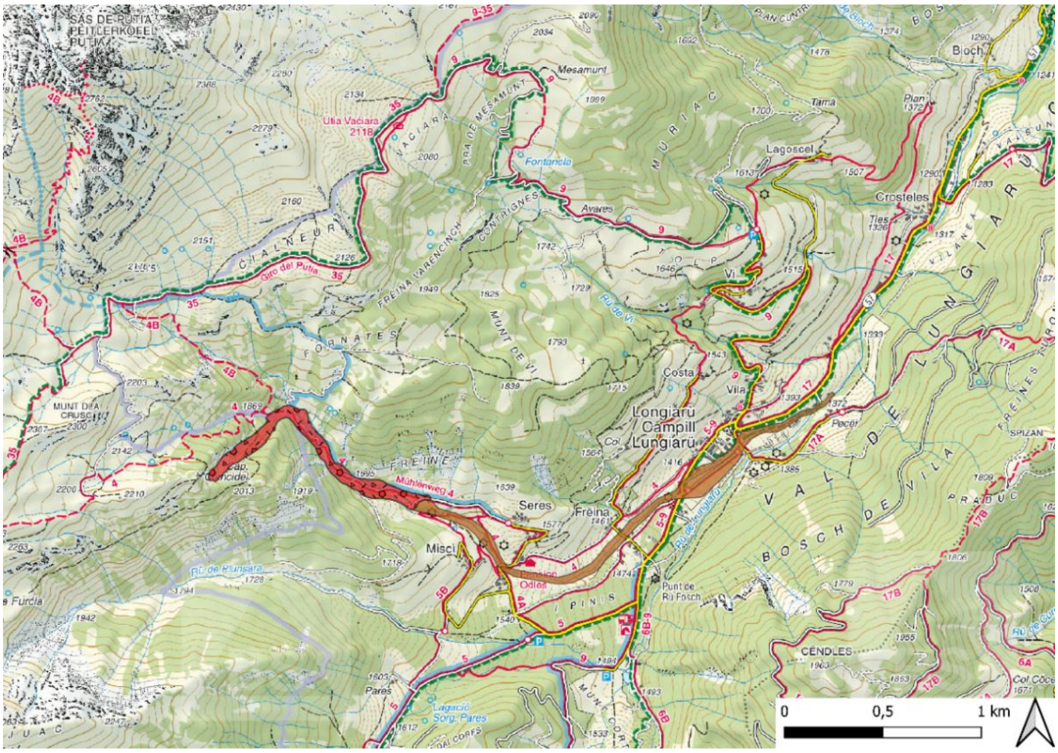

Figure 3: Topographic map of the study area with the process area of the mass movement divided in debris flow (red) and mud flow (brown). Basemap: Tabacco (2024). Important local toponyms in this thesis are: Peitlerkofel, Ciancidel (S of source area), Fornates (NE of Seres creek) and Rü de Plunsara = Bronsara valley.

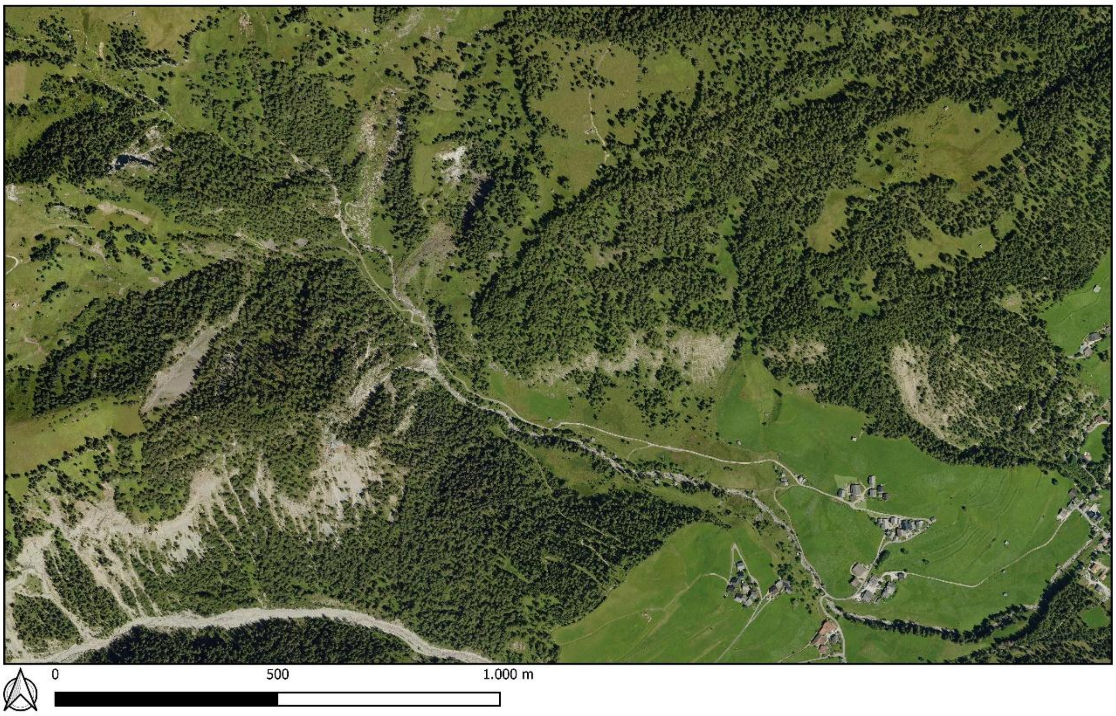

Figure 4: Orthophoto of 2023 of the study area.

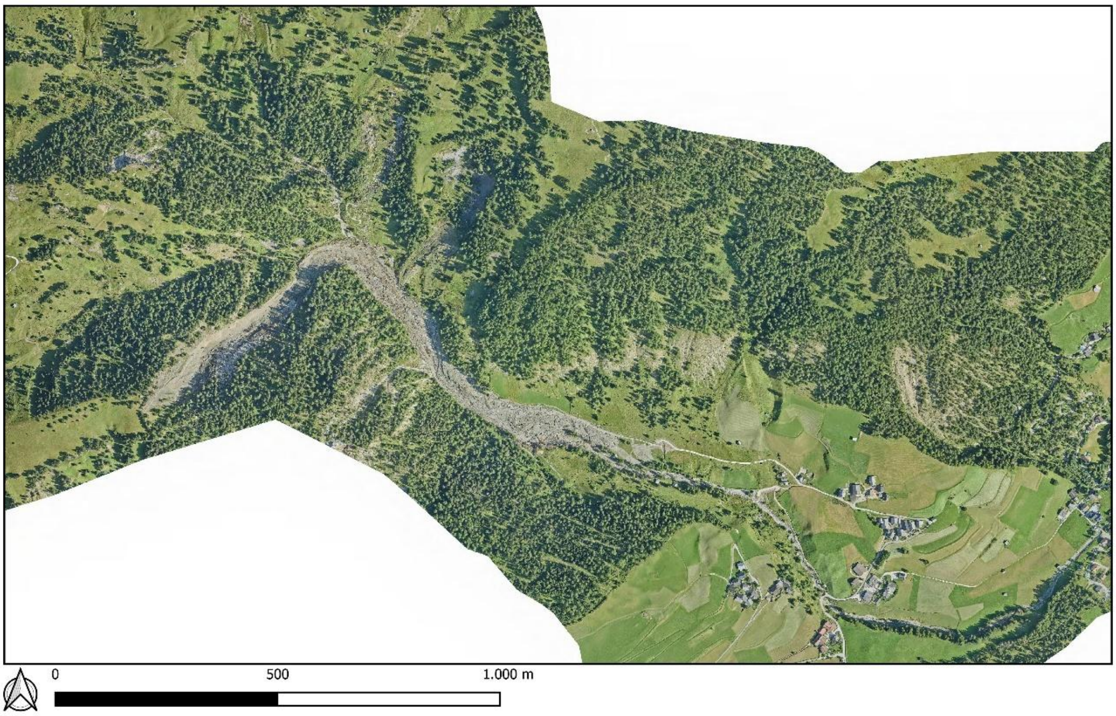

Figure 5: Orthophoto of September 2024 of the study area.

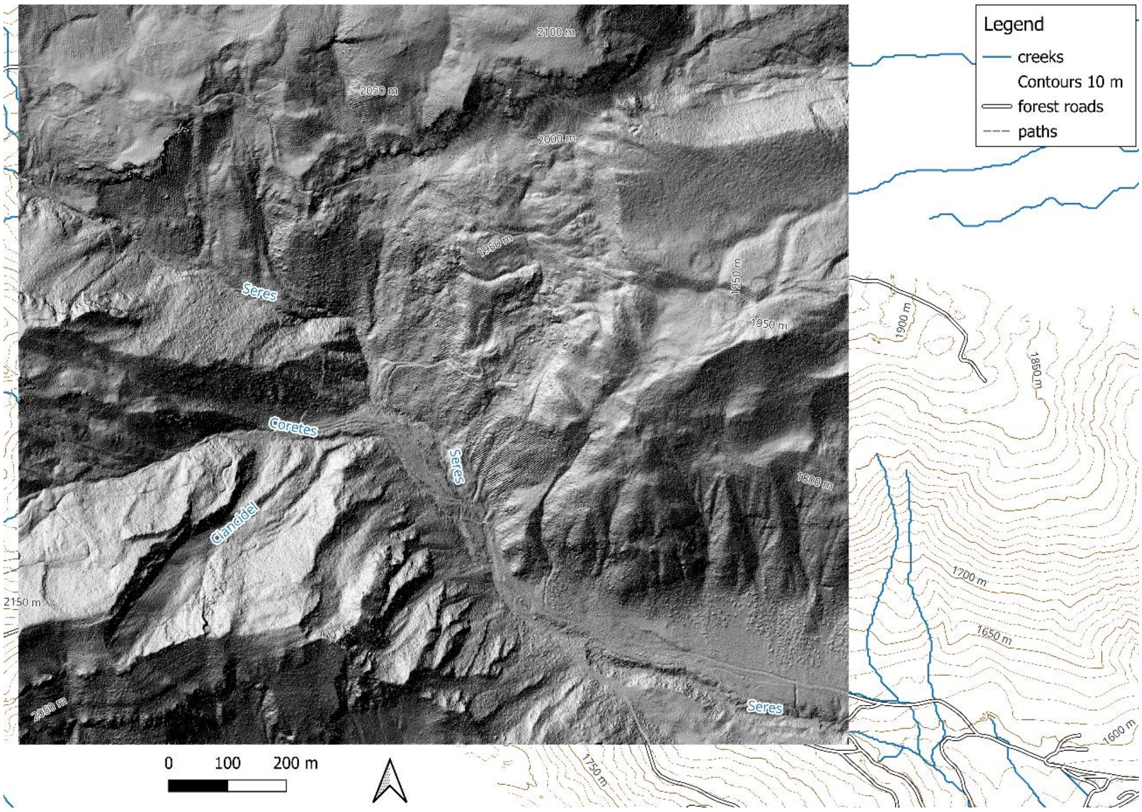

Figure 6: pre-event 1 m DTM of 2006 of the study area.

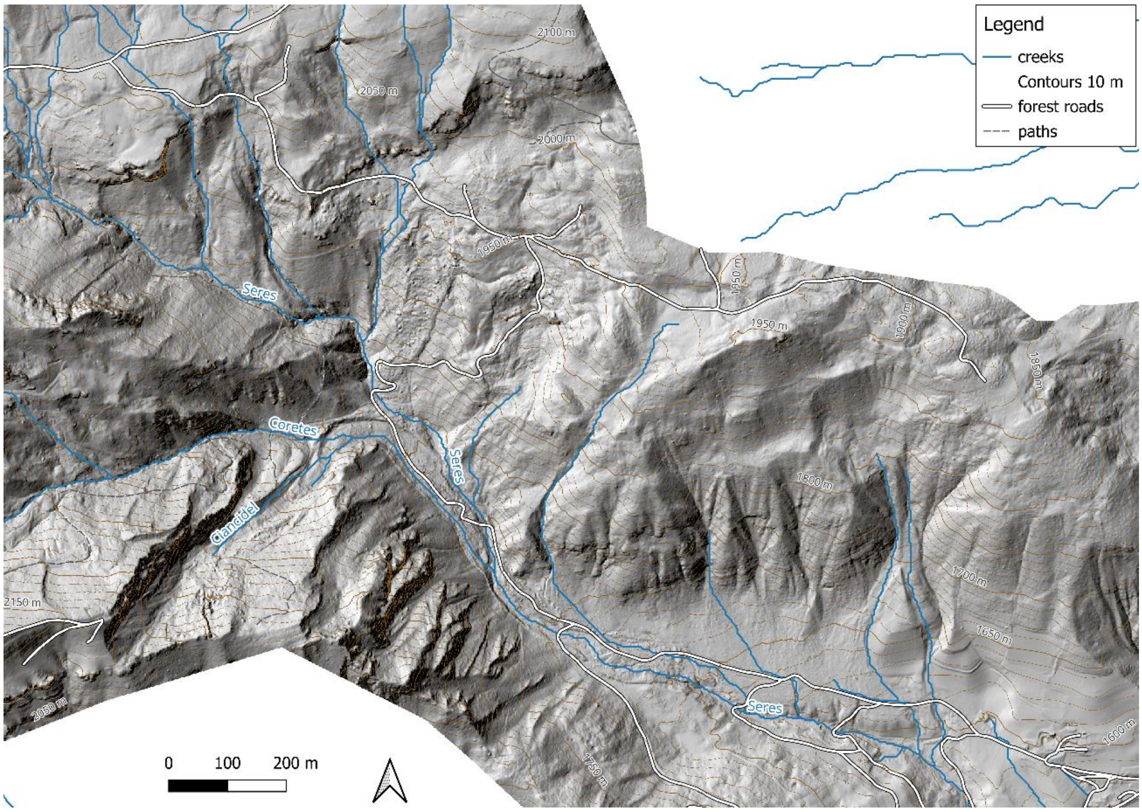

Figure 7: post-event 1 m DTM of September 2024 of the study area.

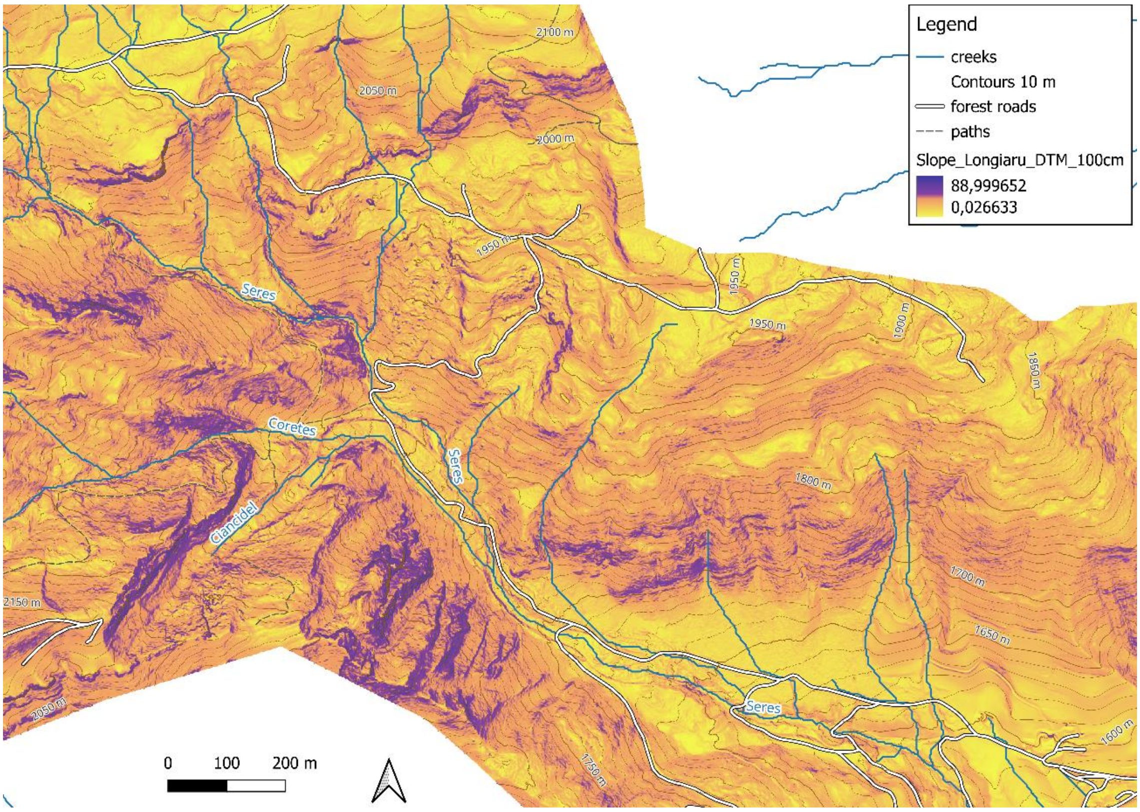

Figure 8: Slope map from the 2024 post-event DTM.

2.2 Geological Overview

The development of mass movements is often connected to the geological conditions. The spatial distribution of different lithologies, structural geological features and quaternary geomorphological deposits result from the geological evolution and shape today's landscape. Therefore, this chapter provides an overview of the relevant stratigraphic and tectonic developments of the Western Dolomites from Permian to Triassic to better understand and interpret the stratigraphic and structural geological conditions in the study area. The overview focuses on the Triassic, as the landscape controlling geological conditions of the study area result from that period. Detailed descriptions of the stratigraphic formations and lithologies within the study area are given in chapter 5.1.1.

2.2.1 Southalpine and Dolomites

The study area is located within the tectonic mega-unit of the South Alpine, more specific in the northern part of the Western Dolomites. The South Alpine unit was part of the Adria microplate and is characterized by (1) mainly magmatic and sedimentary units, (2) a south-vergent fold-and-thrust belt and (3) low-grade to absent Alpine metamorphic overprint (Doglioni, 1987). The Variscan metamorphic rocks (e.g. Brixner Quarzphyllite) are regarded as the basement of the South Alpine, while the permomesozoic cover is composed of Permian volcanics and

Mesozoic marine sediments (carbonates), which build up the Dolomites (Doglioni, 1987; Bosellini et al., 2003).

Extensional tectonics and differential subsidence rates during Mesozoic, especially during Triassic, led to partly different sedimentation history in the Dolomites. Therefore, they are often subdivided in Western and Eastern Dolomites (Bosellini, 1996). The boundary between the Western Dolomites (Trento Horst) and Eastern Dolomites (Belluno Graben) can be approximately positioned along the N-S trending Val Badia (Bosellini, 1967, 1967; Curzi et al., 2023; Winterer & Bosellini, 1981).

During the Alpine orogeny (Cretaceous to Miocene) the South Alpine experienced various deformation phases, which changed the region from a passive margin of the Tethys Ocean into a non-metamorphic south-verging fold- and thrust belt (Castellarin et al., 1998). The NE part of the South Alpine, where the Dolomites are positioned, behaved as a rigid block (Indenter) during the compression of the Alpine orogenesis (Reiter et al., 2018). The Dolomites are described as an approx. 60 km wide Neogene pop-up structure in the South Alpine (Doglioni, 1987), which is approximately bounded by the S-verging Valsugana thrust to the SE, the Giudicarie fault to the W and the Periadriatic strike-slip fault to the N, which constitutes the border to the Austroalpine mega-unit of mainly crystalline metamorphic units (Bosellini, 1996; Brandner & Keim, 2011; Castellarin et al., 1998). At the NW edge of the Dolomites the permomesozioc cover of the Dolomites does not extend until the Periadriatic fault but terminates around the N-verging Villnöss (Funes) and Pikolein backthrusts (Curzi et al., 2023). North of them Variscan metamorphic basement is exposed. Due to this synclinorium structure of Neogene age, the low-grade Alpine metamorphic overprint and the relative small tectonic movements the Dolomites could preserve several structures almost in their original depositional geometries (Gianolla et al., 2008; Maurer, 2000).

The inherited Mesozoic architecture (normal faults and strike-slip zones, carbonate platforms to basins transitions) acted as inhomogenities to the Alpine orogeny, therefore some Mesozoic features might also have been reactivated or inverted (Doglioni, 2007). In Miocene age the Dolomites were exhumed (Keim, 2008) and were modelled out also during the Quaternary ice age, like the LGM (Würm glacial; Van Husen, 1987)

The most relevant tectonic and magmatic phases, which shaped the geological structures of the Dolomites and are controlling the present landscape were (Doglioni, 1987):

1. **Permian-Early Cretaceous E-W Rifting causing Extensional Tectonics and Magmatism**: Crustal extension (sinistral transtension) through rifting caused magmatism and volcanism in Lower Permian (Etschtaler Vulkanit-Gruppe), N - S-trending normal faults and intracontinental horst and graben zones (e.g. Trento Horst and Belluno Graben in Triassic-Jurassic; (Bosellini,

1967), which were repeatedly reactivated up into the Cretaceous (Brandner et al., 2007). Accordintg to Bosellini (1968) the Val Badia developed along a Jurassic N-S striking normal fault.

1.1. Middle Triassic (Anisian) E-W Extension: Transtensional or strike-slip tectonics caused differential subsidence, e.g. Göma Fault to the E of the study area (Doglioni, 1987; Broglio Loriga et al., 1990).

1.2. Middle Triassic (Ladinian) Volcanic Event: Volcanic eruptions partly interrupted the carbonate production and deposited volcanoclastic material into basins and sea straits around the dolomitic buildups (Bosellini, 1996; Gianolla et al., 2008).

2. Late Cretaceous to Miocene Alpine orogeny

2.1. Paleogene (mesoalpine) ENE-WSW Compression: The compression (dextral transpression) produced a thin-skinned thrust belt, marking the end of sedimentation that had persisted since the Early Permian (Doglioni, 1987; Doglioni, 2007).

2.2. Neogene (neoalpine) NNW-SSE Compression: The compression was accompanied by S-vergent folding and back-thrusting along the S-directed thrust faults (Doglioni, 1987).

2.2.2 Stratigraphy of the Dolomites

The stratigraphy of the Dolomites records a variety of events which indicates a polyphase history of tectonic and magmatic events, as well as sea transgression and regression cycles. During periods of tectonic activity through rifting (crustal extension) magmatic and volcanic activity is registered in the Dolomites, while in tectonic less active periods subsidence with following sea transgression were predominant, which caused the sedimentation of the characteristic carbonate platforms (Bosellini, 1996; Bosellini et al., 2003).

From a palaeogeographic perspective, the Dolomites were located on the W shelf of the Tethys during the Triassic, within a nearshore to shallow-marine environment characterized by numerous islands dissected by deeper sea straits and basins. Depending on the depositional setting (shallow marine vs. pelagic deeper marine) and the relative sea-level position (transgression vs. regression) different sedimentations occurred. On highstanding shallow marine zones biogenic carbonates were precipitated, while deeper marine environments experienced pelagic carbonate sedimentation with micritic carbonates, marls and clays (Mutschlechner, 1933; Fois, 1982; Bosellini, 1996; Keim, 2008; Gianolla et al., 2008).

Also, the characteristic landscape of today's Dolomites of white dolomite mountains sticking up above the hilly alpine meadows with underlying dark volcanoclastic sediments is the result of different sedimentation history between platform carbonate highlands and marine basins in Triassic times. The lithologies in the study area were all deposited in Triassic period.

2.2.2.1 Permian: Athesian Volcanic Group, Gröden- and Bellerophon - Formation

Permian rifting led to crustal thinning, the formation intracontinental basins (grabens or half-grabens) accommodated by normal faults and accompanied by widespread effusive and intrusive magmatism (Brandner et al., 2016; Cassinis et al., 2008; Morelli et al., 2012). The volcanic products of 285 - 275 Ma ago are summarized under the name Etschtaler Vulkanit-Gruppe or Athesian Volcanic Group, in the past denominated as Bozner Quarzporphyr (Stingl & Mair, 2005) and reach thicknesses until 3000 m (Bargossi et al., 2004) while spanning over an area of approximately 2000 km² between the Periadriatic fault in the NW and the Valsugana thrust in the SW (Bargossi et al., 2004). The volcanic products, mainly lavas and ignimbrites (pyroclastic flows) of mainly andesitic to rhyolitic composition, were deposited between 285 Ma - 274 Ma (Bargossi et al., 2004; Marocchi et al., 2008).

From the erosion of the Athesian Volcanic Group and subordinate the Variscan basement alluvial red bed sandstones and conglomerates of the Gröden-Formation sealed the Lower Permian graben system and therefore vary in thickness (Bosellini, 1996; Broglio Loriga et al., 1990; Gianolla et al., 2008; Massari & Neri, 1997). Just N of Peitlerkofel, at Würzjoch, a threefold division of a lower red part, a middle grey part, which is linked to a transgressive phase and an upper red part is possible (Baur, 2019).

The Bellerophon-Formation of the uppermost Permian shows the first progressively sea-level transgression of the Tethys from east to west. The depositional environment was first an arid coastal plain (flood peneplain) with lakes, sabkhas and lagoons and developed later into a shallow marine shelf. Therefore, the lithologies span from evaporites (sulphate evaporites, gypsum or anhydrite) to marly or dark dolomites, marlstones and limestones (Gianolla et al., 2008; Massari & Neri, 1997).

2.2.2.2 Early Triassic: Werfen - Formation and Anisian Tectonics (Peres-, Morbiac- and Contrin - Formation)

Continuous subsidence and the result of at least four transgression-regression cycles in the Lower Triassic led to the deposition of alternating shallow-marine carbonate and terrigenous sediments of the Werfen-Formation, with thicknesses reaching 400 m (Bosellini, 1996; Gianolla et al., 2008). The colorful and mainly finely bedded formation consists of marly limestones and dolomites, marls, silt- and sandstones and calcarenites, (Gianolla et al., 2008). The Werfen-Formation has been subdivided into nine subunits (members and horizons) based on the macroscopic lithostratigraphic characteristics (prevalent lithologies, color, strongly evident fossiliferous levels) (Bosellini, 1968; Farabegoli & Viel, 1982; Loriga et al., 1982; Broglio Loriga et al., 1990).

With the Mid Triassic (Anisian), a period of tectonic reorganization began, which is responsible for the present-day landscape of the Dolomites (Gianolla et al., 2008). Extensional (transtensional) tectonics associated with the breakup (rifting) of Pangaea (Broglio Loriga et al., 1990; Stingl & Mair, 2005), combined with block tilting (Brandner et al., 2016) led to differential evolution of the Dolomites. The eastern Dolomites subsidenced and experienced shallow marine conditions, while the western Dolomites W of Val Badia were uplifted, silted up and subaerial erosion began to act (Gianolla et al., 2008; Keim, 2008).

Worth to mention is hereby the Anisian Göma Fault. This N-S trending Normal Fault displaced the eastern part downwards, while the western part was uplifted and slightly tilted towards W ("Dorsale Badioto Gardenese" or "Gardena Ridge" after (Bosellini, 1968). This is the case for the study area, where the westwards tilting of the crustal block W of Göma Fault led to differential erosion of the Werfen-Fm. Through this erosional phase of the western Dolomites rocks of the upper and middle Werfen-Formation were eroded and fluvially deposited (Gianolla et al., 2008). The resulting reddish and component-supported conglomerate (Richthofen-Conglomerate), sand-and siltstones are summarized as the Peres-Formation and were deposited with a bigger or smaller erosional disconformity (hiatus) within the Werfen-Formation in the western Dolomites. Contrary in the eastern Dolomites (east of Göma Fault) the Werfen-Formation is complete and because of the continuing marine evolution in Lower- and Middle Anisisan age further successions like the Sarl-Dolomite or Dont-Formation deposited (see stratigraphic scheme in Bosellini (1996) or Broglio Loriga et al. (1990) (figure 9).

Renewed sea transgression through subsidence caused by the ongoing rifting brought marine environments also to the western Dolomites. Tectonic differential movements along crustal blocks (block tilting) led to differential subsidence and topographic differentiation subdividing the Dolomites into an articulated area of marine basins and sea straits, shallow marine islands and terrestrial plains (Brandner & Keim, 2011; Gianolla et al., 2008). Thus, a variety of depositional environments developed close to each other, which is recorded by the occurrence of different carbonate lithotypes.

In shallow sea environments (high zones) where subsidence was less extreme the Anisian carbonate platform was able to develop. First, the carbonates of the Morbiac-Formation mark the transition from terrigenous-coastal into a shallow marine (lagoonal) environment (Bosellini, 1996; Gianolla et al., 2008). Above the first biologically built reefs of the carbonate platform of the Contrin-Formation could deposit. The massive Contrin-Formation essentially consists of light grey massive dolomites and ranges from 30 m thickness in areas with little subsidence to a maximum of about 200 m (Gianolla et al., 2008). Due to its hardness, the

Contrin-Formation frequently forms a characteristic terrain step of 50 to 70 m recognizable at the base of the huge Triassic carbonate platforms in the western Dolomites (Bosellini, 1996; Bosellini et al., 2003).

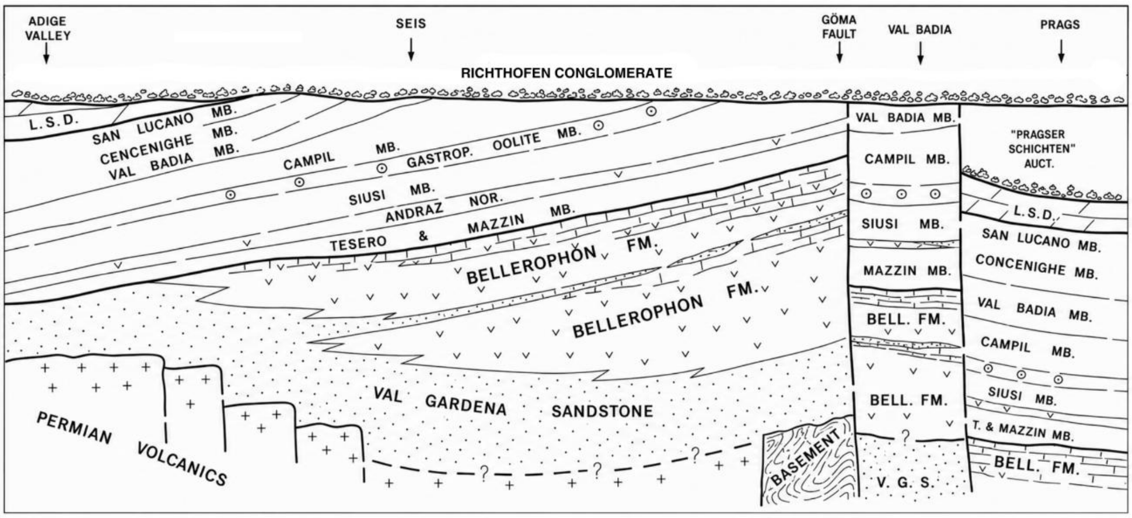

Figure 9: Stratigraphical setting of the Werfen-Formation after the Anisian tectonics from the Western Dolomites (left) and Eastern Dolomites (right). Vertical scale great-ly am-plified (modified after Broglio Loriga et al., 1990).

2.2.2.3 Ladinian: Pre-volcanic platform (Buchenstein-Formation, Schlerndolomite and Zoppé - Formation)

Between Anisian and Ladinian subsidence intensified, causing the Contrin Platform to tilt or break up into blocks. On the highest points of these blocks, reef-building organisms such as sponges, algae and the first calcareous corals could settle, forming the carbonate platform of the Schlerndolomite (pre-volcanic carbonate platforms of the Schlern-Group [Rosengarten-Formation]). Despite the progressive subsidence (about 800 - 1000 m in 3 - 4 Ma; (Bosellini et al., 2003; Brandner & Keim, 2011) the speed with which the reefs produced calcium carbonate kept pace with the rapidly rising relative sea level and resulted in a constant upwards growing reef aggradation (Brandner & Keim, 2011; Maurer, 2000). This development led to isolated platform carbonate buildups (reef and lagoon facies) divided by marine basins and sea straits. As the subsidence rate decreased in Upper Ladinian, the reefs expanded horizontally (reef progradation; Maurer, 2000). Reef progradation is proven by about 30 - 40° dipping reef slopes, so called clinoforms, reaching down towards the surrounding marine basins. The clinoforms were originally called “Überguss-Schichtung” (sensu Mojsisovics, 1879; Maurer, 2000). Parallel to the development of these reef islands (atolls) the basins experienced/recorded a much slower sedimentation history of 50-70 m over 3 Ma (Brandner & Keim, 2011). The basinal facies sediments of the Buchenstein-Formation are composed of thin stratified pelagic, cherty, dark micritic limestones and bituminous limestone laminites. Through the progradation of the Schlern-Dolomite the clinostratified reef slopes episodically shifted reef debris downwards towards the reef foot (distal reef slope, basin). Therefore, the cliniforms of the Schlerndolomite interfinger with the basin sediments of the Buchenstein-Formation (Fois, 1982; Brandner et al., 2007). Intercalated within the Buchenstein-Fm. thin volcanic tuff or ash layers (pyroclastic products), intensely green in color, called “Pietra Verde”, can be found.

Suddenly in the Upper Ladinian, siliciclastic, arkosic sediments coming from S of the Dolomites (Venetian foreland basin) were transported northwards by prograding turbidite lobes into the basins of the Dolomites. This Zoppé Sandstones exhibit turbiditic stratification and are composed of grey, arkosic siltites and pelites, alterned with dark marls (Viel, 1979; Gianolla et al., 2008). The Zoppé-Sandstone is characterized by volcanic clasts and clasts derived from the erosion of the metamorphic basement, indicated by phyllites, quartzites and mica components (Viel, 1979). These turbiditic sediments can be found nearly until the Pustertal Valley (Siorpaes et al., 2018). The Zoppé-Sandstone is the formation that is exposed is the source area of the mass movement.

2.2.2.4 Upper Ladinian Volcanic Event (Caotico Eterogeneo, Fernazza- and Wengen-Formation)

The Upper Ladinian volcanic event of regional scale partly interrupted the reef growth around 238 Ma ago. The eruptions developed mainly on sea floor but also basaltic dykes which cut through the carbonate reefs as well as collapse structures are observed in the Dolomites. Magmatic intrusions and eruption centers are exposed further south at Predazzo (Fassa valley; Bosellini, 1996; Gianolla et al., 2008). Effusive or pyroclastic products include pillow lavas, hyaloclastites, tuffs and volcanic breccias, which were spread across the western and southern Dolomites. These volcanic and volcanoclastic products of the Fernazza-Formation were mainly deposited in basins and partly deposited on top (onlap) of the riff slopes.

At the base of the Fernazza-Formation, through submarine mass movements due to volcanic eruptions, huge material deposits of chaotic and heterogeneous megabreccias accumulated in the marine basins (Caotico Eterogeneo, formerly called “agglomerates”). The Caotico Eterogeneo essentially consists of submarine megabreccias with coarse polymictic components and volcanoclastic matrix, locally with whole fragments (olistoliths) of the preceding formations (Buchenstein-, Contrin-Fm., Schlern-Dolomite or seldom Werfen-Fm.), which were literally torn out of their original position by the rising magma (Gianolla et al., 2008).

With the fading of the volcanic activity the volcanics of the Fernazza-Formation were eroded and resedimented as volcaniclastic material together with marine basin sediments. Close to the eruptive centers coarse volcanoclastics accumulated (Marmolada-Conglomerate), while further away finer volcanoclastic sediments deposited like the Wengen-Formation (Bosellini et al., 2003). The Wengen-Fm. comprises volcaniclastic Sand-Silt-or Claystones with carbonates and marls, which mainly sedimented as turbidites (Bosellini, 1996).

Between the Middle and Upper Triassic (Ladinian to Carnian age) subsidence decreased and volcanic activity stopped. The St. Cassian-Formation records the last depositions of the resedimented volcanoclastic material in the basins together with an increasing marl and carbonate amount (Bosellini, 1996). These three volcanoclastic formations (Fernazza-, Wengen and St. Cassian-Formation) filled up the Triassic basins and sea straits. Together with these formations the post-volcanic carbonate production (Schlern-Group [Rosszähne-Formation and Cassian-Dolomite]) prograded towards the basins leading to lateral facies interfingering with Wengen- and St. Cassian-Formation (Brandner & Gruber, 2019b).

At the beginning of the Upper Triassic (Carnian) the sea level sank. The western Dolomites silted up and experienced a terrigenous-fluvial sedimentation with siliciclastic and carbonatic material (sandstones and conglomerates) of the Raibl-Group. Above, the well stratified, m-thick banks of the Upper Carnian to Norian Hauptdolomit deposited and sealed the last topographic differences (Keim, 2008).

The stratigraphic overview ends with the Upper Triassic as the uppermost formation in the study area is the Schlern-Group. The Hauptdolomit constitutes the highest formation in the Western Dolomites and the Rhaetian and Jurassic successions were deposited only in the Eastern Dolomites were shallow marine conditions prevailed (e.g. Dachsteinkalk at Heiligkreuzkofel).

After the exhumation of the Dolomites, the development of the present-day relief was governed by selective erosion controlled by the geological framework inherited from the Triassic reef and basin landscape. This means that the basin sediments (Wengen and St. Cassian formations) were far more susceptible to weathering and erosion than the resistant reef bodies of the Schlerndolomite (Keim, 2008).

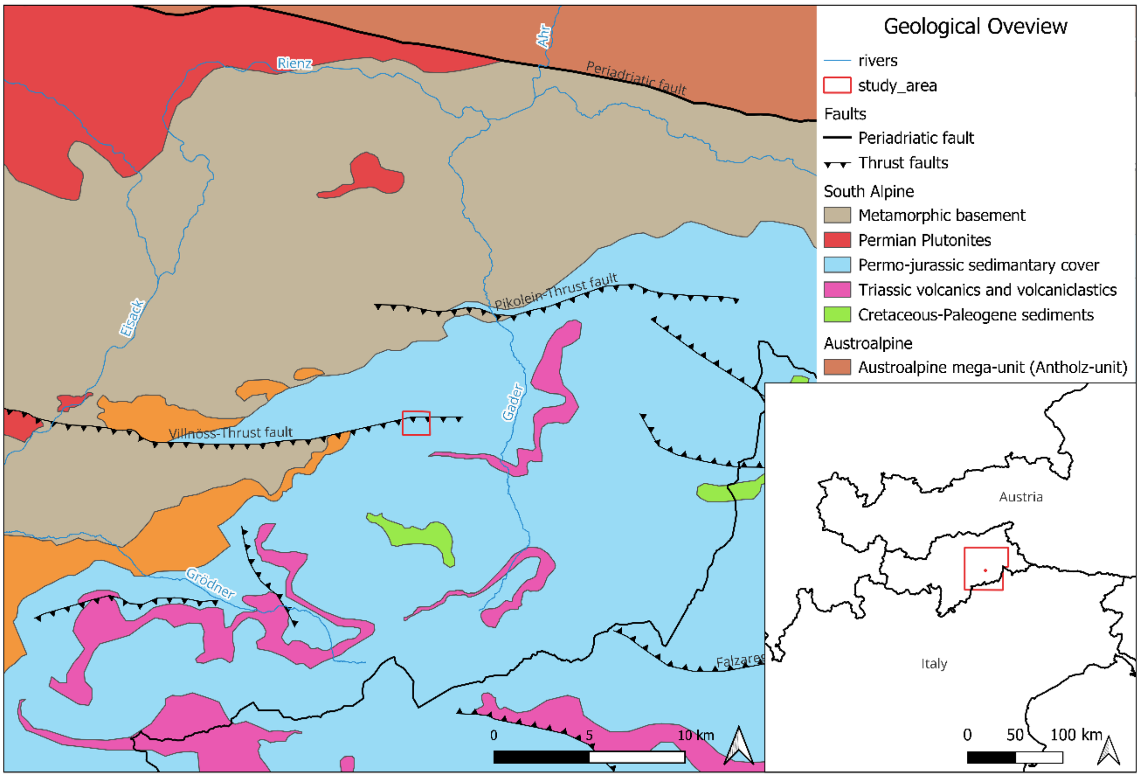

Figure 10: Geological Overview map of the surroundings of the study area (modified according to Office for Geology and Building Materials, Province of Bolzano).

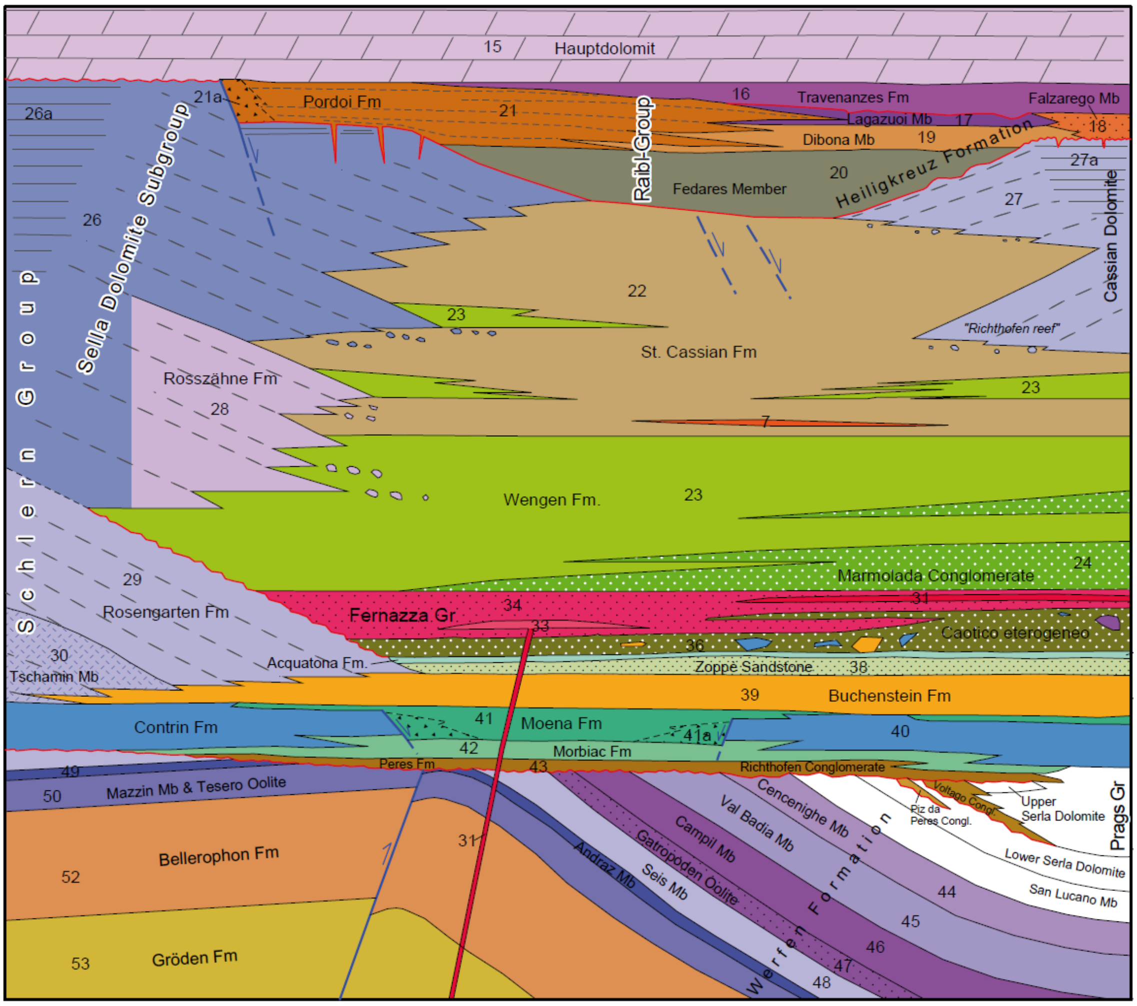

Figure 11: Stratigraphic scheme of the Permian to Upper Triassic succession of the Western Dolomites. Geological Map of South Tyrol, Western Dolomites, 1:25.000 (Brandner & Gruber, 2019a)

2.3 Meteorological Overview

Meteorological conditions, in particular precipitation, often act as the triggering factor of mass movements. Short extreme precipitation events, long-lasting precipitation or snow melt can destabilize in different ways the ground conditions and lead to mass movements. Water for example can enhance weathering, infiltrate in soil or debris material, increase the pore-water pressure or decrease the shear strength. When infiltration capacity is exceeded the resulting rapid overland flow (flashflood) potentially acts as transport medium to debris flows (Iverson, 2000).

Therefore, meteorological conditions need to be considered when investigating the triggering factors of mass movements. It is also important to differentiate between different meteorological events as they have different consequences on the ground conditions. The current climate change as well as climate projections indicate an increasing probability to hydro-geomorphic hazards in alpine terrain (Jemec Auflič et al., 2023). To better evaluate the role of meteorological factors a meteorological overview of the actual and future climate conditions is given here.

The mountainous topography of the Dolomites, exerts a decisive influence on its meteorological conditions, resulting in climatic differentiation from sub-Mediterranean conditions in valleys to nival environments in the highest elevations (Micheletti et al., 2010). Mountains function as orographic barriers to atmospheric circulation systems and induce deflection of frontal systems, thermal circulations, orographic wind uplift, precipitation enhancement on windward slopes and leeside drying as well as a pronounced tendency toward convective storm formation during summer (Micheletti et al., 2010; Zebisch et al., 2018)

Most of the precipitation in the Dolomites comes from the orographic uplift of southern air masses (low-pressure systems) originating from the Mediterranean Sea (Gulf of Genoa and Adriatic Sea; GeoSphere Austria et al., 2015)

Compared to other Alpine regions, the Dolomites exhibit moderate mean annual precipitation totals, typically around 700 to 1000 mm in the valleys and above 1000 mm on mountains (Zebisch et al., 2018). This pattern is characteristic of an inner-alpine climate with relatively low to average precipitation totals and marked seasonal variability driven by summer maximums due to convective precipitation events and relatively dry winters (Micheletti et al., 2010).

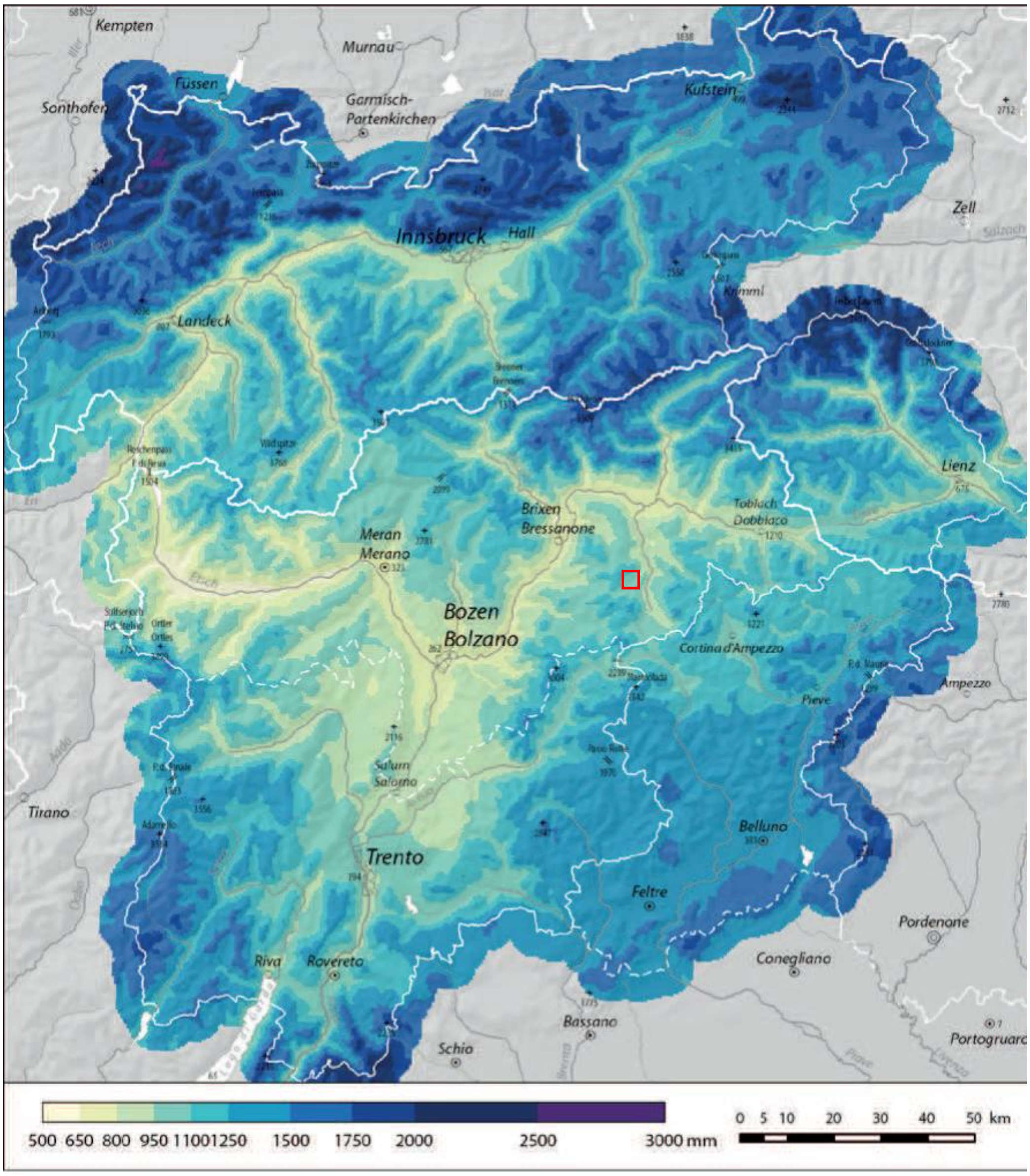

Figure 12: Mean annual precipitation in mm for Tyrol, South Tyrol, Trentino and Belluno (GeoSphere Austria et al., 2015). The figure shows altitude dependency of mean annual precipitation, so while in Val Badia the mean annual precipitation is around 700 - 1000 mm, at higher altitudes (subalpine or alpine level) values up to 1200 mm are usual. Study area is marked in red.

The Climate Change Monitoring of EURAC Research has analysed the climate developments of South Tyrol in the last decades. Following parameters are regarded as relevant with regard to mass movements (Niedrist et al., 2022):

1. Temperature increase of + 2,2 °C since 1980 for all South Tyrol.
2. Mean precipitation increase of + 38 % in winter and + 9 % in summer since 1981.
3. Heavy precipitation increase of one-day heavy precipitation events of +118 mm in 2024 compared to 1980, based on linear trend.

4. Above-average humid conditions in 2024 after Standardized Precipitation–Evapotranspiration Index (SPEI).

The consequences of these climate developments were for example:

- + 30 % discharge increase in winter.
- 77 % of the 2024 timber selection was classified as weather-related (extreme weather events), which is the consequence of the natural hazards in 2024.

Regarding the future climate development in the Dolomites and implications for mass movements, following relevant projected outlooks are outlined:

1. Temperature increase of approximately +2 °C to +4 °C by the end of the 21st century relative to pre-industrial levels (Zebisch et al., 2018). Rising temperatures will reduce snow cover duration and promote permafrost degradation in high-altitude areas (Zebisch et al., 2018).
2. Intensification of short-duration heavy precipitation events:
   Although annual precipitation remain uncertain and may change only moderately, increasing temperatures in the Dolomites enhance convective initiation, which may translate into more intense precipitation events. During intense precipitation events infiltration capacity is exceeded and/or pore-water pressures in debris material is raised, leading to rapid overland flow which can trigger debris flow initiation in alpine catchments (Micheletti et al., 2010).
3. Shift in seasonal precipitation patterns: As already observed in the last decade, summer precipitation will increasingly happen as intense precipitation events leading to strongly variable summer runoff. In winter enhanced precipitation and higher proportion of rainfall to snowfall under warmer conditions (rain-on-snow events), will result in an increased winter and spring discharge (Niedrist et al., 2022; Zebisch et al., 2018).

In order to quantify the meteorological conditions, in particular temperature, precipitation and snowmelt, as potentially triggering factors for the mass movement event, data time series from different meteorological stations from the Office for Meteorology and Avalanche Warning (Province of Bolzano) are statistically evaluated regarded their significance as potentially triggering factor (chapter 4.6).

3 Methods

3.1 Geodata sources

Geodata of the post-event (high resolution DTM and Ortophoto) from September 2024 was provided by the Office of Geology of the Province of Bolzano and was produced by the company ALTO DRONES. Geodata before the event was downloaded from the web GIS platform of the Province of Bolzano {Citation}, especially 2.5 m DTM of 2006, Ortophotos of the years 1999 to 2023 and different vector data (tab. 9).

Table 9: Geodata metadata and sources.

Data Type	Date	spatial resolution (grid spacing)	Source
Digital Terrain Model (DTM)			
DTM Peitlerkofel - Campill	2024	20 cm/pixel (0.2 m) 100 cm/pixel (1 m)	Laserscanner ALTO DRONES
DTM South Tyrol	2006	250 cm/pixel (2.5 m)	LiDAR Province of Bolzano - Office for Regional Planning and Cartography
DTM South Tyrol	2006 - 2026	100 cm/pixel (1 m)	New classification of 2006 pointcloud and production of 1 m DTM with CloudCompare
Orthophoto (OF)			
OF Peitlerkofel - Campill	2024	5 cm/pixel	Laserscanner ALTO DRONES
OF South Tyrol	2023, 2020, 2015, 2014, 2011, 2008, 2006,1999	20 cm /pixel (0.2 m)	Province of Bolzano - Office for Regional Planning and Cartography

The 0,5 m DTM from the Project Solar Tirol 2013 could not be used, as this DTM is restricted to the valley floors and terminates at the village of Seres.

Due to insufficient accuracy of the 2,5 m pre-event DTM of 2006 a new pre-event DTM with 1 m resolution was produced from the original pointcloud of 2006 of the Office for Cartography of the Province of Bolzano. This process is explained in chapter 4.3. Geomorphic Change Detection.

3.2 Geological Mapping, Stereoplots and Profiles

The extent of the geological map focused on the surrounding area of the mass movement, to the extent necessary to clearly identify the geological conditions. The mapping area extends from Mühlental in the SE (upper Seres fields) to the source area in the W, bounded in the N by the occurrence of post-volcanic Schlerndolomite of the Peitlerkofel and in the E up to the Peitlerkofel meadows (locality Fornates, behind the mass movements from the E slope of the Seres Valley) for a total of 1,4 km^2.

Before field mapping, literature research was focused on gathering relevant geological informations for the Western Dolomites, especially for the study area. The current geological map “Western Dolomites (Eastern Sheet)” does not cover the study area, its northern limit lies approximately 1 km south in the Bronsara Valley.
The first geological publication containing the study area is the Peitlerkofel map by G. Mutschlechner (Mutschlechner, 1933). The maps “Carta geologica delle Tre Venezie. M. Marmolada” (1930) and “Carta geologica foglio 11: Marmolada” (1969) have been carried out in a large scale of 1:100 000. For this thesis, Mutschlechner’s geological map proved useful, as it was produced at a smaller scale (1:25 000) and his descriptions refer to the area of the Peitlerkofel. Nevertheless, the stratigraphic nomenclature of the 1930’s was in some extent different from the current classification and therefore it was necessary to adapt it to the current stratigraphical subdivision. The thesis of Jesacher, 1999 (Jesacher, 1999) concentrated on the stratigraphic and tectonic description of the Peitlerkofel area. Another work with valuable informations was provided by Fois, 1982. Her study upon the margin development (interfingering) between the carbonate reefs and the basin sediments was crucial for the (paleo-)geolgical understanding of the study area.
By consulting the mentioned geologic maps, before starting with the field mapping, different aspects were noted:
(1) Peitlerkofel is built by Schlerndolomite with S dipping bedding (Mutschlechner, 1933).
(2) S of the study area the upper parts of the Puez Massif are constituted by the Upper Triassic Hauptdolomit, whereas (3) the massifs to the E of the Val Badia (Eastern Dolomites e.g. Heiligkreuzkofel) also record the deposition of the Uppermost Triassic Graukalk-Group (Dachsteinkalk) due to the more pronounced subsidence in the Eastern Dolomites (Bosellini, 1996).
(4) In the Bronsara valley, just S of the study area, an anticline structure is present (Jesacher, 1999). These Bronsara anticline exposes Bellerophon-Fm in its fold core and on the two valley sides opposing dipping directions occur. This structural geological feature is important as the study area is located on the N fold limb dipping with around 30 - 40° towards N.
Since the bedding at the Peitlerkofel is S, there has to be a syncline between the source area of the mass movement and the Peitlerkofel.

Field mapping was conducted with printed topographic basemap, ortophoto and slope map to identify outcrops for the outcrop mapping. Hammer and magnifier were used for closer inspection of the lithologies. Structural data (dip/dip direction, joints and fold axes) were acquired in the field using the FieldMove Clino mobile application. 10% hydrochloric acid (HCl) was used to differentiate between limestone and dolomite.
Around 150 outcrops were examined and documented in detail. After the outcrop mapping the formations and lithologies were interpolated into a complete geological map in QGIS Version 3.40.1 (QGIS Developement Team, 2024) and geomorphological features were mapped on a separate vector layer.

Structural Geological analyses in the stereonet were performed with Stereonet 11 (version 11.6.6) of 2025 (Allmendinger et al., 2011; Cardozo & Allmendinger, 2013).

Topographic and geological profiles were extrapolated in QGIS with the tools Terrain Profile, qProf and GeoProfile to get the topographic profiles and the geological intersections with the surface (by integrating the polygons of the Geologic Map). When integrating the measured structural data from the field (dip/dip direction) qProf and GeoProfile convert the true dip (α) to an apparent dip (β) regarding the horizontal angle between dip direction and profile line (δ), after following equation:

$$\beta = \arctan(\tan(\alpha) * \cos(\delta))$$

3.3 Geomorphic Change Detection

Geomorphic change detection aims to characterize the differences between pre- and post-event conditions. These analyses on DTMs are essential to determine where and when changes occurred, of which type and dimension. The presented following methods can serve as a workflow for post-event analysis to detect geomorphic changes utilizing QGIS (QGIS Developement Team, 2024), CloudCompare v. 2.13.2 (Girardeau-Montaut, 2023) and the Geomorphic Change Detection software GCD Standalone v. 7.5.0 (Bailey et al., 2020).

To better illustrate the geomorphic changes in the study area a Difference of DTM (DoD) is produced. A DoD quantifies the differences between pre-event DTM and post-event DTM and hereby identifies areas of surface elevation (deposition) and surface lowering (erosion). The challenge of geomorphic change detection is to only detect real geomorphic changes and minimize differences due to miss-alignments between the two DTMs. The prerequisite for producing a clean DoD, is that both DTMs have the same coordinate system and are perfectly superposable in areas where no change occurred (referred to as “stable areas”). If DTMs are not perfectly matching, Co-Registration tools can be used to align them and minimize the false geomorphic change signals (e.g. Nuth & Kääb, 2011; Scheffler et al., 2017). Common methodologies for Digital Elevation Model (DEM) co-registration encompass iterative, topography-based alignment algorithms - such as the classic Iterative Closest Point (ICP) algorithm (Besl & McKay, 1992) and the slope- and aspect-based Nuth-Kääb method (Nuth & Kääb, 2011) - as well as rigid transformations utilizing manual ground control points within georeferencing environments (e.g. QGIS) or automated image features as implemented in the GeoFolki framework (Plyer et al., 2015).

When inspecting the two source DTMs for producing the DoD two issues were noted, which led to the decision to create a new pre-event DTM with better resolution directly from the point cloud:

1. Different resolution: The old pre-event DTM of 2006 has a 2.5 m resolution (grid size) while the post-event DTM of 2024 has a 1 m resolution. This resolution difference leads to small (subpixel), false geomorphic chance signals in the DoD, as the 1 m DTM shows accurate surface details where the 2,5 m DTM linearly interpolates. This effect can be solved by resampling the 1 m DTM to a 2.5 m DTM, which results in a slight loss of surface detail, or by establishing a detection threshold (Level of Detection, short LoD) for the DoD visualization, so that only real geomorphic changes are shown.
2. Aspect-dependent elevation differences: When inspecting the initial DoD, aspect-dependent elevation differences were noted. Specifically, terrain surfaces on north- and east-facing slopes were systematically lower, while those on south- and west-facing slopes appeared slightly higher. The observed aspect-dependent elevation differences in the initial DoD are characteristic of horizontal co-registration offsets between the datasets. These artifacts likely stem from differences in flight geometry during acquisition and inconsistencies introduced during the post-processing and merging of the 2006 point cloud.

To avoid artificially biased results, the original point cloud of 2006 was requested at the Office for Regional Planning and Cartography (Amt für Landesplanung und Kartografie, Provinz Bozen). The point density of this point cloud is 0.82 points/m², which corresponds to an average point spacing of approx. 1,1 m (derived from the inverse square root relationship between density and spacing). For geomorphological analyses in mountainous terrain, this average point density is regarded as acceptable, as previous studies have shown that DTM accuracy remains relatively robust even at point densities of ~0.4 - 0.5 points/m² in steep, forested environments (Cățeanu & Ciubotaru, 2021) and interpolation distance for producing a 1 m DTM is constrained.

The provided point cloud was processed into a 1 m gridded DTM with Cloud Compare. To only choose the ground points (bare-earth surface) and exclude vegetation or buildings point class 2 was selected. These ground points were converted to a DTM with the “Rasterize too”. To fill empty cells interpolation method applied to fill gaps with a linear interpolated elevation. Then the grid was updated and exported as a raster file. Hereby a new pre-event DTM with 1 m resolution is created.

Georeferencing in QGIS is performed to better align the two DTMs and to get the horizontal displacements dX and dY (see table 17). These values are essential for establishing a detection or cut-off threshold named LoD (Level of Detection), which is set up for an accurate calculation of the real geomorphic volume changes. Georeferencing was performed using six ground control points (GCPs), while an additional six points were excluded from the transformation and used for independent accuracy assessment (check points). The GCPs were positioned on visible landmarks by consulting high resolution orthophotos of the province of 2023 (20 cm resolution) and the orthophoto of ALTO DRONES of 2024 (5 cm resolution; see table 9). Residual errors (dX, dY) were calculated for all points.

In order to get an estimation for the displacement in vertical direction (dZ), which is also needed for the LoD determination, a first DoD was produced by subtracting the post-event DTM of 2024 from the pre-event DTM of 2006 through the Raster Calculator in QGIS. Then areas where no geomorphic change occurred were delineated in a vector layer denominated as stable areas. Then the total average dZ from the DoD was calculated for all stable areas with the tools Zonal statistics and Basic statistics for fields.

With dX, dY from georeferencing and dZ from zonal statistics tool in QGIS, the LoD for the volume calculation in GCD Software can be calculated. The LoD is defined with standard error propagation theory (e.g. Brasington et al., 2003; Wheaton et al., 2010), accounting for both systematic error (mean μ) and random error (standard deviation σ):

$$LoD = \sqrt{(\mu_x + \sigma_x)^2 + (\mu_y + \sigma_y)^2 + (\mu_z + \sigma_z)^2}$$

For quantifying the volume of displaced material, e.g. erosion and deposition, the pre- and post-event DTMs are imported in the GCD Software in the field “DEM Surveys” as well as the desired investigation area, e.g. the Debris Flow vector layer, in the field “Masks -> Add Existing Area of Interest Mask”. When uploading the DTMs coordinate system and grid size should be the same, while the extent position (Top, Right, Bottom, Left) should be rounded to whole pixels until they become green. The calculations are started in the folder “Analyses -> Change Detection” and the prior calculated LoD for real geomorphic change has to be inserted. In the field “Area of Interest” it can be chosen if using the mask or not. After calculations tabular areal and volumetric results together with histograms are given out.

Finally, geomorphic changes are visualized through following methods (chapter 4.2):

- DoD Maps visualizing the elevation differences (erosion and deposition areas). The GCD is performed in the GCD Software and then imported to QGIS.
- GCD Histograms showing the amount of areal and volumetric erosion and deposition (outputs of GCD Software).
- Cross-sections along and across the channel with the pre-event vs. post-event profile lines. These cross-sections are created with the Profile tool in QGIS. Cross sections along the mass movement give indications at which angle the mass movement started and at which angle material was transported and deposited. Cross sections normal to the mass movement propagation direction visualize lateral differences of erosion and deposition.

3.4 Laboratory Tests

Geotechnical and geological laboratory tests were performed to characterize the lithologies and the residual soil at the source area as well as the debris flow material. The characterization of soil and rock aims to evaluate the material properties in terms of a geological predisposition for the mass movement.

At the source area 5 residual soil samples (2.2.; 3; 4.1.; 4.2. and 6) and 4 rock samples were taken (3 of Zoppé-Fm [3; 4.3. and 4.4.] and 1 of Schlerndolomite [2.1.]). In addition, one sample of 10 kg for the debris flow material was taken at the deposition area in the upper Seres fields and sample 7 from the Wengen-Fm. was taken at the eastern edge of the older Earth slump. For the debris flow sample the maximum collected grain size was boulder size.

The samples were analysed at the geotechnical laboratory of the Office of Geology of the Province of Bolzano, while Slake Durability and XRD were performed at the laboratory of the Institute of Applied Geosciences at TU Graz.

Table 10: Sample descriptions with sample no., material type (lithology) and locality.

Sample	Material type (lithology)	Locality & date
1.	Debris Flow Material	upper Seres fields (25.09.2024)
2.1.	Schlerndolomite sliding surface	source area, SE-slope (01.10.2025)
2.2.	Residual soil at Schlerndolomit sliding surface	source area, SE-slope (01.10.2025)
3.	Sandstone at sliding surface (light grey-greenish)	source area, SE-slope (25.09.2024)
4.1.	Zoppé-Sandstone, residual soil	Upper source area (07.05.2025)
4.2.	Zoppé-Sandstone, residual soil	Upper source area (07.05.2025)
4.3.	Zoppé-Sandstone competent bank	source area, NW-slope (01.10.2025)
4.4.	Zoppé-Sandstone, weak siltites between competent banks	source area, NW-slope (01.10.2025)
6.	Zoppé-Sandstone, residual soil	source area, NW-slope (2024 & 2025)
7.	volcanoclastic- carbonatic rocks (Wengen-Fm.?)	NE edge of Earth slump at E-slope of Seres valley (01.10.2025)

3.4.1 Grain size distribution

Grain size distribution of the debris flow material was performed according to norms: DIN EN ISO 17892-4, UNI EN 933-1 (sieving method), DIN 18123 (hydrometer analysis) and classified according to UNI EN ISO 14688-2.

Of the 10 kg in total, 2,665 kg (= 26,95 %) of fine-grained material (< 0,063 mm) was washed out and 7,305 kg were sieved. A representative part of the fine-grained material was taken for the sedimentation (hydrometer) analysis and extrapolated for the fine-grained portion.

During sampling different spots in the debris flow deposition zone were sampled to try to collect a representative sample of the debris flow material. Blocks over 10 cm in diameter were not collected, as it is anyway difficult to characterize the whole highly heterogeneous debris flow grain size distribution as blocks up to a few meters were transported. Therefore, the grain size distribution curve was normed without block grain size (> 63 mm) as it is common practice in debris flow studies (e.g. Bolliger et al., 2024) and suggested by ASTM D4718.

3.4.2 Slake Durability (SDT)

Slake Durability (SDT) is performed to characterize the resistance against weathering. This test method assigns quantitative durability index values to weak rocks. The test simulates natural weathering such as rainfall, drying and minor mechanical disturbance by wetting–drying cycles combined with abrasion in a rotating mesh drum. This test is especially relevant for engineering geological characterization of weak rocks with poor mechanical properties like mudstones, siltstones, marls or volcanoclastic rocks. The SDT was performed after the American Society for Testing and Materials (*ASTM D4644-16, n.d.*) and the DGGT Recommendation No. 20 (Herzel, 2002).

The test procedure involves the preparation of 10 roughly equidimensional rock pieces, each 40 - 60 g (total mass 450 - 550 g). After oven drying at 105°C until constant mass is reached (12 - 16 h) the pieces are rotated at 20 rpm (revolutions per minute) for 10 minutes in a partially submerged mesh drum, filled with 20°C water until 20 mm below the drum axis.

Afterwards the material in the drum is re-dried and the mass is measured to complete the first cycle. After the second cycle the slake durability index SDI2 is calculated as a mass percentage difference.

According to the DGGT Recommendation No. 20, up to six cycles are performed on the material. The result can be evaluated through the classifications of Gamble (Gamble, 1971).

Gamble (1971)	
SDI_2 (%)	**Classification**
> 98	Verh high
98 - 95	High
95 - 85	Medium High
85 - 60	Medium
60 - 30	Low
< 30	Very low

SDI_2 classifications after Gamble (1971).

3.4.3 Liquid and Plastic Limits

The determination of liquid limit (LL) and plastic limit (PL) of the fine-grainde part of the residual soil of the source area were performed after standard EN ISO 17892-12 with EN ISO 17892-6 for the fall cone penetration of the liquid limit (LL). For every sample the PL was determined through the mean of five subsamples and the LL through the linear regression of five differently saturated subsamples and the water content reading at 20 mm cone penetration. The Plasticity Index (PI) representing the range of plastic behavior is calculated as $PI = LL - PL$ and the Liquidity Index (LI), which indicates the current soil state relative to limits (solid / plastic / liquid; figure 13) is calculated as $LI = \frac{w - PL}{PI}$. Consistency Index (CI) is $CI = \frac{LL - w}{PI} = 1 - LI$.

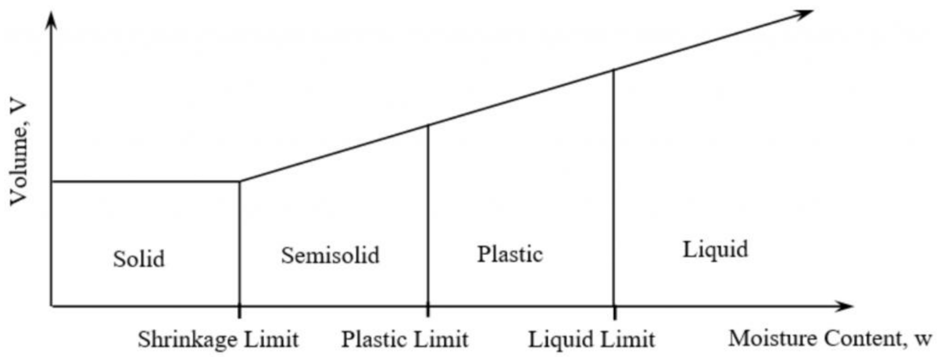

Figure 13: Qualitative positions of Atterberg limits relative to moisture content (EN ISO 17892-12)

These fine-grained soil parameters together with their classification tables help to characterize the soil properties (*ASTM D2487-17*, n.d; Holtz & Kovacs, 1981).

Table 11: The degree of plasticity based on the plasticity index (PI) can be classified into non-, low-, medium-, high-, and very high plasticity ranges (Holtz & Kovacs, 1981).

PI	Degree of Plasticity
0 - 4	Non/Very low
4 - 7	Low
7 - 17	Medium
17 - 35	High
> 35	Very high

3.4.4 Water content

Water content was measured after one of the field inspections. This samples were taken at moist conditions in the source area. Sample 6 was taken from residual soil at NW flank of the source area (about 45° steep) while it was slowly failing in some cm-dm big soil fragments towards the gully.

3.4.5 Mineralogy (XRD Analysis)

The X-Ray Diffractometry (XRD) semiquantitatively identifies the mineral phases from powder of the samples. To measure minerals of the mica-, chlorite-, smectite-, and kaolinite group, samples were prepared with ion exchange with potassium and magnesium and on ceramic plates. Identification of clay minerals is based on expansion characteristics following solvation with glycerine and dimethylsulfoxide.

The used equipment of the IAG laboratory at TU Graz were a Diffractometer Panalytical XPert (Co-tube), Philips PW 1830 (Cu-tube) and the Panalytical Highscore Plus Software.

The procedure was carried out after Recommendation No. 25 of the Commission on Rock Testing of the Deutsche Gesellschaft für Geotechnik e. V. and ON B 4810.

3.5 Slope stability analysis

Slope stability analyses were carried out using the GEO5 geotechnical software package (Fine Software, version 2024), applying 2D limit equilibrium methods (resisting vs. driving forces). The analyses were performed with the Janbu method of slices implemented in GEO5. It satisfies force equilibrium and moment equilibrium and supports both non-circular (polygonal) and circular sliding surface.

The slope geometry was defined in a 2D cross section and material properties were assigned to individual soil or rock layers according to site investigation data (without EC7 partial factors).

In the Janbu Simplified Method the slope mass above a trial slip surface is divided into vertical slices. For each slice following forces act:

- Weight W_i
- Normal force on the base N_i
- Shear resistance on the base τ_i
- Driving shear force due to weight and geometry

For each slice:

- Driving force: $W_i * \sin(\alpha_i)$
- Resisting force: $c' * b_i * N_i * \tan(\varphi)$

GEO5 applies the Mohr - Coulomb (shear strength) failure criterion on the base of each slice: $\tau_i = c' + \sigma' * \tan(\varphi)$

where:

- c' = effective cohesion [kN/m^2 = kPa]
- φ = effective friction angle [°]
- σ' = effective normal stress [kN/m^2 = kPa]
- α = slope angle [°]
- b = brightness of slice

In case of groundwater, the normal effective stress is reduced by the pore water pressure. Finally, the global Factor of Safety (FOS) is computed from force equilibrium.

The potential failure mechanism was modelled using a polygonal failure surface, which permits a realistic representation of translational or composite slide surfaces. With the calculation option “optimization” the software automatically searches the critical failure surface by systematically generating and evaluating multiple potential slip surfaces within a predefined search domain. The surface associated with the minimum FOS is identified as the critical failure surface. This optimized search reduces subjectivity compared to manually defined slip surfaces and ensures that the most unfavourable stability conditions are captured.

The analyses were performed on two profiles. The first profile concerns the source area of the mass movement, named “Profile: Col Ciancidel”. Here different scenarios were analysed to try to reconstruct the stability conditions and possible starting mechanisms at the source area. The second slope stability analysis was performed on the Earth slump - Earth flow. Here the question was if reactivation through future Seres creek incision at the foot is possible.

The profiles were exported from QGIS in dxf. files which contain x and y coordinates of every point. In Geo5 the profile was simplified redrawn.

3.6 Analysis of Meteorological Data

The analysis of Meteorological data aims to statistically quantify the significance of precipitation as well as the meltwater as potentially triggering factors for the mass movement event. Together with discharge data from a hydrograph of the superordinate Val Badia catchment area the significancy of water in the catchment area is checked.

Meteorological time series data was downloaded from the closest meteorological stations from the Office for Meteorology and Avalanche Warning of the Province of Bolzano. Discharge data from the Office for Hydrology and Dam Facilities was downloaded from the Meteo Browser South Tyrol (Meteo Browser Südtirol).

The closest meteorological stations where precipitation, temperature and snow height data were taken are the stations of St. Martin in Thurn and Campill Kreuzkofeljoch (see table 12). Since the source area of the mass movement is at ~ 2000 m.s.l., it is preferable to use meteorological data recorded at similar altitude, as weather conditions in the valley might differ, e.g. thermal inversion in winter. Therefore temperature [°C] and snow height [cm] records were taken from Campill Kreuzkofeljoch meteorological station at 2295 m.s.l. as it is the closest to the study area (see table 11) and is positioned at similar alpine-subalpine altitude zone, reflecting mountainous climate conditions. Precipitation [mm] is not recorded at Campill Kreuzkofeljoch but at St. Martin i. T. and St. Peter in Villnöss.

Meteorological data was compared with other stations in the area (Seiser Alm Zallinger, Abtei Piz La Ila, Corvara and Stern) to (1) check for data correlations, (2) compare with longer time series and (3) possible errors, as the open-source data from the Meteo Browser is raw measurement data. In general, very good data correlation with other stations was determined (see tables 12, 13 and 14). Incorrect or missing values were not filled but left empty.

Table 12: metadata of meteorological stations: coordinates, elevation, linear distance from source area and direction, precipitation and snow height recording time span.

Meteorological stations	Coordinates [WGS84]	Elevation [m.a.s.]	Distance & orient. from source area [km - orient.]	Precipi-tation	Snow height
Kreuzkofeljoch	46.637689; 11.812249	2295	1,3 km to WSW	-	Sept. 2022
St. Martin	46.679181; 11.897935	1152	7 km to NE	1981	-
Villnöss	46.647927; 11.689372	1325	11 km to W	2022	-
Seise Alm	46.511879; 11.688789	2050	18 km to SW	2014	Aug. 2014
Abtei Piz La Ila	46.564962; 11.903624	1997	10 km to SE	-	Aug. 2014

3.6.1 Precipitation

Precipitation [mm] is taken from St. Martin meteorological station as it has a much longer timeline back to 1921, while the meteorological station of Villnöss records back only until 2022. Precipitation is measured using heated pluviometers with either a tipping-bucket mechanism or a weighing principle (pers. comm. M. Pernter, Office for Meteorology). Comparing the two stations shows medium-good correlation of the datasets, capturing the same precipitation events with similar amounts and exhibiting close annual totals. That means that both stations record relevant precipitation data for the study area. Finally, it was chosen to take the data from St. Martin due to the longer recording history, which enables statistical analysis.

The station of St. Martin exhibits daily precipitation data from 1981 and monthly and annual precipitation data from 1921. Monthly and annual data were used to evaluate the significance in the long-term calculating monthly and annual mean, 90-percentile, as well as periodical amounts of 6 months and 3 months of the first-year half, regarded as relevant historical time references for accounting the statistical relevance regarding the triggering of the mass movement. For the years

1978, 2009 - 2011 no data was recorded. The daily data was used to evaluate the mid- and short-term precipitation distribution of 2024 some weeks before the event.

For the precipitation analysis the raw data from St. Martin is used without accounting any precipitation correction for the conditions at the source area at 2000 m a.s.l.. This precipitation corrections of increased precipitation related to orographic uplift are usually done by applying precipitation gradients, which have to be established by two stations which lay relatively close to each other. For the alpine regions precipitation gradients typically exhibit values around 5 - 10 % increase per 100 meters of elevation gain (Beniston, 2006; Daly et al., 1994; Sevruk, 1997). Since this gradient varies depending on local climate (season, humidity) and topographic effects, for the reconstruction of precipitation in the study area, it would be preferrable to establish a local gradient from St. Martin station. For the study area this correction could have only been done with the Seiser Alm station (2050 m a.s.l.), which is one of the few stations in South Tyrol recording precipitation at alpine level. For the observed 10-year period (2014 - 2024) about 26 % more precipitation on average fell at Seiser Alm. This would correspond to a gradient of + 27 mm / 100 m elevation gain, which is equivalent to + 2,9 % / 100 m elevation gain. As mentioned before this correction is not used for reasons of straightforward reproducibility and comparability, and due to the distance of 18 km microclimatic differences can´t be fully excluded. Still this gradient could be used to approximate for instance the annual precipitation in the study area.

Table 13: Precipitation correlations between the stations St. Martin, Villnöss and Seiser Alm.

Precipitation	Villnöss	Seiser Alm
St. Martin	0,77	0,79
Villnöss		0,89

3.6.2 Temperature

Temperature data is of relevance to (1) account the thermal differences (daily or seasonal), (2) to check if freezing-thaw cycles (physical weathering) occur, (3) if precipitation falls as snow or rain and (4) to calculate the daily Snow Water Equivalent (SWE). Air temperature is recorded using electronic sensors.

Mean daily temperature was taken from Kreuzkofeljoch station, which is regarded as representative for the study area as is positioned only 1.3 km far and 250 m higher. Temperature at Kreuzkofeljoch shows high correlation of 0,92 with St. Martin, indicating almost equivalent temperature shifts, except for the winter period, where thermal inversion plays a role.

Table 14:Temperature correlations between Kreuzkofeljoch, St. Martin, Villnöss and Seiser Alm.

Temperature	Villnöss	Seiser Alm	Kreuzkofel
St Martin	0,97	0,93	0,92
Villnöss		0,97	0,96
Seiser Alm			0,99

3.6.3 Snow height

Snow height is recorded at Kreuzkofeljoch meteorological station and is used to identify the time of snow melt in the study area and calculate the Snow Water Equivalent (SWE). To check the accuracy of the snow height measurements the snow height of other two meteorological station in the region, namely Seiser Alm Zallinger (2050 m.a.s.l.) and Abtei Piz La Ila (1997 m.a.s.l.) were checked and showed good correlation in capturing the same snow fall events and thus recording really similar snow heights (table 15).

Table 15: Snow height correlations for period winter and spring 2024 (01.12 2023 - 01.05. 2024)

Snow Height	Abtei Piz La Ila	Seiser Alm
Kreuzkofel	0,93	0,88
Abtei Piz La Ila		0,97

Snow depth at Kreuzkofeljoch is measured using an ultrasonic time-of-flight method (pers. communication M. Pernter, Office for Meteorology, Province of Bolzano). In the absence of a snow cover, vegetation can significantly affect the measurements and is a major contributor to the “noise” observed in the summer.

The total SWE is calculated with following formula:

$$SWE = D * \frac{\rho_s}{\rho_w}$$

Where:

- D = snow depth (m)
- ρ_s= snow density (…kg/m³)
- ρ_w = water density (≈ 1000 kg/m³)

Snow density was estimated with a conservative value for spring snow of 300 kg/m^3 (= 0,3 g/cm^3; see table 16). In case of snowfall events during the snow melt period (defined by decreasing snow height trend), these are added with their snow height and an assumed snow density of 50 kg/m^3 for typical fresh snow.

Table 16: Snow densities for alpine snowpacks (Jonas et al., 2009; Pistocchi, 2016).

Snow condition	**Typical density [kg/m³]**
Fresh cold snow	50 - 120
Settled mid-winter Alpine snow	150 - 300
Spring / melt-phase snow	300 - 500

3.6.4 Discharge

Another parameter indicating moist or wet conditions can be retrieved from 4discharge measurements taken at gauging stations. The closest gauging station measuring discharge is in Montal, at the end of Val Badia and records the whole Badia river (german Gaderbach) catchment area (384 km^2), which is much bigger than the catchment of the Seres creek at the study area (3,5 km^2). The discharge graph (hydrograph) gives indications on how the catchment reacts to seasonal variations like winter baseflow, spring meltwater and heavy summer precipitations. From a hydrograph two flow components can be derived, namely the (1) Baseflow and the (2) Overland flow. The baseflow of a hydrograph represents the water component which arrives with some delay to the stream network and the measuring station as it infiltrates in the ground (groundwater) before reaching the stream network. Therefore, the baseflow component can be regarded as a rough approximation of the soil saturation in the catchment.

3.7 Conceptual Ground Behaviour Model

A Conceptual Ground Behaviour Model (CGBM) is a qualitative to semi-quantitative representation of the geological system that describes how ground conditions control mass movement processes (Baynes & Parry, 2024). Conceptual models are widely used in engineering geology to synthesize complex datasets into a simplified, interpretable framework that captures the spatial variability and process interactions within a slope system (Giles, 2013). A CGBM describes the materials, structures, processes and mechanisms controlling ground deformation or failure. For landslides and related processes, the CGBM explains (1) the ground conditions and (2) which failure mechanisms can happen according to (3) the different triggering mechanisms. Therefore, predisposing factors (geological and geomorphological properties) and triggering factors (meteorologic or anthropologic events) are typically integrated.

The Conceptual Ground Behavior Model in this study is a simple conceptual and descriptive interpretation of the slope conditions and how this slope system behaves at certain hydro-meteorologic events. It integrates the gathered geological, geomorphological and geotechnical field observations of the study area together with regional insights from mass movement literature of the Val Badia region.

The aim is to give a general outline on which slope processes develop at which geological conditions and triggering events. Further this model can serve as a general basis for landslide susceptibility mapping, hazard assessment or numerical modelling.

4 Results

The detachment of the mass movement near Campill was primarly controlled by (1) geological, (2) geomorphological, (3) structural geological, (4) hydrogeological and (5) meteorological factors. The presentation of the different type of results aim to characterize and evaluate the different processes in order to discuss the role of the different factors (predisposing or triggering factors) within the Ground Behaviour Model (chapter 6.3)

4.1 Geological Model

A geological model constitutes the first essential step for an extensive mass movement analysis, as the detachment of the mass movement was controlled by (1) geological factors, like the competence difference of the stratigraphic sequences (lithologies) and (2) structural geological factors like the orientations of bedding planes due to a large anticlinal structure. This geological model was produced by merging geological, structural geological and geomorphological field observations and data of the study area together with relevant regional geological information's from the literature.

Chapter 4.1.1. Geological Mapping summarizes the essential lithological characteristics of the formations and lithologies encountered within the study area, as the geologic conditions seem to have played a crucial role in the activation of the mass movement. This lithostratigraphic or geological characterizations are essential, firstly for the reader to recognize the described formations and lithologies in the field and secondly because lithologic properties such as strength, mineralogical composition, weatherability, bedding surfaces or joints constitute important first criteria when assessing weathering behaviour or stability of certain lithologies or finally to assess susceptibility or hazards for mass movements.

Chapter 4.1.2. Geological Profiles visualizes the geological formations and geometries in 2D to better visualize the geological conditions in the source area, which favoured the development of the mass movement.

Chapter 4.1.3. Structural Geological Analyses complements the tectonic and neotectonic background of the Dolomites with relevant structural geological observations from the field and from relevant literature.

4.1.1 Geological Mapping

Stratigraphically speaking, the study area ranges between the Bellerophon Formation and the post volcanic Schlern-Group, which were deposited between Upper Permian to Middle Triassic epoch.

In the study area the stratigraphic subdivision between these formations of mainly carbonatic and volcanoclastic lithologies becomes somewhat complex, as several formations occur within meter-scale intervals, due to the thin stratigraphic successions and the lateral interfingering between slope carbonates and deeper marine basin carbonates as well as turbiditic and volcanoclastic sediments. This complex Triassic evolutionary history is exposed in the study area.

After the mapping the Triassic palaeogeographical position of the source area is interpreted to have been a transitional position at the distal slope where slope carbonates (debris and megabreccias) from the prograding Peitlerkofel reef prograded (Schlerndolomite) onto the basinal carbonates and marls (Buchenstein-Fm.) and were later covered by turbiditic sedimentation (Zoppé-Sandstone) and resedimented volcanoclastic material (Caotico Eterogeneo and Wengen-Fm.).

4.1.1.1 Bellerophon - Formation

The shallow marine sediments of the Bellerophon-Formation of Upper Permian epoch is only exposed in the SE of the study area. Especially one huge outcrop NW of the Seres village, described in more detail by Baur (Baur, 2019), allowed a more detailed view on this formation. The lower part (Fiammazza facies) with evaporitic sequences (gypsum, anhydrite) and dark dolomite banks is not exposed in the study area but is reported W of Misci at the beginning of Bronsara valley (Mutschlechner, 1933; Jesacher, 1999). In the study area only the upper part (Badiota facies), composed of well bedded dark grey and strongly bituminous smelling limestone, which weathers in light grey color is exposed. In between thin marl layers could be observed in the field (figure 13). The limestone banks are mostly dm-thick, sometimes slightly dolomitized and lack of macroscopic visible fossils. The name-giving index fossil, the gastropod Bellerophon, could not be found.

The dark limestones are permeated by white calcite veins and geodes, as well as stylolites. The limestones weather with a rough surface and grey to brown color and exhibit a splintery breaking. At the transition with the Werfen-Formation the thin marl layers occur with more frequency. The microfossils in the Badiota facies are mostly foraminifers and calcareous algae, thus the lithologies can be classified as Pack-and Wackestones after (Dunham, 1962) classification.

From a tectonic point of view the lower part of the Bellerophon-Formation (Fiammazza facies) is described as a sliding-horizon, because of the rheological softer properties of these layers which allows tectonic deformations (strain) to localize (Mutschlechner, 1933). In fact, many folds were observed in the Fiammazza facies all over the Dolomites, as in Bronsara valley (Jesacher, 1999).

Figure 14: a) Outcrop NW of Seres hamlet (denominated as “Seres Profile” in Baur, 2019) of the upper Bellerophon-Formation (Badiota facies) composed of 1 - 2 dm-thick limestone banks and thin, easier weathering marl layers in between. b) bituminous limestone W of Seres creek.

4.1.1.2 Werfen - Formation

The Werfen-Formation of Lower Triassic period is characterized by colorful sequences, depending on whether carbonate (limestone, dolomite and marls) or fine-grained siliciclastic sediments are predominant, which reflect transgression or regression phases. In comparison to the Bellerophon-Formation the Werfen-Formation is containing much more marl layers and smells less bituminous. In the study area, through the Anisian erosional phase, all members above the Seis member were eroded. E of Seres creek the Werfen-Formation appears to be only about 30 - 35 m thick constituting the lower Tesesro-, Mazzin- and Andraz-Members, while in the W the formation seems to slightly thicken as the Seis-Member is lensing in, which is confirmed by the appearance of many bivalve fossil imprints, especially the index fossil of the genus Claraia, confirms (fig. 15d).

The first member, the Tesero-Oolite, is about 2 - 3 m thick and was recognized by its typical composition of small, rounded calcium carbonate components known as ooids. These limestones display distinct bedding surfaces and are generally somewhat lighter in colour (white to light grey) compared to the dark limestones of the Bellerophon-Formation. The mainly oolithic grainstone is mostly dm-thick banked. Towards the Mazzin-Member the oolithic content decreases, whereas the marl content increases (Jesacher, 1999). On the W side of Seres creek a fold could be observed with measured fold axis (plunge: 08 / azimuth: 082).

The Mazzin-Member is composed of light grey to grey, thin-layered limestone and marl layers. Characteristic is the apparent bimodal distribution of layer thickness: some parts are dm-thick layered, while other parts are cm-thin layered. Characteristic of the Mazzin Member are the recurrent shell and tempestite layers. The Mazzin Member is about 20 m thick and after (Dunham, 1962)classification is mainly composed of mudstone and wackestone.

The Andraz-Member can be recognized by the thinly layered ochre to yellow and red coloured (dolomitic) marl and limestone layers, occasionally perlites or fine sandstones occur. This about 5 m thick member has higher terrigenous input, expressed by higher marl content, because of its peritidal/intertidal deposition environment during a regression phase (Gianolla et al., 2008). It was observed on the E of Seres creek, but not at the W.

The Seis-Member was observed lensing in at the W of the Seres creek. Lithologies are mostly well-bedded marly limestones and micrite layers. The typical weathering colour is yellow ochre. At the outcrop the beds displayed a similar thickness of about 5 - 10 cm, with distinctive boundaries between the beds. Also here shell and tempestite layers occur repeatedly. From a paleontological perspective the layers bear many fossils but usually consist of a single species or genus. Typical features of the Seis-Member in the study area are the Clarai clarai and Clarai aurita bivalves and bioturbation marks. Sediment structures like wave ripples could be observed in some bedding surfaces laying below the outcrop of the Seis-Member (fig. 15f).

The lensing in of the Seis-Member is probably attributable to Anisian block tilting tectonics and the erosional event (Jesacher, 1999). This led to differential erosion of the Werfen-Formation in the Western Dolomites, which is reflected also in the study area as the eastern part eroded until the Andraz Horizon (orographic left), while the western part preserved the Seis-Member and the Gastropod-Oolite further west. Therefore, the upper Werfen-Formation is missing in the study area and display a stratigraphic hiatus (erosional disconformity), which is observed with different extensions in the Western Dolomites.

Between the Werfen-Fm. and the Contrin-Fm. the stratigrphy results different regarding to the typical stratigraphic succession:

The Peres-Formation with its typical Richthofen-Conglomerates, which mostly follow the Werfen-Formation in the Dolomites was not observed. This situation is represented in the western part of the stratigraphic scheme (Brandner & Gruber, 2019a). According to Baur (2019) the Richthofen-Conglomerate is exposed about 6 m thick at an outcrop NW of Seres village, some hundred meters E of the study area. This would mean that the Richthofen-Conglomerate lenses out between Seres valley and Seres village.

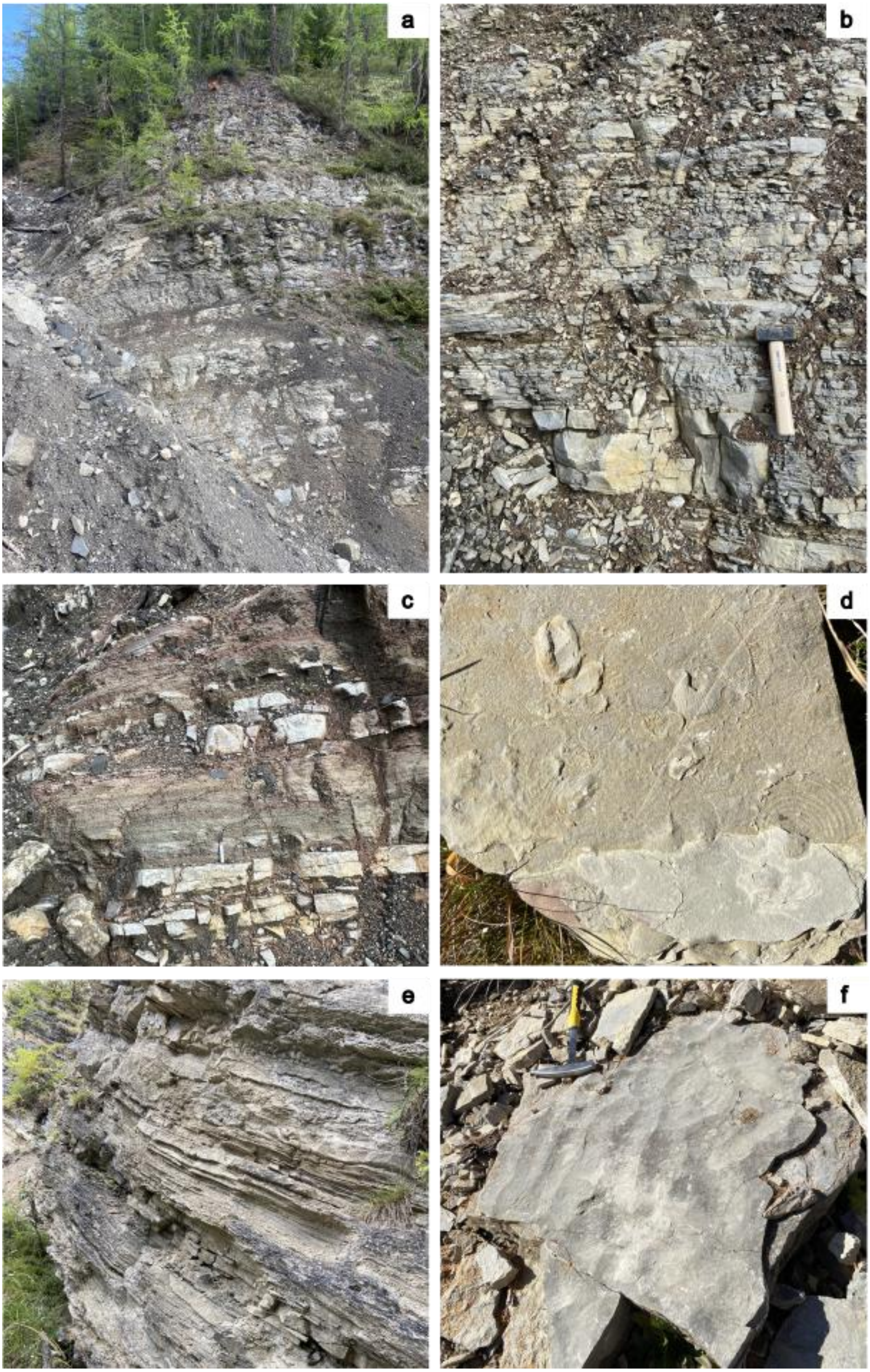
a
b
c
d
e
f

Figure 15: Outcrops of the Werfen-Formation. a) Mazzin-Member on the E side of Seres valley. b) Mazzin-Member close-up view. c) Andratz-Member with typical yellowish colors at the base and reddish tones on top. d) Claraia clarai bivalves from the Seis-Member. e) outcrop of Seis-Member W of Seres creek. f) Wave ripples on bedding surface of Seis-Member.

4.1.1.3 Morbiac - Formation

The Morbiac-Formation was observed on both sides of the Seres creek. With the missing of the Peres-Formation in the study area it is the Morbiac-Formation to cover the Anisian erosional disconformity to the Werfen-Formation. The Morbiac-Formation was deposited under renewed subsiding conditions (transgression) in a shallow lagoonal or coastal environment (De Zanche et al., 1992; Masetti & Neri, 1980). At the outcrop on the E side of the Seres creek the Morbiac-Formation exhibits well-layered, grey to dark, silty-marly, micritic limestones. In the lower part the marl content is more common due to terrigenous input. Compared to the Andratz-Member the footwall of the Morbiac-Formation seems to have a slightly flatter dipping angle (around 5° difference). The outcrop on the W side of Seres creek shows the characteristic nodular bituminous limestones (packstones and wackstones). Here the bedding in cm- to dm-range is often laminated and has a nodular appearance due to intense bioturbation (Gianolla et al., 2008). Between the nodular bituminous layers thin marly limestone layers of maximum 10 cm exhibit reddish-greenish color. Sometimes the bedding is obliterated by the intense bioturbation resulting in amalgamated beds of several dm.

As also observed by Baur (Baur, 2019) the uppermost part of the Morbiac-Formation is composed of red marly limestones, which were only found on the W side and are overlain by the Contrin-Formation. In total the formation is about 10 m thick E of Seres creek and seems to thicken out towards the W. The differential out lensing of Peres-Fm. and Morbiac-Fm. was also reported in the western part of the stratigraphic scheme of the map of the Western Dolomites (Eastern part; fig. 11)

4.1.1.4 Contrin - Formation

The dolomites of the Contrin-Formation were clearly identifiable due to their relative compact and massive appearance and their light crystalline white to light grey color (figure 16). These dolomites create a steep wall and a morphological step in the landscape and typically form a base platform over which the large Ladinian carbonate platforms arise. The primary stratification of the limestone is not observable in the study area because of the dolomitization, which makes this formation more weathering resistant. Orographic right of the Seres creek the Contrin dolomites seem to be thicker (around 60-80 m) than on the left (around 30-40 m).

Figure 16: Morbiac-Formation left (a and c) and Contrin-Formation right (b and d). a) outcrop of Morbiac-Formation W of Seres creek with cm-dm stratified, partly nodular strata and an about 0,5 m thick bed with obliterated stratification due to strong bioturbation. b) Dolomite cliffs of the Contrin-Formation W of Seres creek. c) nodular limestone of Morbiac-Formation with white chert. d) Contrin-Dolomite with porous structure.

4.1.1.5 Buchenstein - Formation

The Buchenstein-Formation can be distinguished through their characteristic appearance of good, generally 5 to 20 cm thick stratified limestone layers. These pelagic limestones layers were deposited in deeper marine environments of several hundred-meter-deep basins and sea straits. Open marine conditions are mostly represented by radiolarians and sometimes ammonites or pelagic bivalves (Stingl & Mair, 2005), but macroscopic fossils were not found in the study area. The composition of these strata is dominated by cherty micritic limestones, with subordinate dolomites and thin green tuff layers, called Pietra Verde.

The thickness of this formation is about 15 m on the W side towards Col Ciancidel and northern side of Bronsara valley and about 5 - 10 m thick E of Seres creek (similar numbers were also reported by Mutschlechner, 1933 and Jesacher, 1999).

The typical threefold subdivision into lower platy limestones (Plattenkalke), middle nodular limestones (Knollenkalke) and upper banded limestones (Bänderkalke) could be identified in the field, although not within a single outcrop.

The lower **platy limestones (Plattenkalke)** appear as black shales and consist of distinctly, cm- to dm-thick bedded, laminated and micritic limestones. Their dark colour and bituminous smell is attributed to the high content of organic material. The planar, platy splintering limestone beds of typical 5 cm to 15 cm are locally interlayered with thin marl (chert) layers. The Plattenkalke attain a total thickness of up to 5 m. They were observed at an outcrop at a small creek about 100 m E of Seres valley, just above the Contrin dolomite (fig. 17a). At the W side they appear at the easternmost tip of the E-W striking Buchenstein outcrop while they couldn´t be find outcropping further E. At the contact between Contrin-Formation and Buchenstein-Formation near Col Ciancidel about 1-2 m thick carbonatic breccias with red matrix were observed.

The **nodular limestones (Knollenkalke)** are also cm- to dm-thick bedded and can be distinguished from the Plattenkalke by their light grey color, dark laminae and wavy to nodular bedding surfaces. The nodular limestones comprise cherty and micritic limestones, calcarenites and marls. Upon weathering, these limestones display grey-ochre tones. Their distinctive structure is the differently developed, dark chert nodules, which were produced by radiolarians and impart a distinctly hummocky appearance to the bedding surfaces (fig. 17d). Bioturbation in the basin floor sediments created the characteristic nodular fabric (Jesacher, 1999). The Knollenkalke reach a maximum thickness of 5 m, which was also reported by Baur (Baur, 2019) for the Peitlerkofel area.

In places, the bedding planes are coated with thin, green or red tones. The green color derives from mm-thin, intensely green, volcanic ash and tuff horizons, called Pietra Verde. They were reported by many authors for the Knollenkalke and Bänderkalke (Mutschlechner, 1933; (Bosellini, 1996); Gianolla et al., 2008) but here they could not be found outcropping but only on rock fragments (fig. 17f).

The nodular limestones are often made of carbonate turbidites of neritic origin (peloids, ooliths, bioclasts) or of pelagic turbidites (Gianolla et al., 2008; Maurer & Schlager, 2003).

The Knollenkalke appear at the W side between Seres creek and Ciancidel huts, as well as 100 m W of Ciancidel huts. Knollenkalke also appear just some 20 m E of Seres creek. At this position they show a shallower dip angle, probably attributable to the slightly tilting due to the outcropping or due to the fossil mountain slope deformation.

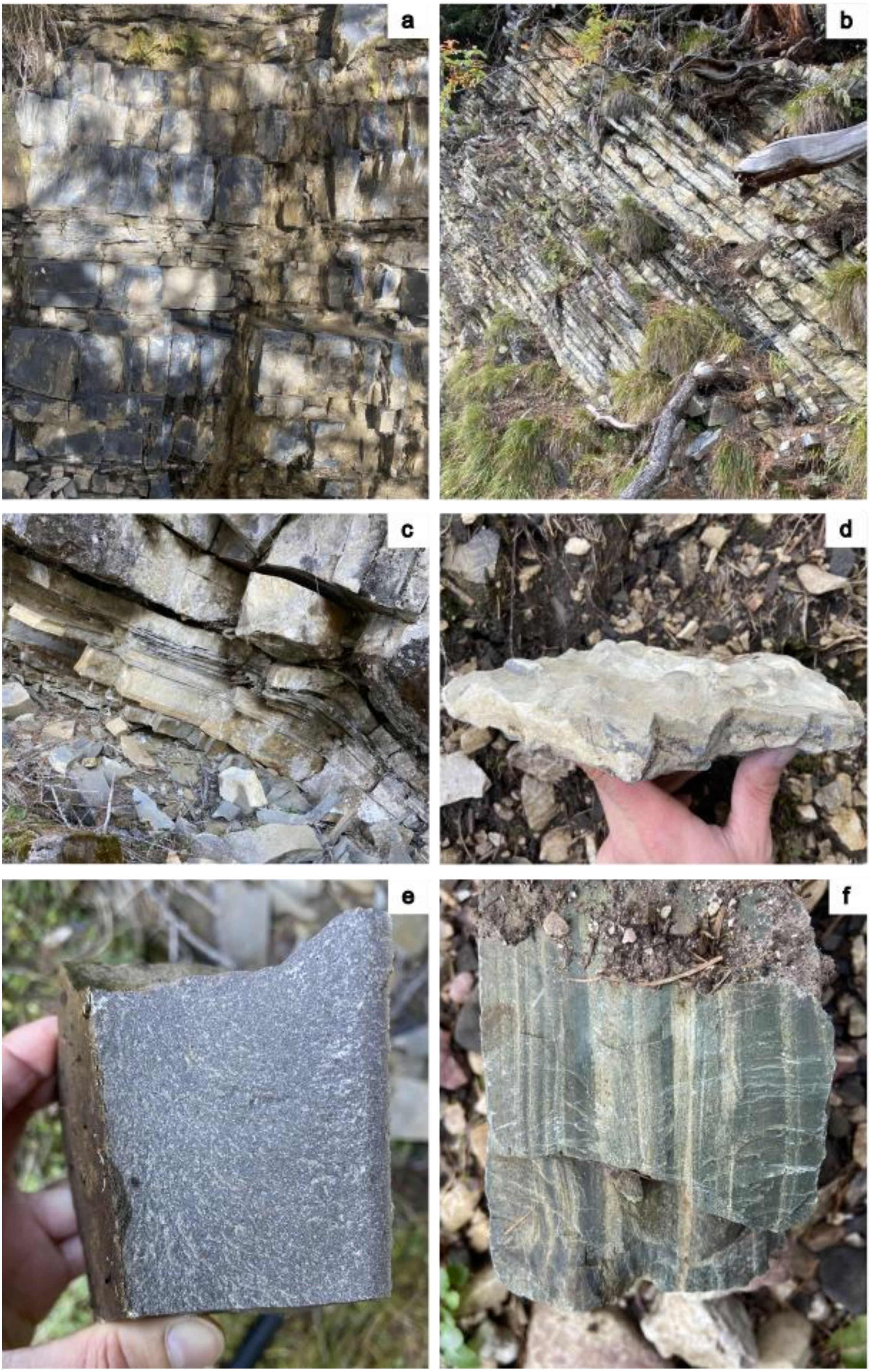

Figure 17: Buchenstein-Formation. a) dark platy limestones (Plattenkalke) at a creek about 100 m E of Seres valley. b) Planar and nodular bedding surfaces of nodular limestones

(Knollenkalke) close to Col Ciancidel.c) banded limestones (Bänderkalke) above Schlerndolomite close to the watershed towards Bronsara valley. d) Detail of chert nodules producing hummocky bedding surface of the Knollenkalke. e) dark (bituminous), micritic imestone of the Bänderkalke. f) Pietra Verde laminae.

At the W side between Seres valley and Ciancidel the top of the Knollenkalke is composed of chaotically deposited, clast supported breccias of coarse calcareous components (gravel to boulder size). As noted in Fois, 1983 the basinal settings close to the prograding platforms (proximal to the platform slope), as it is the case in the study area, experienced turbidity currents and deposition of carbonatic reef debris material from the prograding reef and slope.

This outcrop shows an erosional discontinuity which separates planar and wavy bedded Knollenkalk layers in the footwall from the coarse carbonatic breccia in the hanging wall. This lithology appears to represent the so called megabreccias unit, described by Fois, 1982 and Jesacher, 1999 in the area SE of Peitlerkofel. A similar outcrop was described by Fois (picture 5, p.572), when investigating the interfingering between platform carbonates (Schlerndolomite clinoforms) and basinal carbonates (Buchenstein-Fm.). Analogous to the scheme of Fois, 1982 the Knollenkalke of the Buchenstein-Fm. in the footwall would correspond to level a, while the megabreccia in the hanging wall would correspond to level b (calcareous megabreccia) or to the Untere Magabreckzie after Jesacher (Jesacher, 1999). This unit of reef debris breccias and calcarenites indicate the progradation of the Peitlerkofel reef (Schlerndolomite clinoforms) into the basin by submarine slope processes into the foot of the reef slope. The sediment deformation structures at the erosional discontinuity, like syn-sedimentary slump folds or load casts developed through early diagenetic deformation due to the sudden load of the reef and slope debris deposition.

The **banded limestones (Bänderkalke)** are lithologically very similar to the Plattenkalke, consisting likewise of well bedded, dark (bituminous), micritic and laminated limestones interstratified with marl layers. The banding is produced by numerous thin, often very dark chert layers, whose dark coloration is attributable to organic matter. Fine lamination is locally marked by hair-thin, white calcite seams. Towards the top brighter calciturbiditic layers increase. The Bänderkalke are typically several cm-thick, locally reaching decimeter scale. Intercalated with both the nodular and banded limestones is Pietra Verde. Above the about 8 m thin Schlerndolomite layer, a small outcrop of Bänderkalke above the source area witnesses the interfingering of basinal facies (Buchenstein-Fm.) with slope carbonates (Schlerndolomite). This approx. 1 m high Bänderkalke outcrop is again overlain by Schlerndolomite.

The ductile behaviour of the Buchenstein-Formation towards stress is documented by folds NE of the study area (p. 46 and 89 in Jesacher, 1999).

Figure 18: Megabreccie at the transition between Buchenstein-Formation and Schlerndolomite. a) erosional discontinuity with load casts separates the Knollenkalk layers in the footwall from the megabreccia in the hanging wall (outcrop between Seres valley and Col Ciancidel. b) outcropping megabreccia. c) finer grained reef debris breccia (calcarenite).

4.1.1.6 Schlerndolomite

The Schlerndolomite is a light grey, compact, fine-crystalline dolomite. It behaves brittle which expresses in splittery breaking. Fossils could not be observed due to dolomitization, which also cancelled the primary limestone stratification. It builds up the Peitlerkofel as slope and reef facies, where it reaches thicknesses of about 600 m (Mutschlechner, 1933).

In the study area the Schlerndolomite is developed as slope facies (clinoform) interfingering with Buchensteiner-Fm., with Caotico Eterogeneo and Wengen-Fm at the NE part and is overlain by Zoppé-Sandstone at the source area. Below the alpine meadows SE of Peitlerkofel (locality of Fornates) pre- and post-volcanic

Schlerndolomite composed as slope facies (clinoforms) with megabreccia horizons (levels d and f after Fois, 1982) can be found. The post-volcanic Schlerndolomite is outcropping as several meters steep, nearly vertical bedrock faces and is bounding the Caotico Eterogeneo and Wengen-Fm. to the N. The post-volcanic Schlerndolomite clinoforms did not reach the same extent as the pre-volcanic Schlerndolomite clinoform and are thus stepped back by about 200 m compared to the pre-volcanic Schlerndolomite clinoform (Fois, 1982), which is developed in the source area.

The pre-volcanic Schlerndolomite (Rosengarten-Formation or Lower Schlerndolomite after Jesacher, 1999), which per definition lays stratigraphically below the volcanoclastic units (Caotico Eterogeneo and Wengen-Fm.), could be identified as an approx. 8 m thick band. It stretches from the Kreuzkofeljoch in the W over the source area, where it behaved as a sliding plane. It is outcropping at the curve of the mass movement and is believed to continue to the E, as one outcrop E of the fossil rock slump has been found. The extension towards E cannot be continuously traced due to the fossil rock slump and the recent earth flow.

The pre-volcanic Schlerndolomite is outcropping on the S slope of the source area where it dips with about 40° towards N. Above the source area there is a N-S trending, about 7 m high rock face, which splits the more massive in-situ rock mass on the W from a block field under the rock face to the E (see fig. 19e and 28). Here the Schlerndolomite dips around 30-40° N towards the source area. When the mass movement happened the lowermost blocks of the blockfield slided down over the sliding plane, which is slightly steeper inclined (around 40°).

The sliding plane is composed of the lowermost part of the pre-volcanic Schlerndolomite, which still partly contains the original calcareous composition (grey-brown colour) and shows dm-thick bedding planes. This basal, around 1 m thick Schlerndolomite is dm-bedded and partly appears slightly nodular. This could be observed at the base of the the N-S trending rock face and was also noted by Jesacher (Jesacher, 1999). At the base of the rock face a slump fold was noted (fig. 19f), which is a structural feature occurring at the transition between Buchensten-Fm. and Schlerndolomite (Brandner et al., 2016). W of the N-S trending rock face, the Schlerndolomite is massive and shows E-W trending tension cracks and a deep tension crack parallel behind the N-S trending rock face. This part is regarded as metastable, as the depth of the tension cracks could not be established, and this rock mass rests above a potential sliding plane. This Schlerndolomite band at the source area is interpreted to have its origin as a reef slope clinoform into the basin (onlap) and was later tectonically steepened together with the adjacent formations during alpine orogeny.

Another Schlerndolomite occurrence is between the two recent mass movements on the E side of the study area, where it occurs as highly fragmented and broken apart.

The N dipping northern fold limb of the Bronsara-Anticlinal is assumed to terminate around Ru de Coretes, because to the N towards Peitlerkofel about 30° S dipping post-volcanic clinoforms from the Peitlerkofel reef are exposed. Therefore, the axis of the syncline is assumed to be positioned approx. along Ru de Coretes. Also, the occurrence of brittle Schlerndolomite means a change in reaction towards tectonic stresses. While the basin sediments between Peitlerkofel and Puez behaved ductile and reacted with folding to the alpine compression (Bronsara anticlinale), in the Schlerndolomite of Peitlerkofel NW-SE trending slike-strip faults, reported by Mutschlechner, 1933 and Jesacher, 1999, accommodate the compressional stress.


a
b
c
d

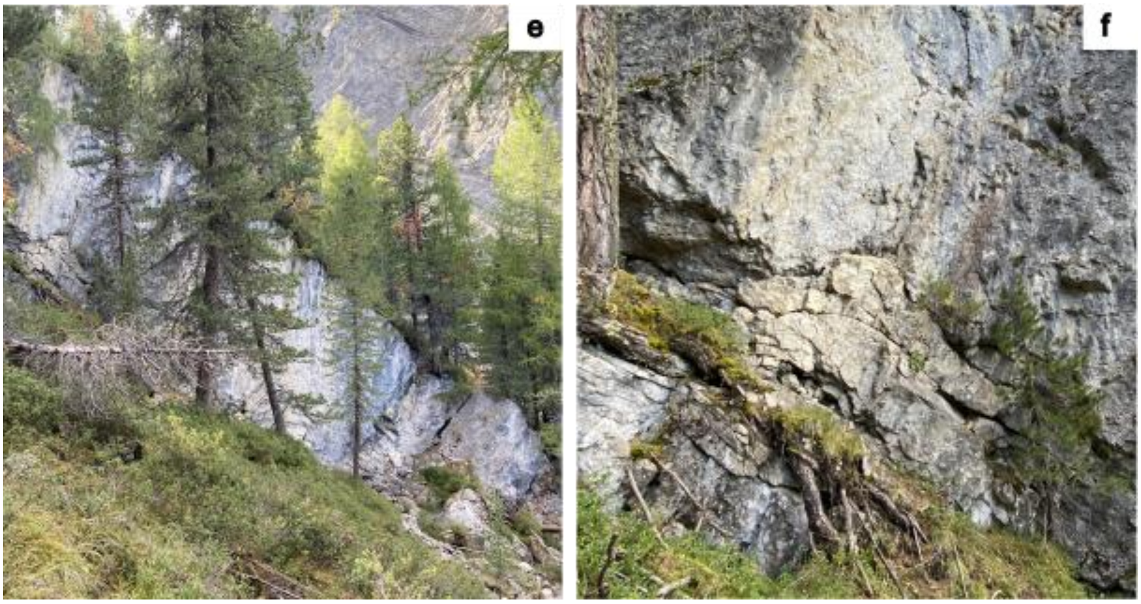

Figure 19: Schlerndolomite. a) Schlerndolomite at the watershed (ridge) S of the source area towards Bronsara valley. b) white Schlerndolomite on top and darker, more calcareous Schlerndolomite with bedding surfaces at from the basal Schlerndolomite. c) Schlerndolomite creating the sliding surface at the source area (dipping ~40° towards N). d) slickensides (Harnischfläche) with striations on the Schlerndolomite sliding plane. e) N-S trending Schlerndolomite rock face. f) basis of the N-S trending rock face with massive, unstratified Schlerndolomite on top and basal stratified Schlerndolomite with slump fold.

4.1.1.7 Zoppé - Formation

Zoppé-Sandstone was only found in the source area of the mass movement. This formation is characterized by well stratified, distal turbiditic, pelitic to sandy sequences of cm- to dm-thick layers of arkosic composition. In the field the strong in-situ weathering of the formation was noticed, especially the bedding surfaces were easily weathering and erosive. The grey siltites, mostly cm-thick bedded layers are weathering stronger than the dm-thick bedded reddish-brown weathering sandstones. At the base thinly layered, laminated dark calciturbidites and micritic marls are found, which expose dark to ochre weathering color. Organic plant remnants (vegetal frustules) are found on top of the dm-thick sandstones, as it is typical for Bouma-sequences like deposition of turbidite beds. From what could be seen in the field the lithologic transition towards the Schlerndolomite in the footwall (onlap) seems to be rather abrupt and erosive, which fits the sudden deposition as turbidite currents of the Zoppé-Sandstone. The highly weatherable material with its slope parallel, about 40° towards N dipping bedding, seems the reason for the developement of the Ciancidel channel.

Below the sliding plane rock fragments of a coarse to medium grained sandstone were found (fig. 21d). This sandstone could not be found outcropping, but from descriptions of the Zoppé-Formation it is likely to come from the base of the formation. It has a lower strength as it is easier to break with the hammer compared to the Schlerndolomite. The sandstone is of arkosic composition with small amounts of calcite cement and probably also contains iron oxides as iron oxidation is visible (fig. 21d). Volcanic clasts or clasts from the metamorphic basement, as described in the localities further south, were not found (Viel, 1979; Gianolla et al., 2008).

Pietra Verde layers were observed above calciturbidites and siltites, but with the difference that flute casts are exposed on the bedding surface (fig. 21c).

Macrofossils found in the source area are imprints of the bivalves Daonella lommeli and Posidonia wengensis, as well as one ammonoid of the Protrachyceras genus (fig. 22i). All three fossils were reported for the Zoppé-Sandstone by Gianolla (Gianolla et al., 2008) and indicate marine conditions during deposition. In total the formation is about 15 m thick.

Deformation of this ductile behaving formation was noted through structural features like monocline folds, rounded parallel concentric folds and a tight fold.

The Aquatona-Formation follows with a clear discontinuity the Zoppé-Sandstone and is exposed as a thin, competent and plane parallel stratified band at the base of the rock face (fig. 21a). On top of this about 5 m thick formation the unstratified Caotico Eterogeneo follows with an erosional disconformity (fig. 23c). Throughout the formation two orthogonal joint sets control the outcrop pattern. The lower part is characterized by carbonate lithologies like limestones and calcsiltites. In between 3 volcaniclastic layers or tufites of about 20 - 30 cm thickness were identified (21b). This is a typical feature of the Aquatona-Formation in the Western Dolomites and is linked to the beginning of Mid Triassic basic volcanism (Gianolla et al., 2008). The Aquatona-Formation was mapped together with the Zoppé-Fm. The upper part could not be investigated, but a new increment in the siliciclastic component, e.g. marls and sandstones is reported (Gianolla et al., 2008).

Figure 20: Zoppé-Formation. a) easily weathering siltstones and more competent calciturbidite banks in the upper part of the source area. b) easily weathering siltstones producing regolith. c) detail of siltstones (grey) between reddish-brown weathering competent calciturbidite banks.

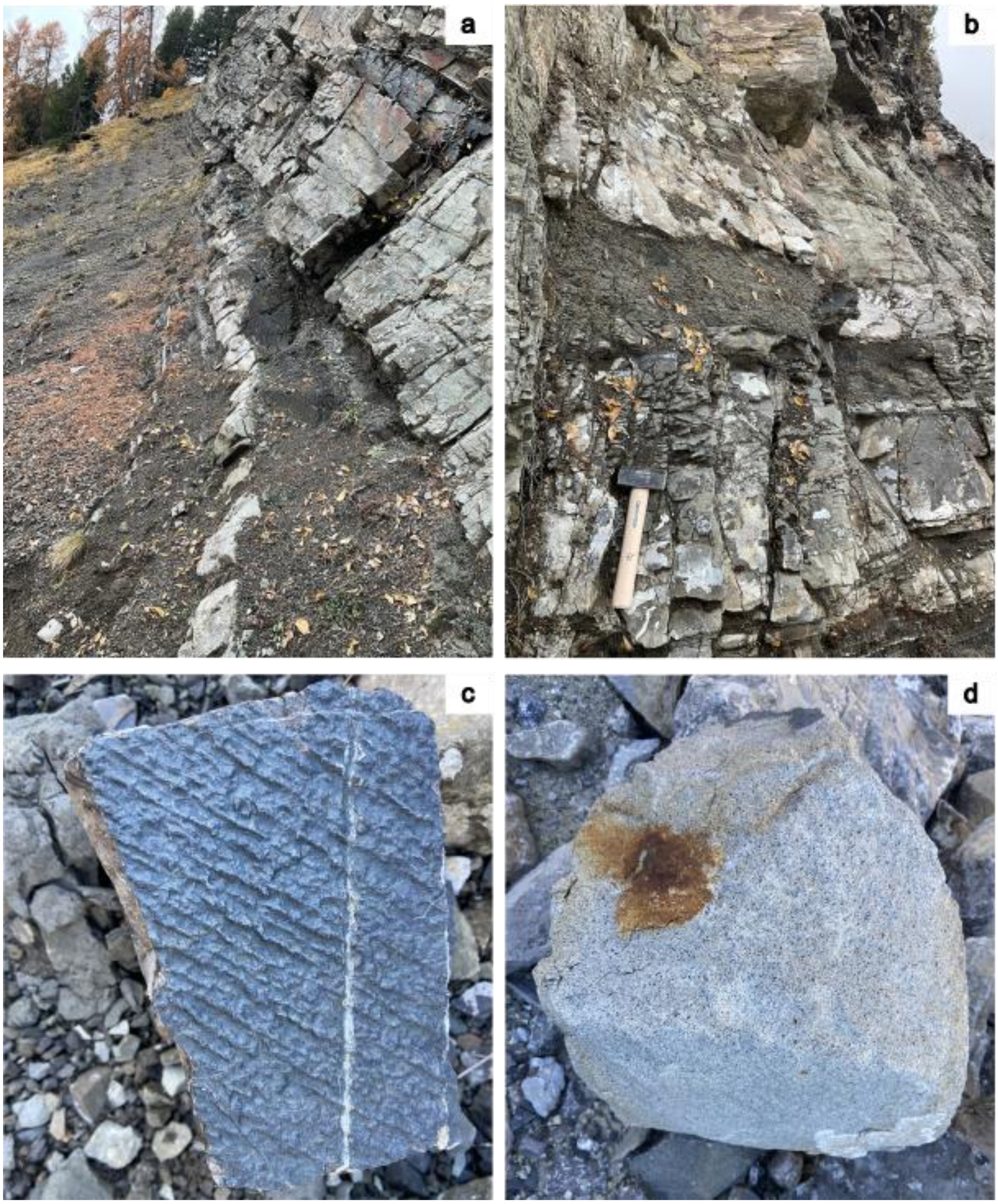

Figure 21: a) erosional discontinuity between Zoppé-Fm. (left) and Acquatona-Fm. (right) constituting the base of the rock face N of the source area. The tuff layer is eroding faster than the carbonates of the Acquatona-Fm.. b) volcanoclastic, 30 cm thick tuff layer in Acquatona-Fm. at the base of the rock face N of the source area. c) Pietra Verde with flute casts on top of a reddish calciturbidite bank. Arkosic sandstone of Zoppé-Fm. with rust iron oxidation.

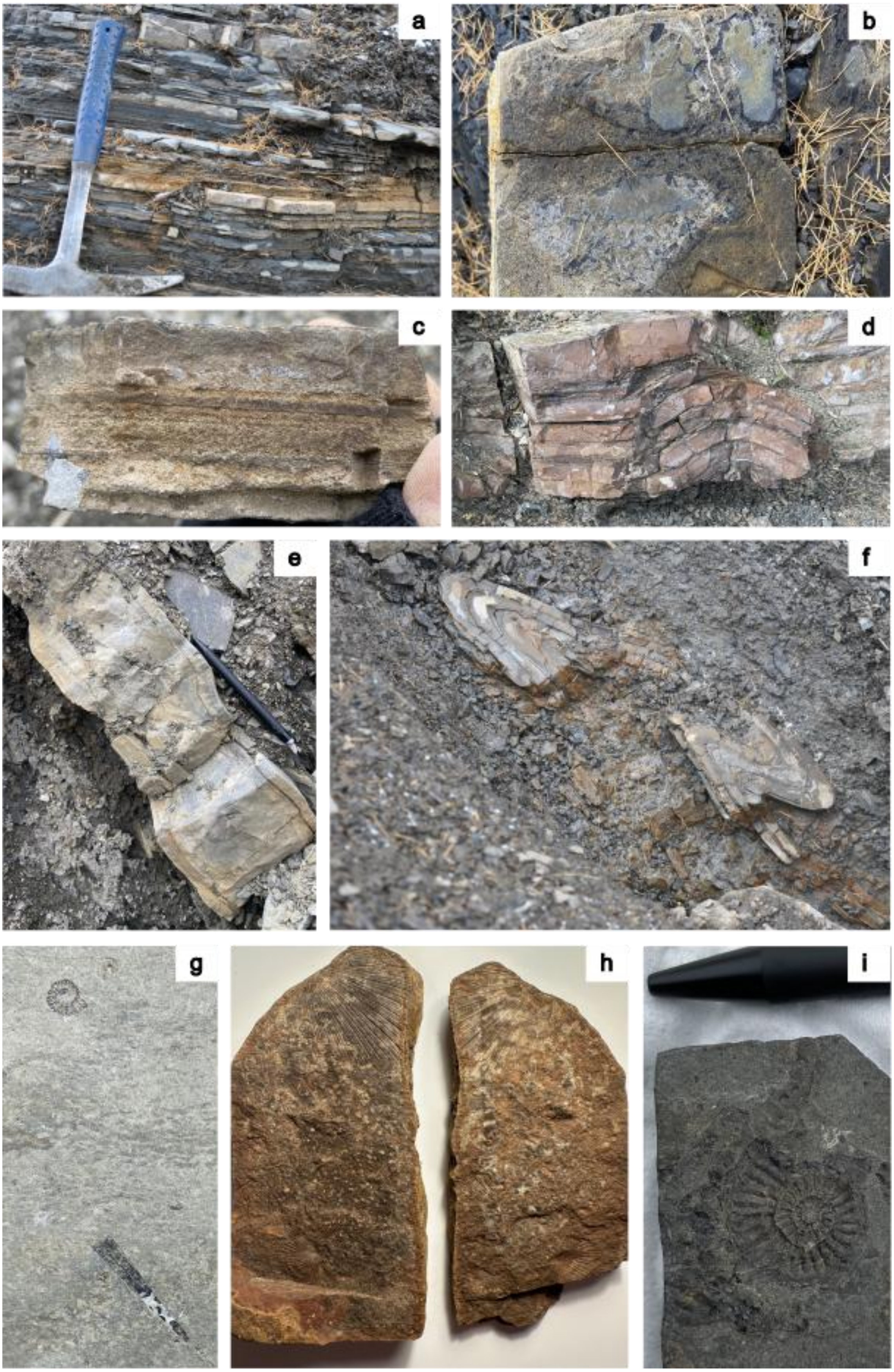

Figure 22: Zoppé-Formation. a) fine calciturbidites at the base of Zoppé-Fm. b) organic plant remnants on top of a calciturbidite (Bouma sequence). c) detail of calciturbidite. d) parallel concentric fold in Zoppé-Fm. e) monocline folding of calciturbidite bank. f) tight fold

g) ammonite imprint on top and belemnite below. h) Daonella lommeli i) ammonoid of the Protrachyceras genus.

4.1.1.8 Caotico Eterogeneo

The chaotic and heterogeneous megabreccias with dark volcanoclastic matrix and carbonate components witnesses the begin of the mid triassic (Ladinian) volcanic activity. The eruption centers were located further south in the Fassa Valley, near Predazzo (Bosellini, 1996). The volcanic activity triggered eruptions and earthquakes, which moved large masses of debris into the basins by mass resedimentation and thus without selective sedimentation processes (Gianolla et al., 2008). Therefore, the thickness of this unit varies strongly, depending on the paleo-topography at time of deposition.

The coarse components of mostly gravel to boulder size derive from the preexisting formations of Contrin-and Buchenstein-Formation. Also, black and dark green basalt clasts with pyroxene phenocrystals from the Fernazza-Formation, can be found now and then (fig. 23a, 23b). Locally big fragments appear in the Caotico Eterogeneo, like olistoliths of several tens of meters of pre-volcanic Schlerndolomite, Buchenstein- or Contrin-Formation, like at the rock face above the source area (fig. 23 c). Apart from the rock face Caotico Eterogeneo is outcropping at the creek Ru de Corëtes and in different spots in the easters part of the study area.

Lithologically the megabreccia of the Caotico Eterogeneo contains poorly to rounded, polymict components bounded together by a dark glassy, porous volcanoclastic or tuff matrix. The components alternate from fine- to coarse-grained parts (generally fining upward trend) and matrix-suported parts alternate with component-supported ones. Occasionally thin tuff and lava layers, as well as pelite and limestone layers divide the megabreccia into massive beds. At the base of the rock face some dm of thinly stratified volcanoclastic greenish siltites or marl layers occur.

The Caotico Eterogeneo appears in the field as steep walls, whose surfaces are often somewhat rounded due to their susceptibility to weathering.

In the eastern part C.E. appears alternating with the Wengen-Fm. in different locations (see outcrop map: e.g. NE of the earth slump - earth flow, at the top of the recent debris slide and at the easternmost end of the mapping extent.)

E of the mapping extent Mutschlechner noted that the Caotico Eterogeneo (therein called Buchensteiner Agglomerate) appears already above Buchenstein-Formation. This observation is probably not accurate as one Schlerndolomite outcrop between these two units was found. Still more outcrops of Schlerndolomite as well as probable Zoppé-Sandstone occurrences further east should be considered to refute Mutschlechners observation.

The purely volcanic and volcanoclastic products of the Fernazza-Formation were not found outcropping in the study area, nevertheless, occasionally black basalts with pillow like cooling structure or better recrystallized basalts with green augite minerals (Augitporphyrit after (Mutschlechner, 1933) could be identified in the mass movement material.


a
b
c

Figure 23: a) Caotico Eterogeneo outcrop with typical megabreccia of fine volcanoclastic matrix with carbonate components. b) Caotico eterogeneo as clast supported matrix with components from Contrin-Dolomite, Buchenstein and basalt of Fernazza-Formation (below) with dark pyroxene phenocrystals. c) rock face composed of Caotico Eterogeneo with a Buchenstein olistolith (black circle). At the base an erosional disconfinuity marks the transition towards the thin carbonatic Acquatona-Formation while below the stratificated Zoppé-Fm. is exposed in the source area. Left a local normal fault displaces the right part (E) of about 2 m downwards (black line).

4.1.1.9 Wengen - Formation

The Wengen-Formation is present in the NE part of the mapping area, where it is found above the Caotico Eterogeneo and is overlain by the post-volcanic Schlerndolomite clinoforms. Here it also builds up steeper rock faces of a few tens of meters. The Wengen-Formation contains eroded and mainly as turbidites in marine basins resedimented volcanoclastic material of the Fernazza-Fm. mixed with carbonate material of the basins. (Keim et al., 2006; Brandner et al., 2007). Thus, the most frequent lithologies are alternating dark pelites and graded sandstones of volcanoclastic (tuff) material, as well as dark conglomerates, claystones and marls with plant residues and Daonella lommeli.

In the NE outcrop the Wengen-Fm. appeared as about 10 cm thick layers of grey-brown to green volcanoclastic sandstones (fig. 24a) interbedded with finer marl layers. The surfaces of the Sandstones appear rounded, the layers were the only ones in the whole study area dipping towards SE (120/20). Also, coarse sandstones with volcanic clasts and conglomerates were identified (fig. 24b).

At the NE tip of the earth flow brown calcite banks crop out. They must represent the upper parts of the Wengen-Formation as carbonate and marl amount increases in the upper parts of the Wengen-Formation. It appears that the Wengen Formation presents a strong heterogeneity of lithofacies, both in terms of lateral variation and of vertical evolution, as described by Gianolla et al., 2008).

Marmolada-Conglomerates were not observed since they are not present in areas far away from the volcanic centers.

Figure 24: Wengen-Formation. a) grey-brown to green volcanoclastic sandstones interbedded with finer marl layers. b) coarse volcanoclastic sandstone.

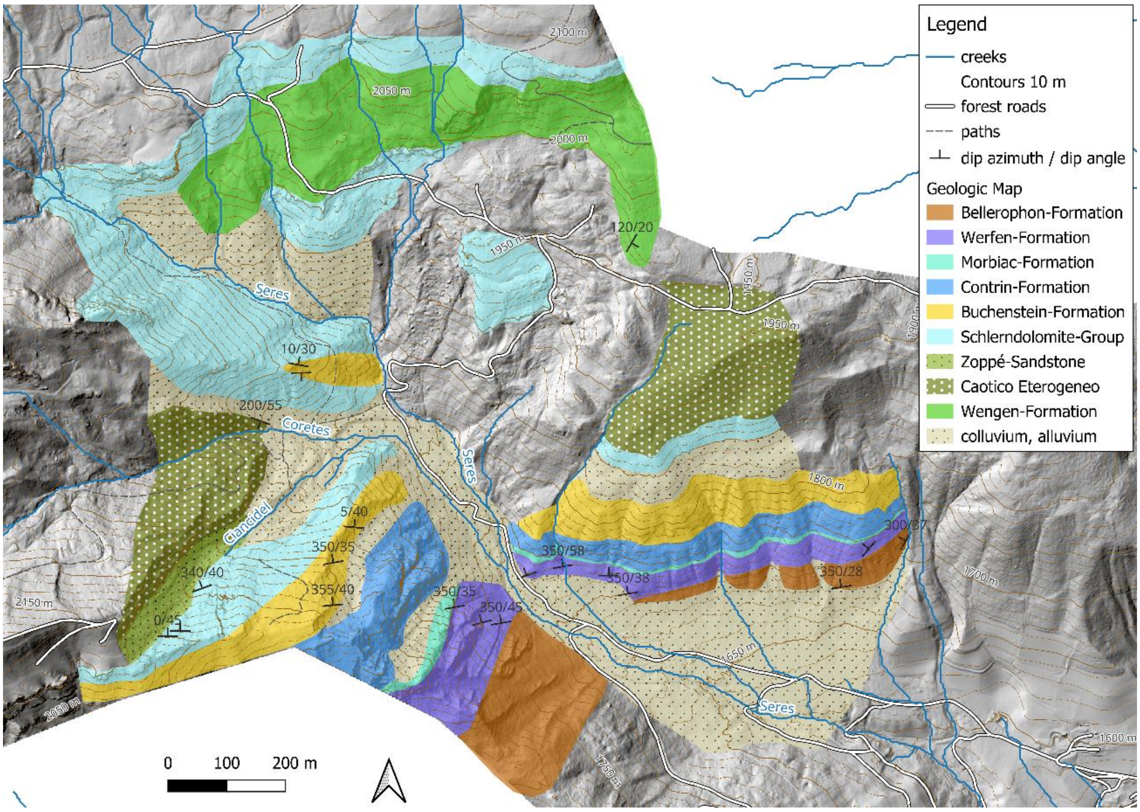

Figure 25: Geological Map of the study area with structural data (dip azimuth / dip angle).

4.1.2 Geomorphological Mapping

From the orthophoto and DTM prior to the event (fig. 4 and 6) the gully of the source area seems to be filled by blocky and gravel colluvial material from the above laying rock cliff composed of Caotico Eterogeneo volcanoclastic mega-breccia. It is speculative to know the structure of the filled gully, however it is assumed that not all of the eroded material from the mass movement was colluvium material, but the lowest parts were likely in-situ destabilized and weathered silt- and sandstones from the Zoppé-Formation.

At the source area prior mass movement activity is indicated by the pre-event DTM which shows convex shaped contour lines at the junction between Ciancidel and Corëia channel, indicating sedimentary deposit. This is highlighted by the incision of two small flow channels dewatering the source area (see figure 37 and cross section 3 in chapter 4.2.3). This prior mass movement event must be at least 100 years old, as indicated by the presence of a forest (forest name "Bosch dal' Ega de Vita") in the Ciancidel channel before the event of 2024. One picture from the junction between Corëtes channel with Seres valley in 2023 (Google Maps, 2023) shows mentioned deposited material in form of a debris fan covered by grass and trees. This testifies the presence of debris depositional events in the past. This material, which from the pre-event DTM seems to mainly origin from the Ciancidel channel, was responsible for keeping the Corëtes creek separated (orographic right) from the Seres creek until 2024.

This geomorphological observation leads to the conclusion that this Ciancidel catchment behaves like a transport-limited catchment. The transport-limited character is explained by an abundance of sediment produced through weathering, colluvial processes and regolith development in the gully. So, the sediment recharge was high and the limited transport capacity of runoff in the small catchment was not sufficient to continuously remove it. As a result, sediment was accumulated in the gully, only being mobilized through significant water saturation. Such catchments are prone to episodic flushing, where large volumes of sediment are suddenly mobilized, mostly coupled with hydro-meteorlogical events (De Haas et al., 2024). Typical processes for transport-limited catchments are shallow landslides, gullying and channels often act as temporary storage zones until sufficient discharge is able to remove the material (Schlunegger et al., 2013).

The event in June 2024 removed most of the unconsolidated material exposing the Schlerndolomite on the S-flank and the stratified Zoppé-Fm. on the N-flank. As today only minor unconsolidated material remained deposited in the channel axis, covering the bedrock in the source area, the source area is now regarded as supply-limited. Still a remobilization of the debris flow material in the transportation zone, especially from the part just below the source area (junction of Ciancidel and Corëtes channels) cannot be fully excluded in case of extreme wet conditions. It is assumed that the hydro-meteorological conditions for remobilization must be heavier than the conditions in June 2024 as the material now is prevalently composed of blocks and gravels while the fine-grained material, which mainly drives the flow behavior, was mostly washed away.

Field indications for long-lasting creeping movement of the SE flank of the source area towards N were identified (fig. 26): (1) several tension cracks of 10 - 30 cm aperture, sometimes covered by roots of trees and bushes and sometimes associated with steps, (2) sickle growth of trees, (3) fractured rock mass, and (4) fibrous calcite vein minerals with striations on discontinuity surfaces of the Schlerndolomite and Zoppé-Sandstone, indicating shear sense towards N. Slickensided surfaces (german Harnischflächen) were found on the exposed Schlerndolomite sliding plane at the source area. All these shear-sense indicators witness a creeping movement of at least some decades or centuries.

Contrary to the Ciancidel catchment, the Corëtes catchment seems to behave like a sediment-limited catchment, as the creek bed is V-shaped and flanks of Caotico Eterogeneo are exposed. The catchment area of the Corëtes channel and its subparallel small and steep northern gully shows hummocky topography with several superficial to shallow slide and flow movements (see chapter DoD), indicating creeping and unstable conditions of the sedimentary cover.

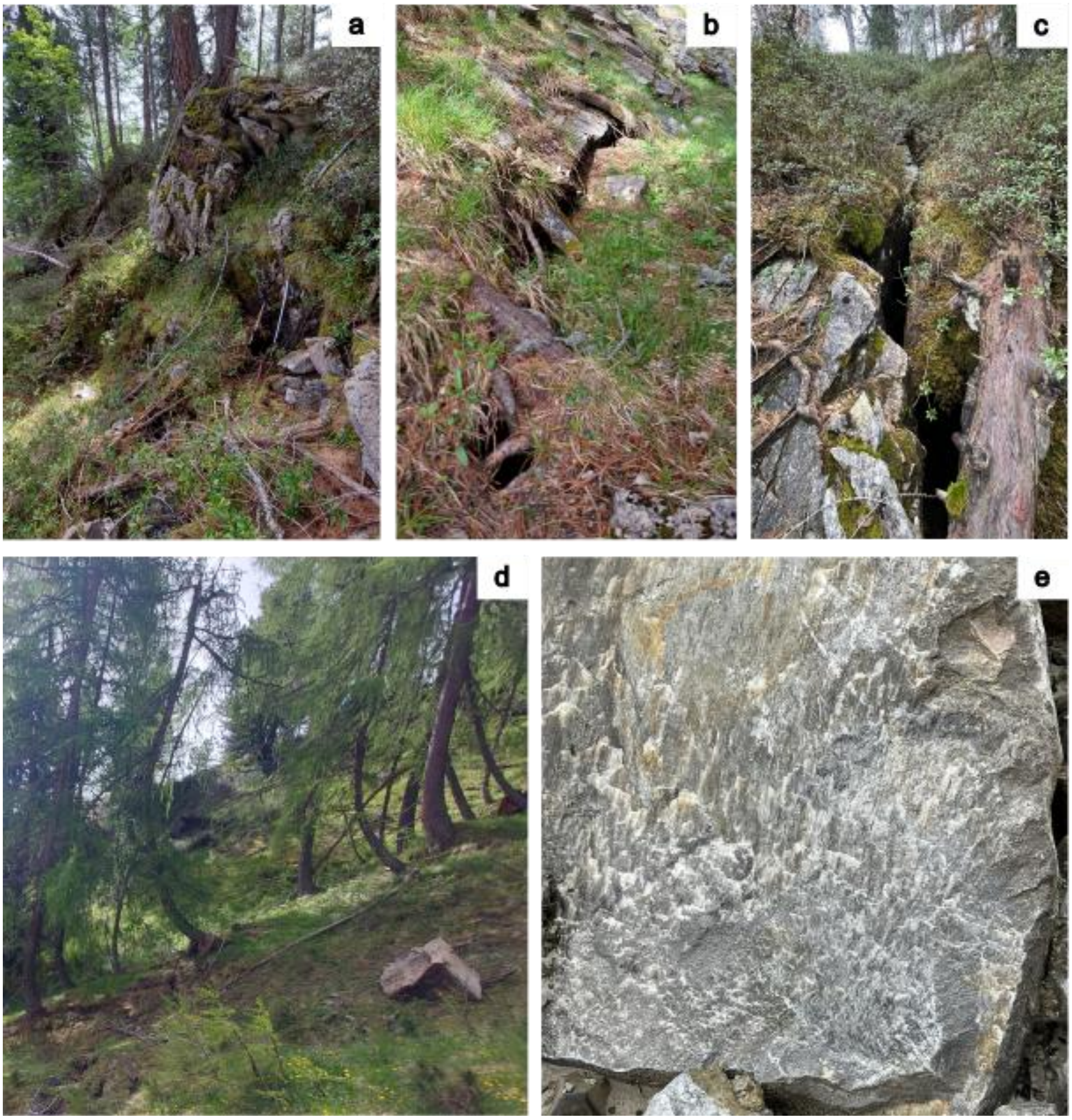

Figure 26: a) tension crack with about 0,5 m step and roots under tension. b + c) tension cracks. d) sickle growth of trees. e) fibrous calcite vein minerals on a Schlerndolomite block.

Between the study area and the Peitlerkofel meadows to the N (locality of Fornates) a marked break in the terrain is visible by about 50 - 70 m high rock cliffs. Consulting the DTM these rock cliffs probably functioned as headscarps of an old (probably Holocene or Pleistocene) huge Rock Slump or Rock Slope Deformation after Hungr et al. (2014) (also slope sagging or “Sackung” in german). The headscarps in N and E, composed of Schlerndolomite and Wengen-Fm. are bounding the rock slump deposit (fig. 28) composed of several meters size fractured Schlerndolomite blocks with occurrences of Caotico Eterogeneo debris and dm to m wide tension cracks forming steps and trenches (German “Nackentälchen”), as well as tension cracks separating little hills on the eastern part, give the deposit a hummocky topography. Below the headscarp at the upper part of the deposit a light settling seems to occur, according to the DoD (see chapter GCD). Movement rates are estimated to be very slow to extremely slow (< 2 cm/year). Above the headscarps more recent tension cracks appear. Within this blocky deposit of about 230.000 m^2 two mass movements developed recently.

The eastern mass movement is classified as an Earth Rotational slide (= Earth slump) - Earth Flow, as it shows a concave geometry in the upper part and scarps in the middle part, while the lowest part shows a flow like transport of silt to gravel, partly blocky material. Regarding orthophotos this mass movement activated before 1999 and especially the lower part was reactivated as an Earth Flow two times before 2011 and once between 2015 and 2020, since than it was inactive.

The western mass movement occurred in spring 2013 (20.05.2013) and is classified as extremely rapid Debris translational slide. Behind the crest tension cracks appeared retrogressively in recent years, a wooden hut was destroyed (fig. 27 c and d) and the forest road at the foot of the Debris Slide had to be restored. NE of this debris translational slide a little creek flows down from the Peitler meadows.

Between the Debris translational slide and the Earth Rotational slide - Earth Flow two huge tension cracks striking E - W are developed in fractured Schlerndolomite. Both tension cracks form an about 2 - 4 m deep trench and appear to be active (see chapter GCD).

Figure 27: E of Seres creek (a - d). a) tension crack N of Earth slump - Earth flow. b) fractured rock mass in Schlerndolomite (picture taken from the E – W striking trench between the

Debris slide and Earth slump - Earth flow). c) scarps on top of the Debris slide. d) retro-gressive evolving scarps displacing the hut.

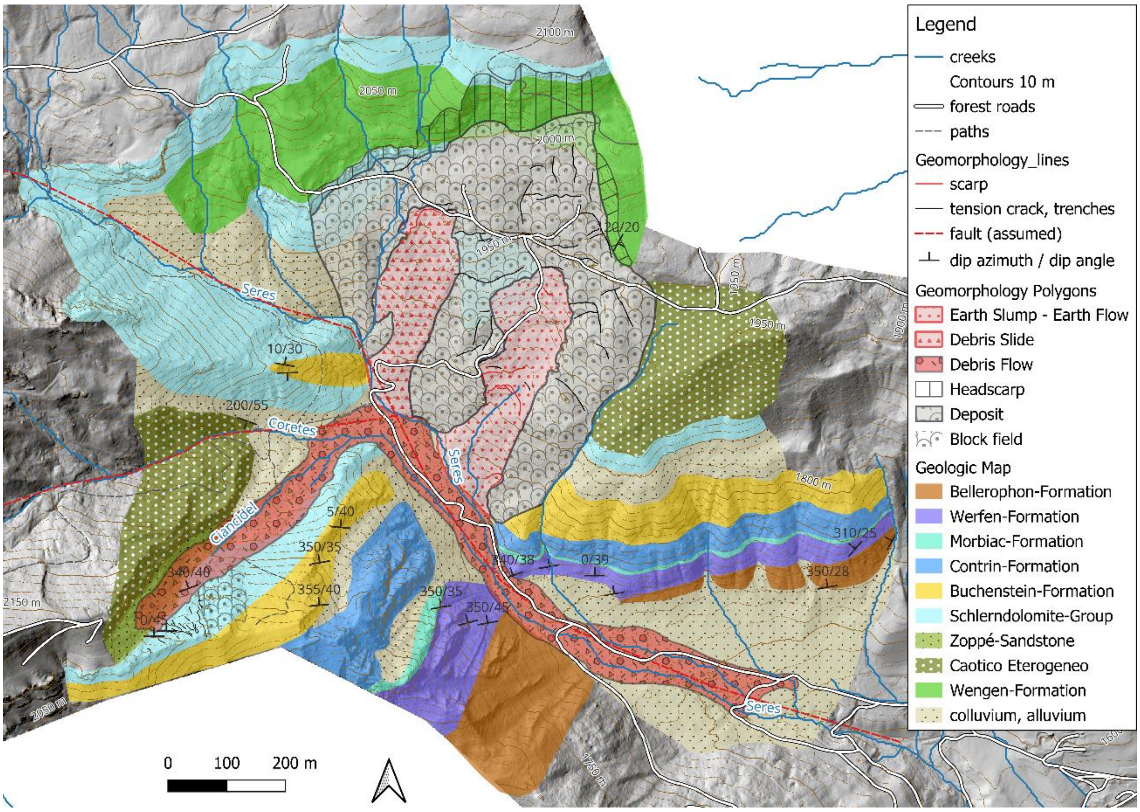

Figure 28: Geological and geomorphological map of the study area.

4.1.3 Geological Profile

A geological profile was drawn through the source area to visualize the geological predisposition with regard to the sliding surface and the mobilized colluvium mass. When drawing profiles it is important to calculate the apparent dip angle, when the profile is drawn in any other direction except from perpendicular to the dip direction.

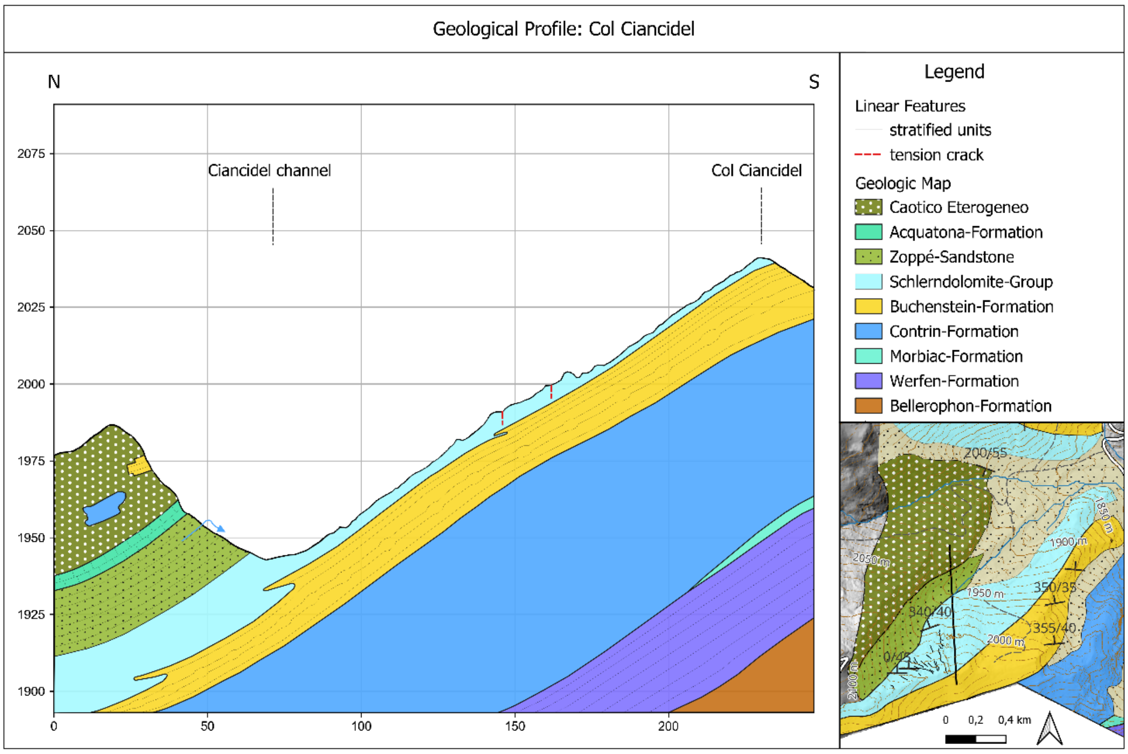

Figure 29: Geological profile from Col Ciancidel in the S through the source area in the Ciancidel channel ("Roa de Coretes") and the rock cliff of Caotico Eterogeneo in the N.

The geological profile in fig. 29 shows a fold limb dipping with 35° to 45° towards N (N-fold limb of Bronsara anticlinal). Towards N the fold limb is drawn gets slightly flatter as it is approaching the synclinal along the Corëtes channel (see chapter 4.1.4 Structural Geological Analyses). Interfingering of basinal Buchenstein-Fm. with Schlerndolomite slope carbonates is indicated with zigzack shaped formation boundary. Aqcuatona-Fm. could be mapped as a separate Formation in the profile. The insered tension cracks are found 20 – 40 m W of the profile line.

From the profile it gets visible that the N dipping makes it possible for water to flow along the bedding planes and saturate the colluvium deposit and weather the Zoppé-Sandstones.

4.1.4 Structural Geological Analyses

Knowledge of the tectonic and neotectonic history of the Dolomites is helpful to identify and interpret structural geological features in the field as possible predisposing factors for mass movements. As structural geological features like folds, faults and joints often control geomorphological or quaternary processes, a regional overview of the possible orientations of faults or fold axes can be helpful to identify new or small scale structural geological features in the field and interpret them. In this chapter the tectonic overview of the Dolomites from chapter 3.2. (Geological Overview) is complemented with relevant structural geological observations from the field or from literature around the study area. Structural geological features are of relevance as folds, faults and joints can act as predisposing factors for mass movements.

Structural geologic features of the Middle Triassic (Anisian) E-W Extension are:

1. The Göma Fault (Col Vercin Fault after Bosellini, 1964) is a N-S striking normal fault about 1 km E of the study area until N of Seres village (Jesacher, 1999). This east-dipping normal fault was responsible for the downward displacement of the eastern crustal block, while the western part was slightly tilted and uplifted (differential subsidence), so that erosion was active in the western crustal block. Due to the westward tilting of the western block, the Werfen Formation experienced increased erosion from west to east towards the Göma Fault (see Broglio Loriga, 1990; Jesacher, 1999). After Jesacher, 1999 the Göma-Fault was reactivated as normal fault during Jurassic/Lower Cretaceous Extension (Rifting), as thrust fault during ENE-WSW Compression in Paleogene and as dextral strike-slip fault during Neogene NNW-SSE Compression.

2. In addition to the light westward tilting of the crustal block west of the Göma Fault, the Seres valley could be considered as an Anisian normal fault dipping to the west. This is suggested by the more massive Werfen Formation W of the Seres valley (Seis member) compared to the reduced Werfen Formation E of Seres valley (=north of Seres village).

Structural geologic features of the Paleogene (mesoalpine) ENE-WSW Compression could not be identified in the study area as they were overprinted by the Neogene compression.

Structural geologic features of the Neogene (neoalpine) NNW-SSE Compression:

1. ENE-WSW striking Bronsara-Anticlinal in the Bronsara valley, SE of study area. This huge anticlinal structure with its 30-40° towards N and S dipping fold limbs was formed under Neogene NNW-SSE compression. Also the fold axis is plunging towards E, which means that the Bellerophon-Fm. in its core is exposed in much higher elevations in the W (until 2200 m) than in the E

(1650 m). This fold axis dipping could be explained by the Paleogene ENE-WSW Kompression (Jesacher, 1999). This anticlinal is highly relevant for the study area as the source area is situated on the N-limb with average dipping of 340 / 40. Just about 200 m N of the source area the Corëtes valley seem to stretch along the synclinal axis with the Caotico Eterogeneo in its core.

2. Several NW-SE trending Neogene dextral strike slip faults occur between Bronsara valley and Peitlerkofel. Most of them dissect the brittle Schlerndolomite of the Peitlerkofel. The most prominent NW-SE Neogene dextral strike slip fault is interpreted to be the Seres valley as the south-eastern continuation of the Scharten-Fault behind the Peitlerscharte (Jesacher, 1999). Further NW-SE trending Neogene dextral strike slip faults with bigger displacements occur 1,5 km W of the study area (area of Kreuzkofel Joch - Schlüterhütte).

3. Funes Fault is a Neogene thrust fault, but its extension towards E still needs to be investigated.

4. South-east of Peitlerkofel S to SE directed thrust faults and folds with E-W to SW-NE striking axes of the Neogene compression occur (Jesacher, 1999), which fit well with the S-vergent folding and back-thrusting along the S-directed thrust faults observed over the Dolomites region (Doglioni & Bosellini, 1987).

5. Measured synclinal fold with E-W axis in the Werfen-Formation (Tesero-Oolite member; fig. 31)

Bedding measurements of all formations show uniform dip direction towards N, with a mean bedding plane of 353 / 40. The southern part of the study area is positioned on the N-fold limb of the Bronsara-Anticlanal, while in the northern part dip direction turns towards S, indicating a synclinal structure around the Corëtes creek. Also the fact that the Corëtes channel is parallel to the Bronsara valley, makes a synclinal around Corëtes channel likely. For the stereoplots of the bedding planes 77 measurements were statistically evaluated. 70 measurements are dipping N and 7 dip S, showing a bimodal bedding distribution, typical for fold limbs. Separating the two sets results in mean N fold limb of 354 / 41 (poles: 174 / 49) and a S fold limb of 174 / 32 (poles: 354 / 58). The inter-limb angle of 107° classifies the synclinal fold as open. Note that the most bedding planes are from the southern part of the study area area.

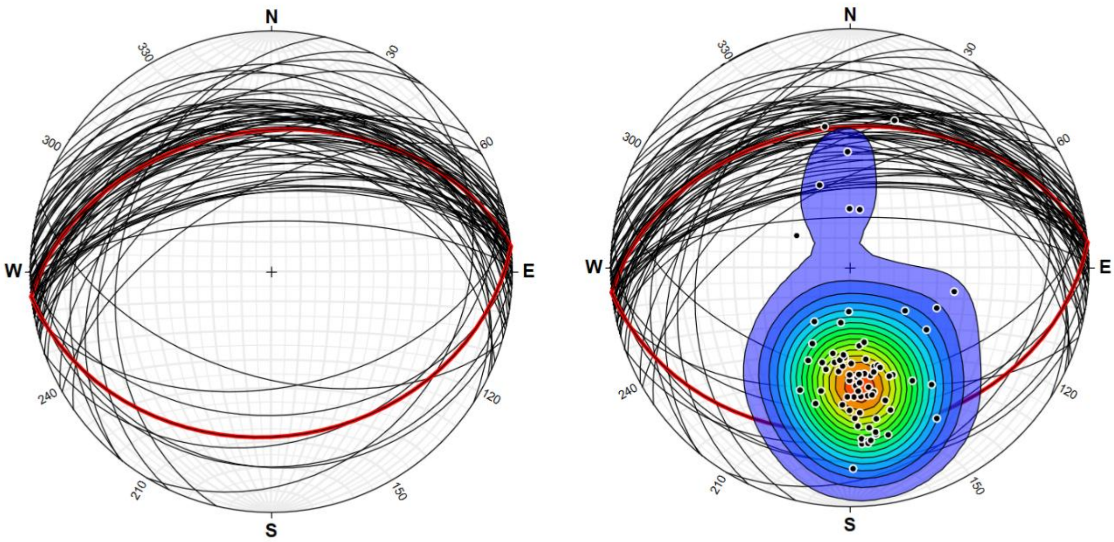

Figure 30: Stereonets of the bedding planes in the study area. Left: mean N and S limb planes of the synclinal. Right: Poles and planes with the Kamb contours.

The resulting fold axis is non plunging and striking E - W (165 - 85) and the axis plane is 355 / 90 (pole of axis plane: 355 / 0), so upright (vertical, non vergent). This means that the measurements indicate a cylindrical fold with upright (non-plunging) fold axis for the synclinal.

One fold was found in Tesero-Oolite (W od Seres creek) with plunge azimuth and plunge of 083 / 08. This fold axis is therefore regarded as a second order Negene fold as the fold axis is parallel to the Bronsara anticlinal and the synclinal around Corëtes creek.

Figure 31: Neogene fold in Tesero-Oolite with with plunge azimuth and plunge of 083 / 08.

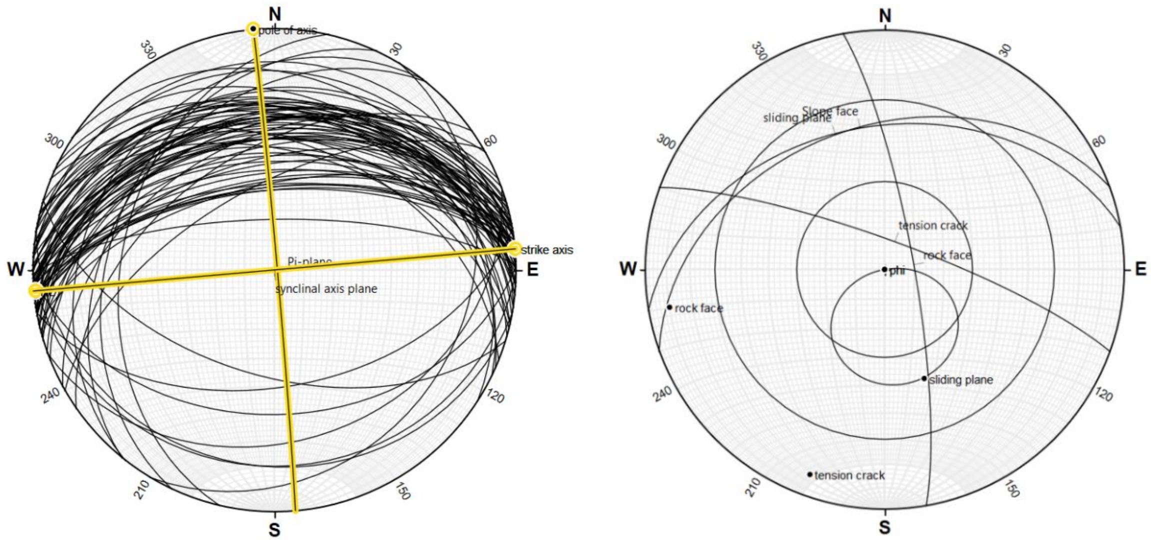

Figure 32: Left: Bedding data showing most measurements dipping N (N fold limb) and some measurements dipping S, building a synclinal structure resulting in E - W (165 - 85) striking fold axis. Right: Stereoplot showing boundary conditions for planar sliding of the fractured Schlerndolomite rock mass above the source area (S side).

Conditions for sliding are only partly fulfilled as slope surface (slope face) and sliding plane are parallel, as they both represent bedding surfaces of the Schlerndolomite. That means that the sliding plane was not daylighting until the colluvium material at the foot of the Ciancidel slope was eroded. As soon as the colluvium material got mobilized the sliding plane could daylight and condition for rock planar sliding of the fractured Schlerndolomite were fulfilled.

Regarding faults, no clear fault planes were observed in the field, but field observations suggest the assumption of two faults. The first is probably occurring along the NW-SE striking Seres valley as continuation of the Scharten graben on the northern side of Peitlerkofel. The formations east and west of Seres valley are possibly only displaced by a few meters, but the probable rightern strike-slip fault must still be verified here, also because (Jesacher, 1999) assumed the striking of this fault only in the upper Seres valley and then further east of it (cutting the two mass movements on the E valley side below Fornates). A second fault is with steep angle is assumed along the Corëtes channel, following the synclinal fold axis.

4.1.5 Hydrogeological Characterization

From a hydrogeological point of view the source area of the mass movement has a small (topographic) catchment area, as it is positioned just below the watershed. In this small catchment area the residual soil of the forested S side above the bedrock is just some dm thick, typical for subalpine slope terrains. Therefore, this small topographic catchment area cannot be the reason for transferring excessive water amounts to the source area.

In the source area several small water outlets (wet points) were observed at all field excursion days on the N slope of the source area (fig. 33). They are positioned in the upper part of the Zoppé-Sandstone and the dripping water leaves an about 5 to 10 m long wet line, at wet conditions a trickle developes in the gully. It is not usual to have water outlets at this side as the bedding is 30 - 40° towards N (anti-dip slope). This observation brings up the question if the water from these water outlets could be groundwater from the Peitlerkofel meadows which infiltrates to the Zoppé-Fm. and flows out in the source area as the synclinal is assumed to be very close to the source area (see section Geological Profile).

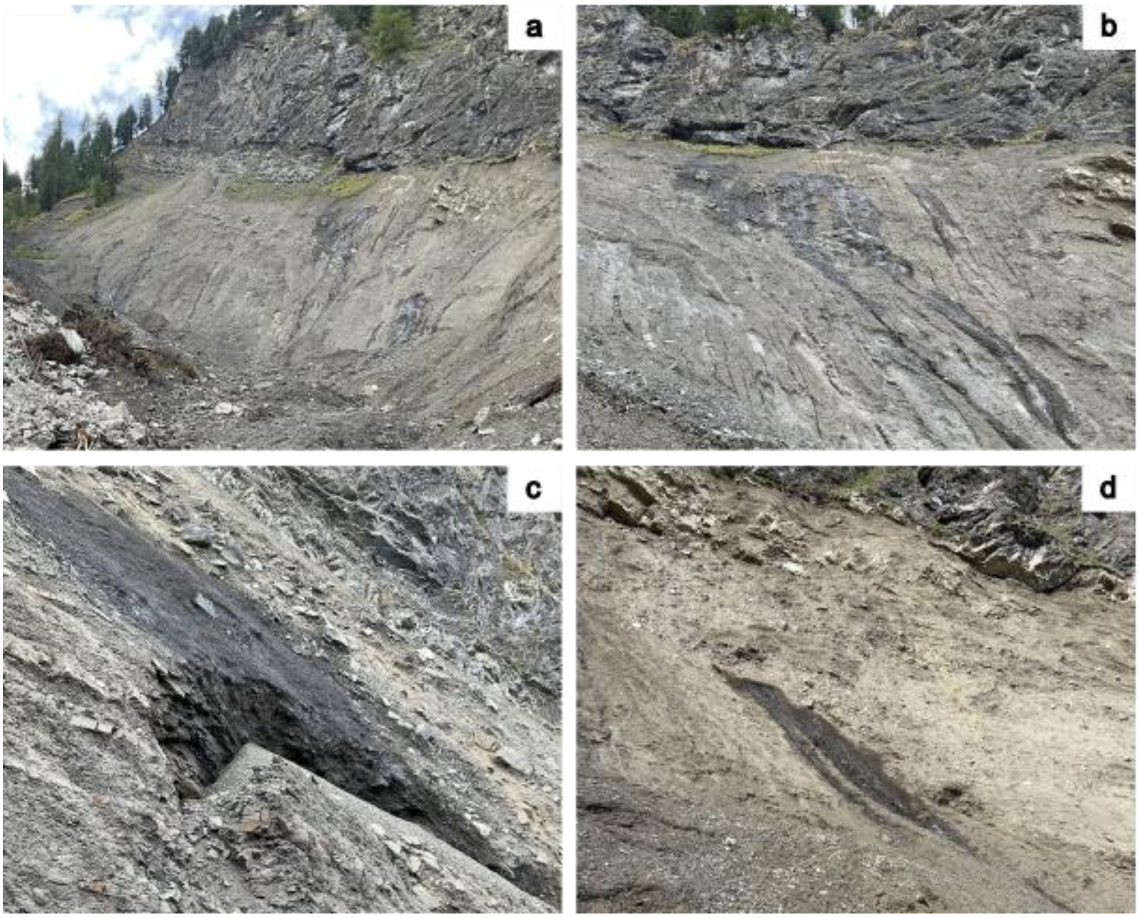

Figure 33: Water outlets on the N slope of the source area (anti-dip slope). a) overview of the different water outlets. b) water outler no. 2. c) water outler no. 4 shows probable local failure of Zoppé beds due to the destabilizing effect of water (reduction of shear resistance). d) water outlet no. 1.

4.2 Geomorphic Change Detection

GCD results are presented starting with the results for the new pre-event DTM and the LoD. In chapter 4.2.1 and 4.2.2. DoD maps and GCD histograms of erosion and deposition of the interested areas are shown. In chapter 4.2.3 cross-sections along and across the channel of the mass movement are shown.

The acceptable quality of the newly created pre-event 1 m DTM from the point cloud of 2006 is verified when comparing it with the 1 m DTM of 2024 which has a much higher point density of 150 points/m². The differences in the stable areas are minimal (see below), while bigger differences are restricted to steep rock cliffs. With this new pre-event DTM a much better DoD can be created as the georeferencing gets more accurate and the dZ of stable areas is constrained.

The georeferencing of the two epochs shows very good agreement (table 17). The remaining horizontal misalignment is within the sub-pixel range and is therefore clearly smaller than the DTM resolution of 1 m.

Table 17: Georeferencing results on 12 points (6 control points + 6 check points). enable = control point; non enabled = check point.

enable	dX	dY
1	0,1737	0,0551
0	-0,2332	0,1965
1	-0,4614	-0,1060
0	0,2275	0,0559
…	…	…
average	-0,0335	0,0194
stdv	0,2399	0,1335

The displacement in vertical direction (total average dZ) is dZ = 0,32 m. Consequently the pre-event DTM was elevated by this amount through the Raster Calculator. This low dZ result confirms that the two epochs are also well aligned in the vertical direction.

With dX, dY from georeferencing and dZ from zonal statistics tool in QGIS, the LoD for the GCD is calculated with standard error propagation theory:

$$LoD = \sqrt{(-0{,}034\ + 0{,}240)^2 +\ (0{,}019 + 0{,}134)^2 +\ (0{,}320 + 0{,}100)^2} = 0{,}5\, m$$

It must be noted that this approach strictly assumes spatially independent errors. In reality, spatially correlated errors do not average out over large areas as effectively as purely random independent errors. Although variogram-based analyses can resolve this issue, such geostatistical approaches were not applied here. Since the errors remain comparatively small (< 0,5 m) at a 1x1 m spatial resolution, it is assumed that the standard error propagation provides a sufficiently robust approximation and the impact of spatial autocorrelation is negligible relative to the actual geomorphic signal.

The LoD determines the smallest statistic significant volume change above the combined measurement uncertainty (noise) of the two DTMs. This means that only elevation changes exceeding 0,5 m are considered statistically significant geomorphological changes and included in the volume calculations.

The DoD map (fig. 34) delineates the geomorphic changes of the studied debris flow, as well as both older mass movements on the E side of the Seres valley. Erosion and deposition areas are clearly visible. Errors due to dZ differences of the two DTMs occur only in extreme steep areas like rock faces. Minor geomorphic changes apart from the mass movements can be individuated in the upper part of the Seres creek and in the Corëtes catchment, where shallow slide and flow events are captured by the DoD and are confirmed by the orthophoto. These observations allow to consider the DoD as qualitatively good.

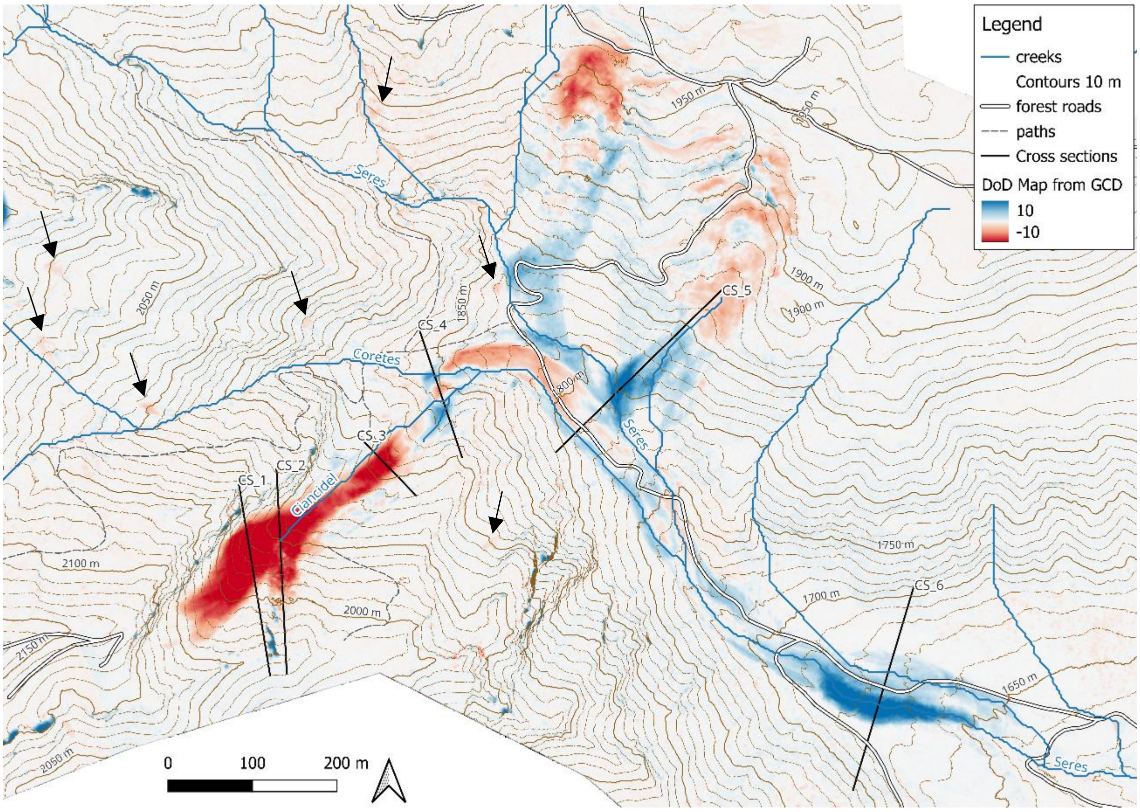

Figure 34: Geomorphic Change Detection (DoD map) showing erosion in red and deposition in blue together with the cross sections (CS_x) of chapter 4.2.3. Together with the debris flow of 2024 also the older mass movements on the E side of Seres valley show erosion and deposition areas. Note that the false GCD signals are restricted to only steep areas. Arrows indicate superficial slope erosion outside the observed mass movements, in the Coretes catchment the erosional areas correspond to small slide and/or flow type mass movements, which were verified in the field and through orthophoto.

The GCD evaluations have been performed on the (1) Debris Flow area, (2) Source area, (3) Debris translational slide and (4) Earth Flow - Earth Flow.

4.2.1 GCD Source Area and Debris Flow

The GCD shows erosion of up to 18 m in the source area and deposition of up to 12 m in the upper Seres fields (fig. 35 and table 18). For the debris flow volumetric relevant erosion occurred between -7 and -11 m, while deposition of material is between +1 and +5 m and around +12 m of material deposition at the deposition area in the upper Seres fields (fig. 36 and 37). There is a negative material imbalance towards erosion of - 6,7 %, which is attributable to the continuing material transport as mud flow further downwards towards Campill village and partly because of cleanup operations after the event.

Source area results show that 88 % of the total eroded material (158 952 m^3 out of 180 984 m^3) come from the source area, indicating minimal channel erosion in the Seres valley (tab. 18).

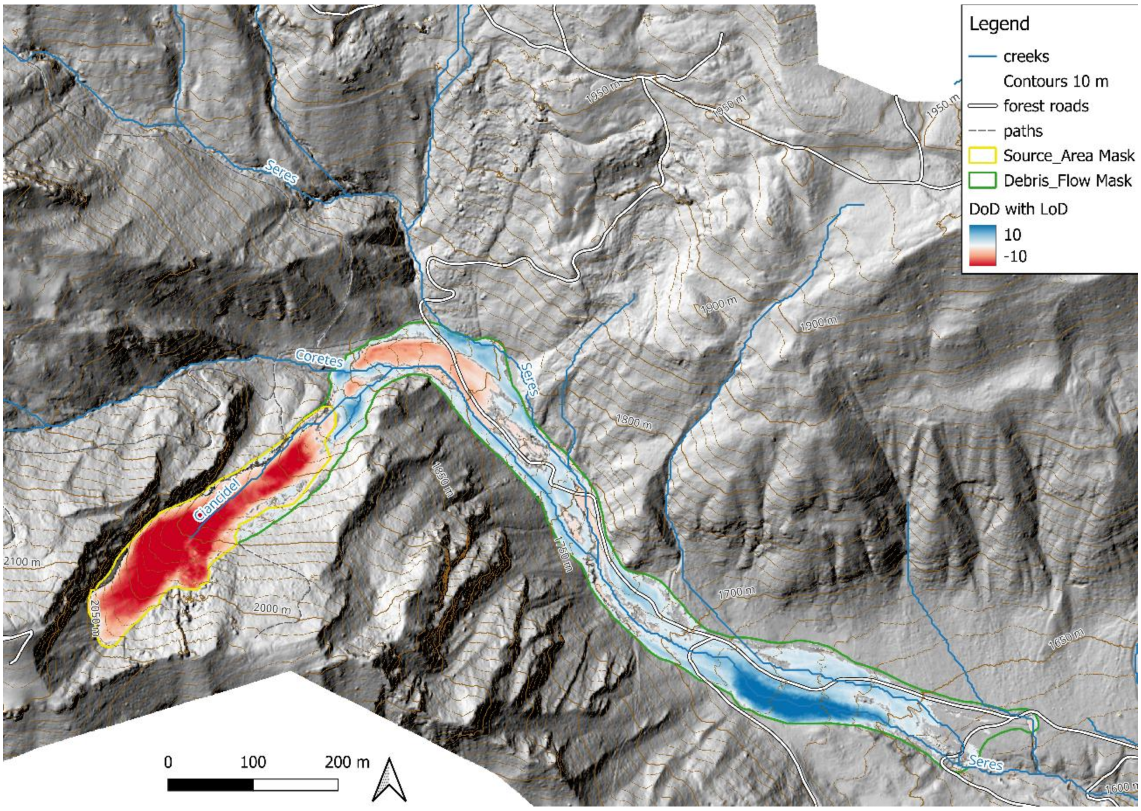

Figure 35: DoD map of the debris flow with LoD of 0,5 m and the masks of source area and debris flow used for the GCD in table 18. Background: Hillshade of post-event DTM.

Table 18: GCD results of the debris flow and source area.

GCD	**Debris Flow**			**Source Area**		
Attribute	Raw	With LoD	% Err.	Raw	With LoD	% Err.
	Area [m^2]			Area [m^2]		
Erosion	40 518	31 506		22 982	21 706	
Deposition	53 513	42 737		1 508	719	
Area of Interest	94 031	NA		24 490	NA	
Detected Change		74 243 (= 79 %)			22 425 (= 91,6 %)	
	Volume [m^3]			Volume [m^3]		
Erosion	182 785	180 984	8,7	159 267	158 952	6,8
Deposition	139 856	137 401	15,6	944	733	46,5
Difference	322 642	318 384	11,7	160 211	159 725	7,0
Net Difference	-42 929	-43 583	-60,9	-158 323	-158 179	-6,9
	Vol. %			Vol. %		
Erosion	56,7	56,8		99,4	99,5	
Deposition	43,4	43,2		0,6	0,5	
Imbalance	-6,7	-6,8		-49,4	-49,5	

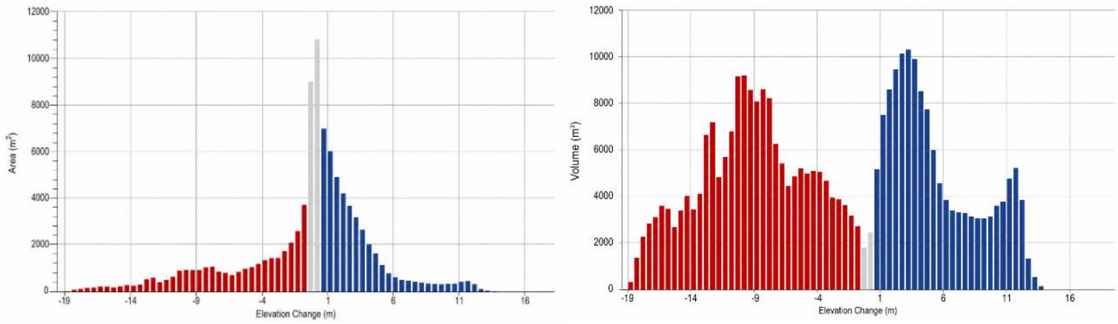

Figure 36: Debris flow areal and volumetric histograms for erosion (red) and deposition (blue) with the LoD of ± 0,5 m (grey).

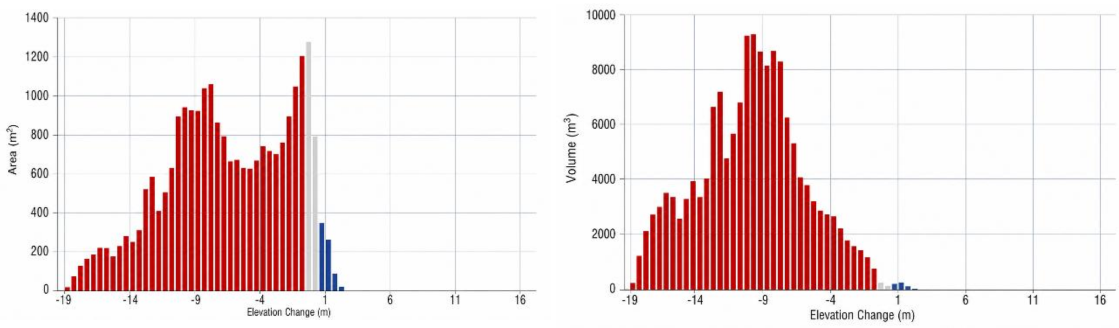

Figure 37: Source area areal and volumetric histograms for erosion (red) and deposition (blue) with the LoD of ± 0,5 m (grey).

4.2.2 GCD Debris Slide and Earth Slump - Earth Flow

For the debris slide and the earth slump - earth flow the results are given in table 19 and figure 38, 39 and 40. For the Debris slide, which occurred in 2013 the GCD recorded the difference between pre-event and post-event, while this is not the case for the Earth slump - Earth flow, which was active already before 1999 and thus before the pre-event DTM of 2006. Here the differences account only for the period between the two DTMs.

Other geomorphic changes apart from the mass movement can be observed from the DoD in the catchment of the Corëia channel and are confirmed by the Ortophoto. Hereby light fluvial erosion in the creek beds of Seres and Corëtes can be observed as well as the shallow slide and flow processes in the Corëtes catchment mentioned in chapter 4.1.2. Geomorphological Mapping.

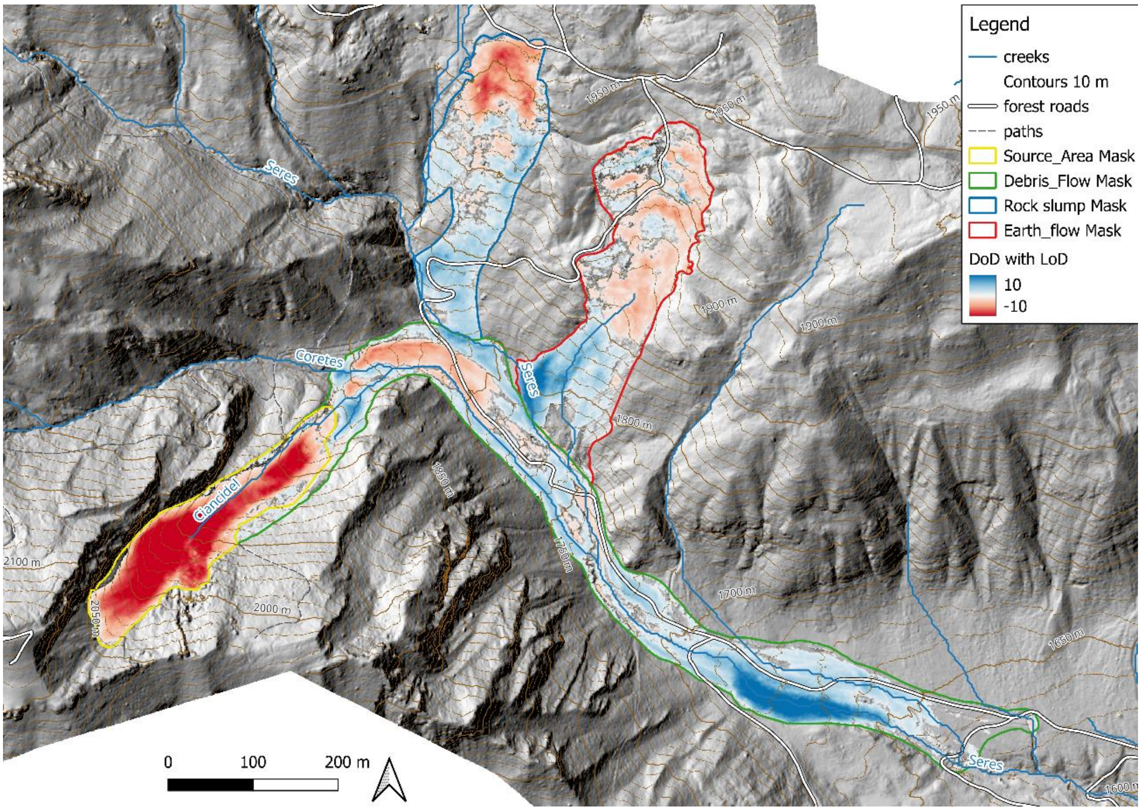

Figure 38: DoD map with LoD of 0,5 m of the debris slide and earth slump - earth flow on the E side of Seres valley together with the debris flow and the related masks used for the GCD in table 19. Background: Hillshade of post-event DTM.

Table 19: GCD results of the debris flow and source area.

GCD	Debris Slide			Earth Slump - Earth Flow		
Attribute	Raw	With LoD	% Err.	Raw	With LoD	% Err.
	Area [m^2]			Area [m^2]		
Erosion	12 437	10 116		21 340	15 872	
Deposition	19 148	16 302		19 553	15 367	
Area of Interest	31 585	NA		40 893	NA	
Detected Change		26 418 (= 83,6 %)			31 239 (= 76,4 %)	
	Volume [m^3]			Volume [m^3]		
Erosion	34 969	34 444	14,7	31 612	30 329	26,2
Deposition	42 077	41 372	19,7	48 681	47 701	16,1
Difference	77 046	75 816	17,4	80 293	78 030	20,0
Net Difference	7 108	6 928	138,5	17 069	17 372	63,6
	Vol. %			Vol. %		
Erosion	45,39	45,43		39,4	38,9	
Deposition	54,61	54,57		60,6	61,1	
Imbalance	4,61	4,57		10,6	11,1	

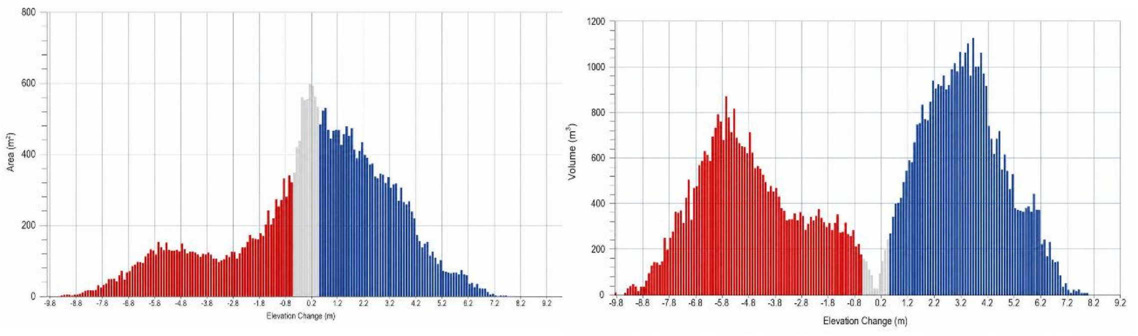

Figure 39: Debris slide areal and volumetric histograms for erosion (red) and deposition (blue) with the LoD of ± 0,5 m (grey). Relevant erosion occurred until -7 m and deposition until +6 m.

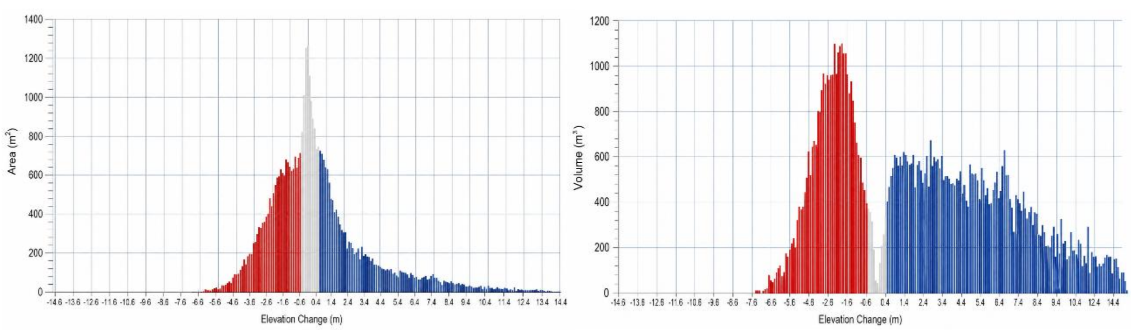

Figure 40: Earth slump - Earth flow areal and volumetric histograms for erosion (red) and deposition (blue) with the LoD of ± 0,5 m (grey). Relevant erosion occurred until -4 m and deposition until +8 m.

4.2.3 Cross-sections

Cross sections (CS) with pre- and post event profile lines are shown in fig. 40. CS_1 is going through the area where the highest erosion depth occurred (18 m). CS_2 is the same as the geological profile. CS_3 is cutting through the lowest end of the scource area. The pre-event profile line shows the probable deposition of unconsolidated sediments in the Ciancidel channel and the light incision of two little creeks mentioned in chapter 4.1.2 Geomorphological Mapping. CS_4 displays the lateral differences in erosion and deposition at the junction between Ciancidel and Corëtes channel. Again, the pre-event profile line shows the deposition of unconsolidated sediments in the Ciancidel channel which seems to get eroded by the mass movement of 2024. Here the first significant deposition volumes of the event occurred on the sides. It is probable that more material was transported and deposited in the core of the transportation path during the first earth-debris flow event, but later during the remobilization as muddy debris flow through water infiltration of the Corëtes creek that material was transported downwards. CS_5 is the cross section for the Geotechnical analysis of the Earth slump - earth flow (chapter 4.3.2.2). At the time of the pre-event DTM the earth slump - earth flow on the E side was already active but from the post-event profile line it seems that in the recent years more material accumulated at the foot. CS_6 shows the deposition thickness at the deposition zone. On the N side (orographic left) deposited material thickness is several dm to some meters, while in the Seres creek bed the deposited material thickness is about 10 to 12 m.

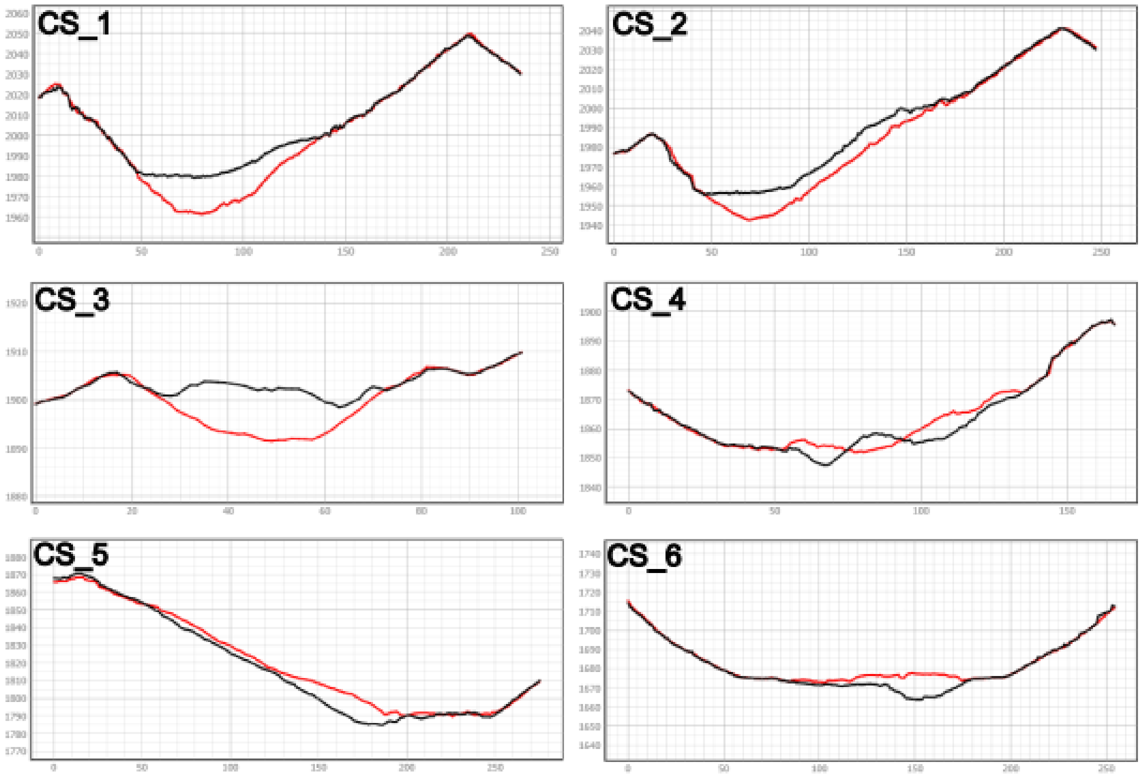

Figure 41: Cross sections with the map view in figure 34. CS_2 = Geological Profile and CS_5 = Geotechnical analysis of the Earth slump - earth flow (chapter 4.3.2.2).

4.3 Geotechnical Model

4.3.1 Geomechanical Evaluation of Parameters

Table 20 shows the results of the different laboratory tests performed on chosen samples.

Table 20: Results from the geotechnical laboratory tests. Abbreviations: XRD = X-Ray Diffraction, SDI = Slake Durability Index [%], LL = Liquid Limit, PL = Plastic Limit, PI = Plasticity Index have as unit water content in %, while LI = Liquidity Index is dimensionless.

Sample	Lithology	XRD	SDI [%]	LL [%]	PL [%]	PI [%]	LI [-]	water c. [%]
1.	Debris Flow Material	x		34,9	14,9	20,0		
2.1.	Schlerndolomite sliding surface		98,2					
2.2.	Residual soil at Schlerndolomit sliding surface	x		38,4	12,8	25,6		
3.	Sandstone at sliding surface (light grey-green)	x	90,2	42,0	17,8	24,2	0,06	19,2
4.1.	Zoppé-Sandstone, residual soil	x						
4.2.	Zoppé-Sandstone, residual soil	x						
4.3.	Zoppé-Sandstone bank		98,2					
4.4.	Zoppé-Sandstone, weak material between competent banks	x						
6.	Zoppé-Sandstone, residual soil	x						18,0 & 13,4
7.	volcanoclastic- carbonatic rocks (Wengen-Fm.)	x	96,8					

(dark grey)	rock sample	
(light grey)	rock & soil sample	
(white)	soil sample	

4.3.1.1 Grain size distribution

Although large boulders are present in the debris-flow deposit, the flow behavior is primarily controlled by the fine-grained matrix (Iverson, 1997; Hungr et al., 2014). Therefore, boulder content was excluded from the grain-size analysis and the remaining grain sizes were renormalized. According to DIN EN ISO 14688-2, the material remains classified as silty-sandy gravel.

According to DIN EN ISO 14688-2, the soil is classified as stony silty sandy gravel (Gm,s + St or siSaGr) or as GM (silty gravel) according to USCS soil classification. The particle size distribution consists of approximately 9.6 % stones, 42 % gravel, 22.6 % sand and 25.8 % silt. Even after normalizing the grain size distribution by excluding the block fraction the classification remains the same.

The debris flow material is dominated by medium to fine gravel (mG - fG) with significant silt content and sand. Note that blocks were not included and a part of the finer fractions (silt and clay) maybe has been washed away during the three months between the event and sampling at the 25th September 2024.

The very high CU indicates a very well graded material (= poorly sorted) of coarse grained material with sand and significant silt content which influences hydraulic conductivity and reduces shear strength due to water content (saturation) sensitivity.

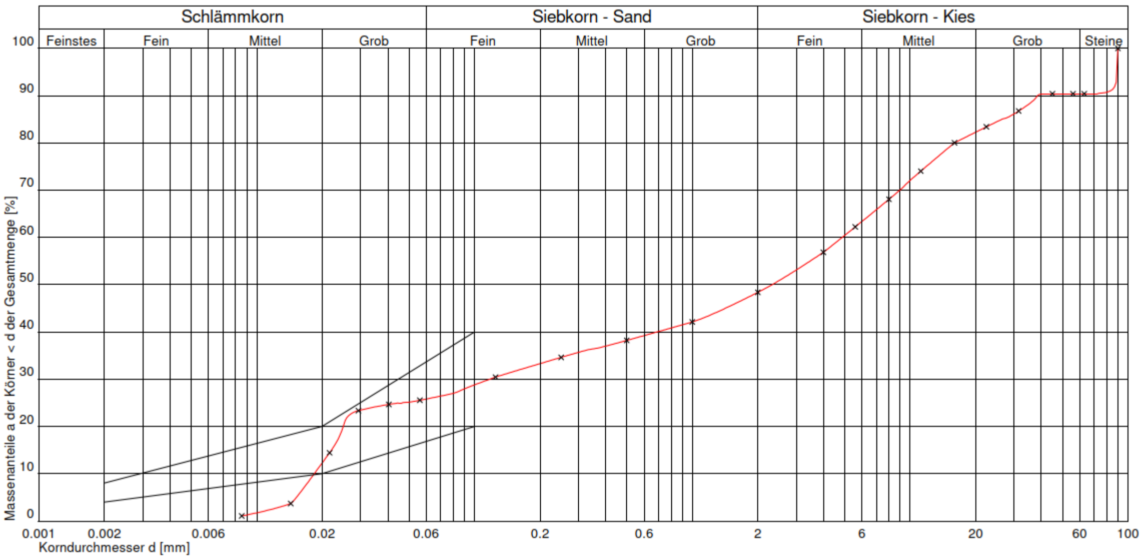

Figure 42: Grain size distribution curve for the debris flow material (sample 1).

Table 21: Results for the grain size fractions and derived parameters.

Grain size	**Amount [%]**	**Normed without blocks after DIN EN ISO 14688-2**
Clay (C)	**0,00**	
Silt (U / M)	**25,8 %**	**28,5 %**
fine / medium / coarse	0,0 - 12,3 - 13,5	
sand (S)	**22,6 %**	**25,0 %**
fine / medium / coarse	7,5 - 5,9 - 9,2	
Gravel (G)	**42,0 %**	**46,5 %**
fine / medium / coarse	15,0 - 18,9 - 8,1	
stones / blocks (St.)	**9,6 %**	
d_{10} =	0,02	
d_{30} =	0,12	
d_{50} =	2,2	
d_{60} =	4,88	
$C_U = d_{60}/d_{10}$ =	265	
C_C =	0,15	
grain or particle density: ρ_S	2,68 g/cm³	
hydraulic conductivity k_f	7,4 * 10^{-7} m/s	

Due to the very well graded material (Cu = 265) empirical estimations for hydraulic conductivity from the grain-size distribution (e.g. Hazen, Beyer or USBR method) cannot be applied, as they are primarily valid for uniform soils (Urumović et al., 2020). Consequently, these methods would lead to unreliable estimates of hydraulic conductivity, typically underestimating values due to the dominance of the fine fraction. Thus, the estimated hydr. cond. $k_f = 7{,}4 * 10^{-7}$ m/s is to interpret as a minimum value.

This grain size distribution classifies the debris flow material as mixed-debris, matrix-supported debris flow after (Jakob & Hungr, 2005).

The material from the debris flow deposit is classified, following (Cruden & Varnes, 1996; Varnes, 1978), as matrix-supported mixed debris. The particle size distribution exhibits dominant coarse fractions embedded in a fine matrix of silt and sand. From a rheologic point of view it can be classified as a viscoplastic debris flow.

4.3.1.2 Slake Durability Index (SDI)

The most important result is that the easily weathering siltstones between the more competent banks of the Zoppé-Sandstone could not be tested, as this lithology was already disintegrating when holding it or barely crushing it in the hands during the field sampling. This rock type is classified as having medium - low slake durability.

Table 22: Results for Slake Durability Index (SDI)

Sample	Lithology	SDI_2	Durability after Gamble, 1971
2.1.	Schlerndolomite sliding surface	98,2	Very high
3	sandstone at sliding surface (Zoppé-Fm)	90,2	Medium high
4.3.	Siltstone bank (Zoppé-Fm)	98,2	Very high
4.4.	Weak siltstone between banks (Zoppé-Fm.)	-	Interpreted as medium - low
7	Carbonatic-volcanoclastic rock (Wengen-Fm.)	96,8	high

4.3.1.3 Liquid- and Plastic Limit

In general sample 1, 2.2 and 3 show PL around 13 - 18 % and LL between 35 - 42 %. According to the Unified Soil Classification System (USCS), LL below 50 % indicate soils of low plasticity (L), typically associated with intermediate silt dominated soils. Also, the PL values are low which means that soil becomes plastic already at low water contents. According to these indices, the investigated materials can be classified as low-plasticity fine-grained soils.

Sample 3 (residual soil derived from Zoppé Sandstone) exhibits a LL of 42 % and was in a plastic state at the time of sampling. Such values are characteristic of silt - clay soils.

However, the PI´s range between 20,0 % and 25,6 %, which corresponds to high plasticity soils according to common geotechnical classifications (PI = 17 - 35 %).

This suggests a significant influence of clay minerals on the mechanical behaviour.

The results indicate a silt - clay mixed residual soil that shows comparatively high PI despite moderate LL due to low PL controlled by the clay fraction.

Regarding the slope stability, soils are regarded as stable in the solid and semi-solid state, in the plastic state (0 < LI < 1) shear strength gets reduced and becomes increasingly reduced at higher water contents (at or above LL ≙ LI >= 1). While water content and water pore pressure (u) increases, effective stress (σ´), cohesion (c) and shear strength (τ) decrease after the Mohr-Coulomb criterion.

Overall, these results show that the residual soils in the source area contain some clay amount which expresses in a plastic soil mechanic behavior of the soil resulting from the weathering of the arkosic, turbiditic Zoppé sand- and siltstones. The relatively moderate LL measured for the Zoppé derived residual soil imply a high sensitivity to water under already moderate moisture conditions and a relatively low threshold towards the (viscous) liquid state.

4.3.1.4 Mineralogy (XRD - Analysis)

The mineralogical content of the Zoppé-Fm. samples in the source area (samples 4 to 6) show moderate quartz contents of about 22 - 29 %. The quartz content reflects the metamorphic protolites of the Zoppé-Fm. The originally arkose composition (> 25 % feldspar) is depleted in feldspar (mainly plagioclase), but high content of clay minerals (considerable vermiculite and minor kaolinite) and mixed-layer minerals (MLM), indicate weathering of feldspar.

Vermiculite typically forms from alteration of mica (e.g. biotite) or mafic minerals.

Sample 4.4. is in-situ bedrock, while samples 4.1., 4.2. and 6 are regolith soil.

Sample 3 sandstone of Zoppé-Fm. has beneath quarz also muscovite, which matches well with the partly metamorphic basement origin/protolites of the Zoppé-Fm. before erosion and turbiditic transport and deposition towards the Dolomites. The high smectite amount indicates chemical alteration (hydrolysis) of the plagioclase and can also occur form volcanic protolite material.

Kaolinite typically forms by strong leaching and hydrolysis of feldspars (especially K-feldspar and plagioclase) as well as biotite or volcanic tuff. Through intense chemical weathering elements like K, Na and Ca are removed and residual Al-rich phase remains, forming Kaolinite. Kaolinite reflects more advanced alteration than vermiculite and smectite.

Mixed-layer minerals (MLM) or interstratified clay minerals, are stacked layers of different clay mineral types within the same crystal structure. They are not pure minerals, but hybrid/transitional phases, typically formed during mineral transformation (Moore & Reynolds, 1997). The mixed-layer minerals in Zoppé-Fm. are most likely smectite, illite and vermiculite interstratifications, formed during incomplete diagenetic transformation of volcaniclastic material (glass).

The occurrence of clay minerals indicate strong chemical weathering through water (hydrolysis) of the Zoppé-Fm in the source area.

Wet smectite and vermiculite have a swelling behavior when hydration of the crystal lattice occurs, while shrinkage occurs during dry conditions (evaporation of water). Such effects also leads to strength loss within the clay minerals.

Debris flow material (sample 1) shows a composition similar to the regolith of the Zopp´s-Fm. Sample 7 from the source area of the Earth slump shows a marly limestone composition with siliciclastic and clay (vermiculite) content, which is in accordance with carbonate-dominated lithologies of the upper Wengen-Fm.

Table 23: Mineralogic composition of the samples in % after XDR-Analysis. Tr. = traces.

Sample no.	Lithology	Quartz	Muscovite	Chlorite	Plagioclase	K-feldspar	Calcite	Dolomite	Mixed Layer Minerals	Vermiculite	Kaolinite	Smectite	Sum
1	Debris Flow Material	25	2	3	12		14		32	12			100
2	regolith at Schlerndolomit sliding surface	10	1	1	8	4	21	27	17			11	100
3	Sandstone at sliding surface (light grey-green)	13	6	?		4	13	12				52	100
4.1	Zoppé-Sandstone, Regolith	23	Tr.	?	10		11		52		4		100
4.2	Zoppé-Sandstone, Regolith	29	Tr.	?	11				35	22	3		100
4.4	Zoppé-Sandstone, weak material between competent banks	22	Tr.		10		11		28	23	6		100
6	Zoppé-Sandstone, Regolith	26	Tr.		17		23	3	9	14	5	3	100
7	volcanoclastic- carbonatic rocks (Wengen-Fm.)	14			9	2	60			15			100

4.3.2 Geotechnical Hazard Evaluation

For the slope stability analyses material parameters as shown in table 24 were used.

Table 24: Parameters for slope stability analysis in GEO5.

Parameters	Block field	Bedrock	Colluvium = Earth Flow deposit
Unit weight γ [kPa]	20	25	21
Sat. Unit weight γ_{sat}	21	-	22
Friction angle φ	37	35	30
Cohesion c	3	500	5

4.3.2.1 Col Ciancidel

The profile lines of the pre- and post-event DTMs showed not only erosion of the colluvium material in the gully but also about 5 - 7 m heigh slope deposit, which from the ortophoto look like block size dominated material. As after the event, the SW slope of Col Ciancidel exhibits the sliding plane (Schlerndolomite), the post-event DTM was approximated as the sliding plane.

For the Col Ciancidel profiles it was tried to reconstruct the most likely failure scenario, hereby the question was what was more likely to fail first: The debris material in the gully or did blocks from the block field fell first on the debris material and then the debris slump/gullying started? Therefore, two scenarios of slope stability analysis were simulated: One with the debris material in the gully and with a groundwater level in the debris and block field, the other scenario considers the prior erosion of the debris material, so it is simulated without debris material in the gully. The results are shown in table 25.

Table 25: Slope stability results with GEO5 Software of the different scenarios for Col Ciancidel Profile.

Scenarios	FOS
with Colluvium + no water	1,16
no Colluvium + no water	0,94
with Colluvium + with water	
GW = 0,5 m	1,14
GW = 1 m	1,12
GW = 2 m	1,08
no Colluvium + with water	
GW = 0,5 m	0,90
GW = 1 m	0,88
GW = 2 m	0,83

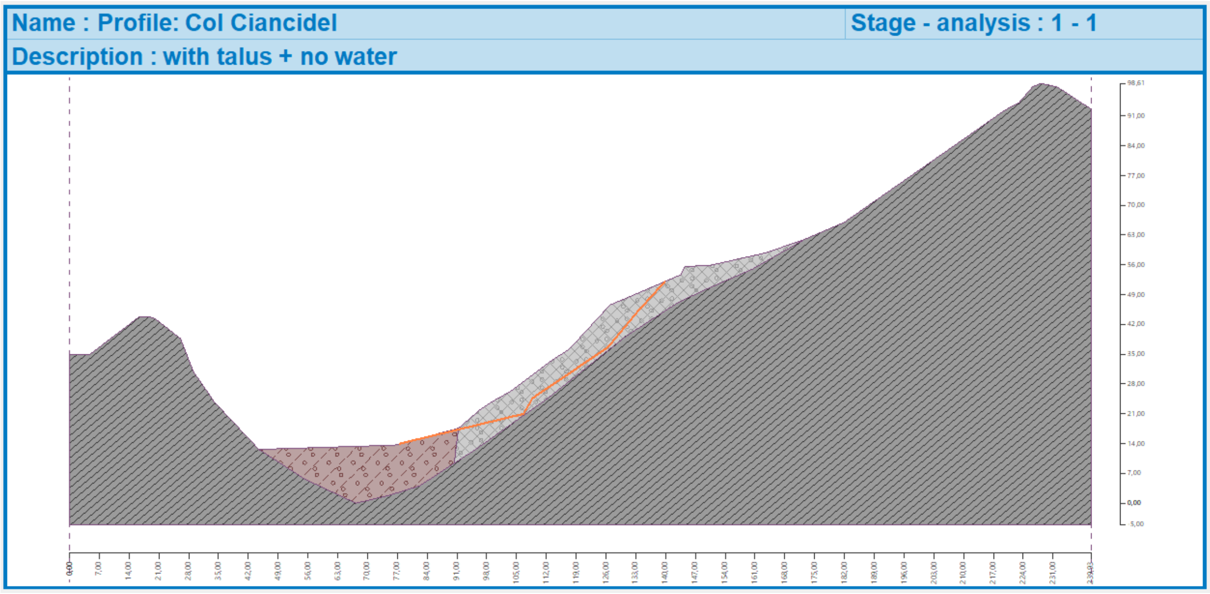

with Colluvium + no water	1,16

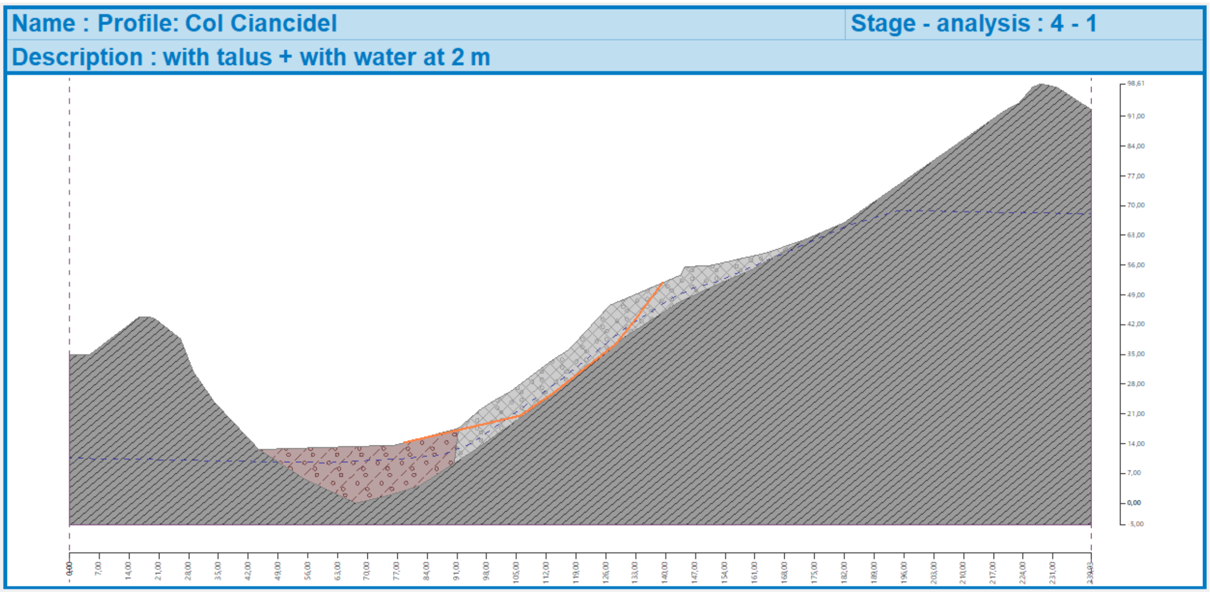

with Colluvium + with GW at 2 m	1,08

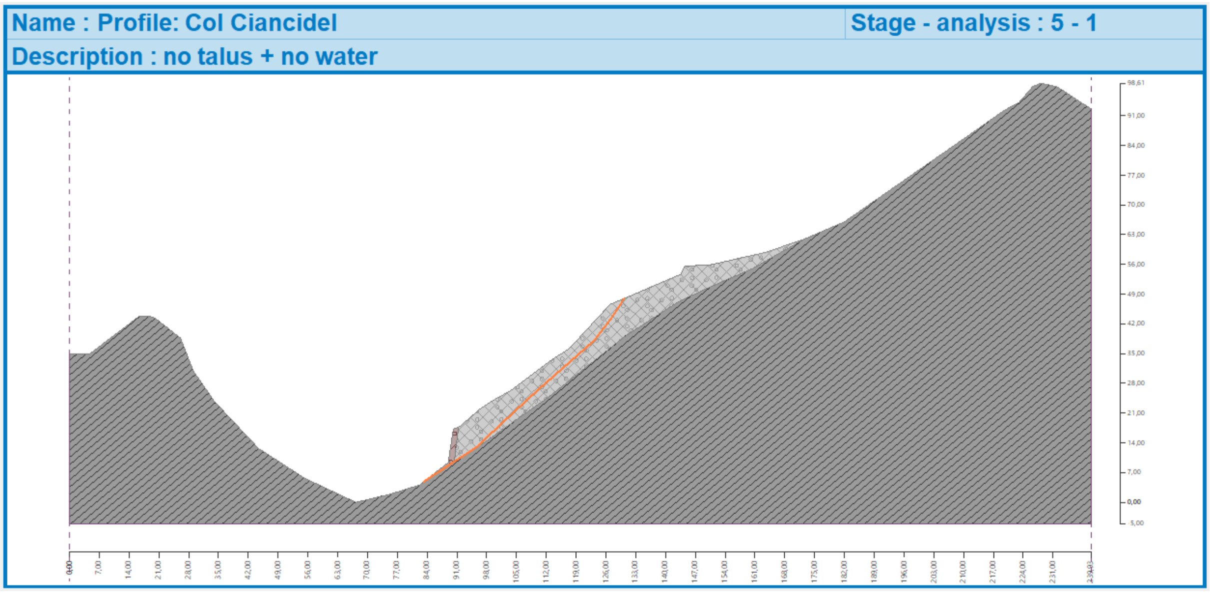

no Colluvium + no water	0,94

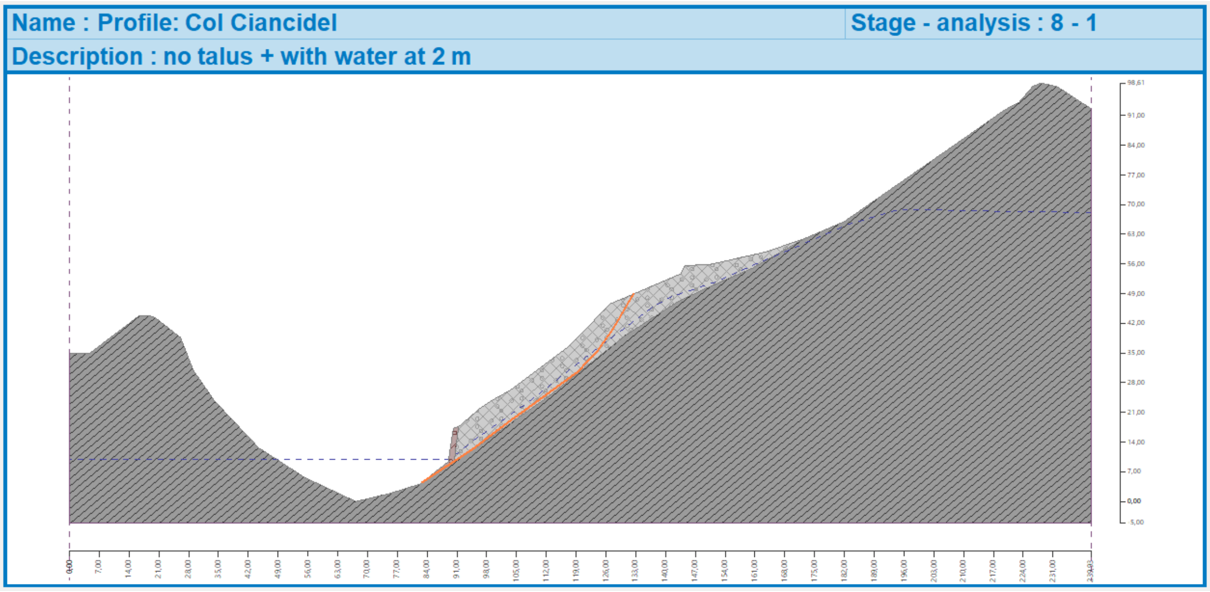

No colluvium + with GW = 2 m	0,83

For the scenario with colluvium in the gully the failure surface does not develop further into the colluvium material but breaks out above the colluvium material. This would mean that, if this scenario would have been the one occurring, the block field material would have slided on top of the colluvium material and consequently would have been transported with the mass movement.

The results indicate that, assuming the adopted soil parameters, the colluvium slope most probably have already failed and have been mobilized before the block field became unstable (difference in FOS of approx. 0.2). All simulations without colluvium exhibit unstable results, which leads to the conclusion that the colluvium material in the gully was most probably first mobilized.

This interpretation is consistent with field observations, which show that the white blocks of Schlerndolomite have slid into the source area and remain there, rather than having been transported downslope by the debris flow, as would have been expected if they had reached the moving mass earlier.

Based on these back-analysis stability calculations, it can be inferred that the colluvium mass most probably failed first, followed by a destabilisation of the block field at Col Ciancidel.

Furthermore, the failure surface within the block field does not propagate all the way upslope. Instead, blocks located on the slightly less steeper middle part of the slope became unstable at a later stage due to the loss of support. This process was also observed in the field, where blocks repeatedly become unstable above the exposed sliding surface as a result of gravity-driven and time dependent loss of strength, deformation and subsequently slide along the sliding surface into the source area.

4.3.2.2 Earth Slump - Earth Flow

The depth to intact bedrock in this profile is not clearly visible in the field, as in the surrounding area bedrock is only cropping out at a few spots and is mainly covered by slope sediments. The bedrock was drawn about 1 m below the profile line of the pre-event DTM of 2006, at this time the earth slump - earth flow was already active (according to orthophoto, since at least 1999). The different analyzed scenarios with varying groundwater table and creek incision are shown in table 26.

In the case of a potential stream incision at the toe of the earth flow, slope stability in the lower part becomes critical once an incision depth of approximately 3 m is reached. Assuming a cohesion value of c = 3 kPa, critical stability conditions are already reached at a 2 m incision in the lower part, while an incision depth of about 3 m would be sufficient to trigger reactivation of the entire earth flow.

Overall the calculated stability values appear relatively plausible, as instability is predicted exactly in those situations where movement has occurred. The FOS decreases with increasing groundwater level, progressive channel incision or decreasing cohesion.

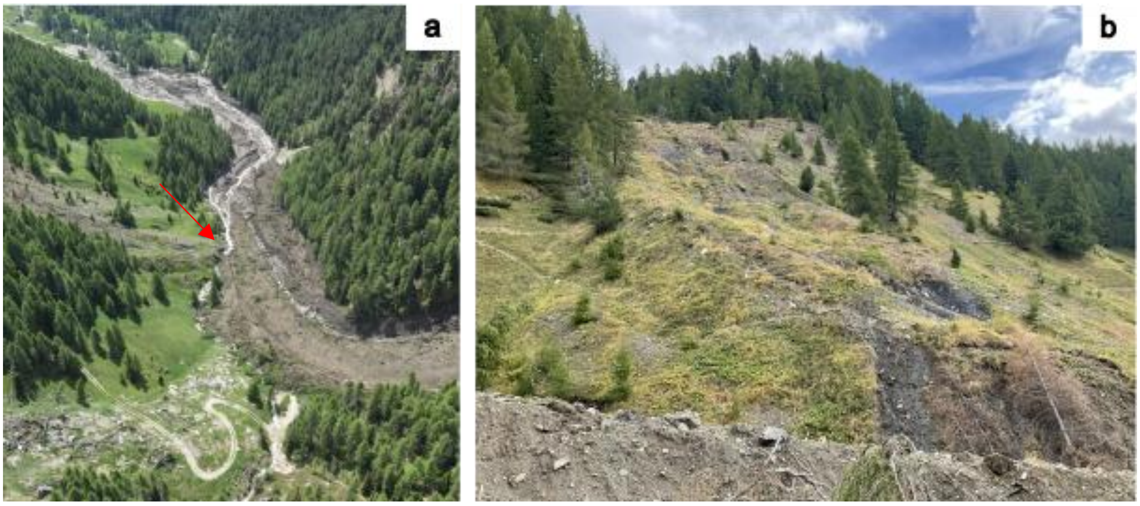

Figure 43: Slope Stability analysis for the reactivation of the Earth Slide - Earthn Flow orographic left of Seres creek. a) aerial image from the Seres valley showing the shift of the Seres creek to the E valley flan where the creek erodes the foot of the Earth Slump - Earth Flow (red arrow). b) lower Earth Flow part of the Earth Slide - Earth Flow mass movement photographed from the Seres valley.

Table 26: Slope stability results of the different scenarios for Earth Slump - Earth Flow Profile.

	c = 5 kPa		c = 3 kPa	
	whole profile	lower part	whole profile	lower part
no water	1,43; 1,46		1,43	
with water	1,13		1,09	
1 m creek incision	1,12	1,17	1,09	1,08
2 m creek incision	1,10	1,10	1,06	1,03
3 m creek incision	1,08	1,02	1,03	0,96

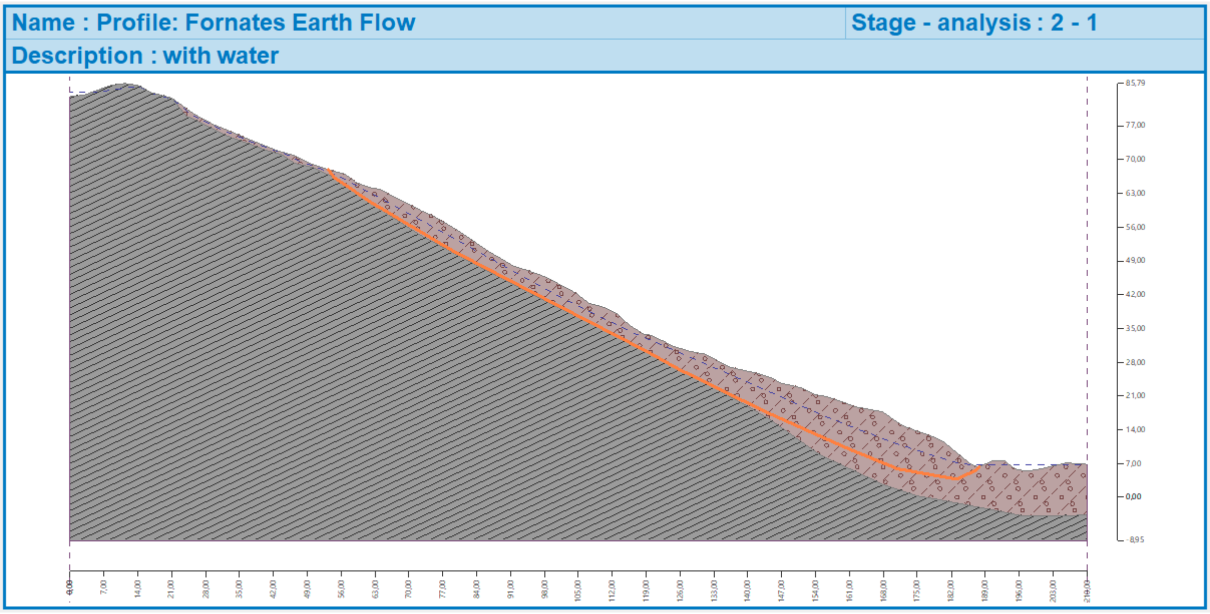

with GW	1,13 - 1,09

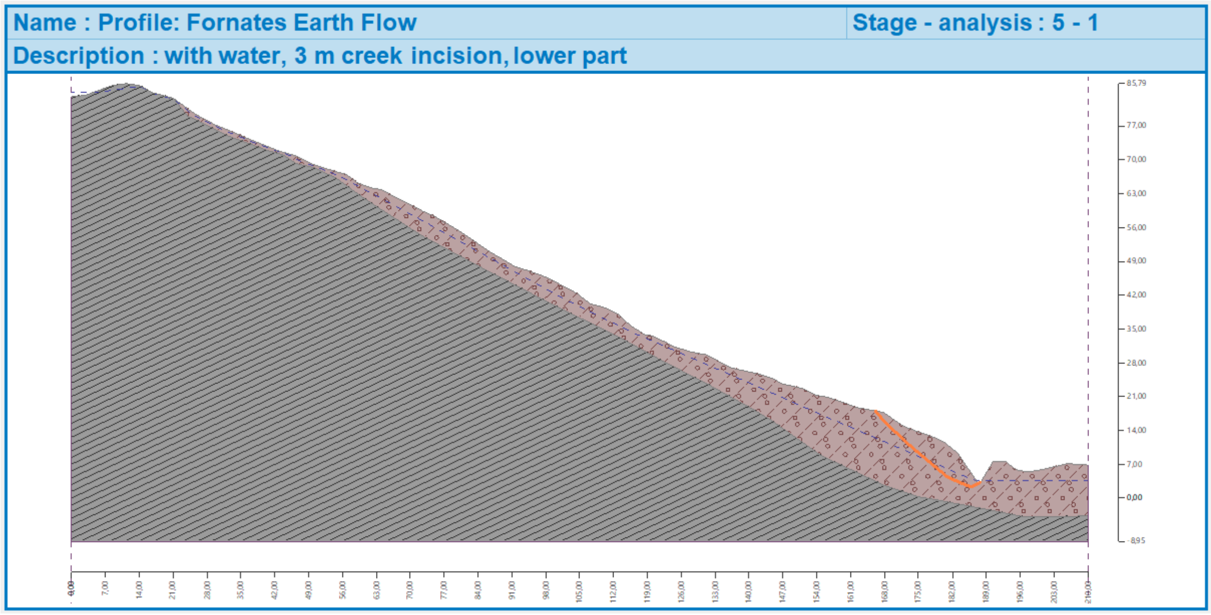

with GW and 3 m creek incision	1,02 - 0,96

4.4 Analysis of Meteorological Data

First, the results of the different parameters are presented and then they are put together to evaluate the triggering factors of the mass movement.

4.4.1 Precipitation

From a long-term point of view, the station of St. Martin recorded a higher frequency of years with more than 1000 mm of precipitation in the last 10 - 15 years. Also, the 10 year mean of 2014 to 2024 of 916 mm is above the 100-year long term mean of 790 mm, indicating a light increase of annual precipitation totals.

In the medium- and short-term, precipitation amounts before the event resulted as significantly high. Two periods were evaluated:

- January to June 30th (6 months period)
- March to May 31st (3 months period)

The precipitation in 2024 in both analysed periods was the 3rd highest since beginning of weather recording, after 1926 and 1975. By mid-June, the cumulative precipitation since the beginning of 2024 reached 490 mm, corresponding to an increase of 215 mm (+78 %) relative to the long-term mean (275 mm) and compared to the 10-year mean (2014 - 2024) an increase of 175 mm (+ 56 %) relative to 315 mm. The return period T for the period January to June after Weibull is 33 years. Moreover, the month of May 2024 was the rainiest since the beginning of weather recordings. In the months before the event, the precipitation of March was above the 90-percentile, April was close to average, May was the rainiest since weather recordings and June was again above the 90-percentile. Also, the weather stations nearby (Seiser Alm, St. Peter Villnöss and Stern) show record like precipitation in May (150 to 220 mm) and above the 90-percentile in March (75 to 120 mm) and June (130 - 160 mm). These statistical evaluations indicate a highly significant precipitation record in the months before the event.

Looking at the shorter-term daily precipitation timeline, from 13th of May 2024 until 17th of June it rained 28 out of 34 days (fig. 44). Through the positive temperatures at Kreuzkofeljoch 255 mm fell accumulated as rainfall in this 34 days before the event. The precipitation event in the days before the mass movement lasted 6 - 7 days and brought about 77 mm of rainfall, which is a considerable amount, but not statistically extraordinary. The cumulative precipitation diagram of 2024 displays the steep increase in precipitation between mid-May and mid-June before the event (fig. 45).

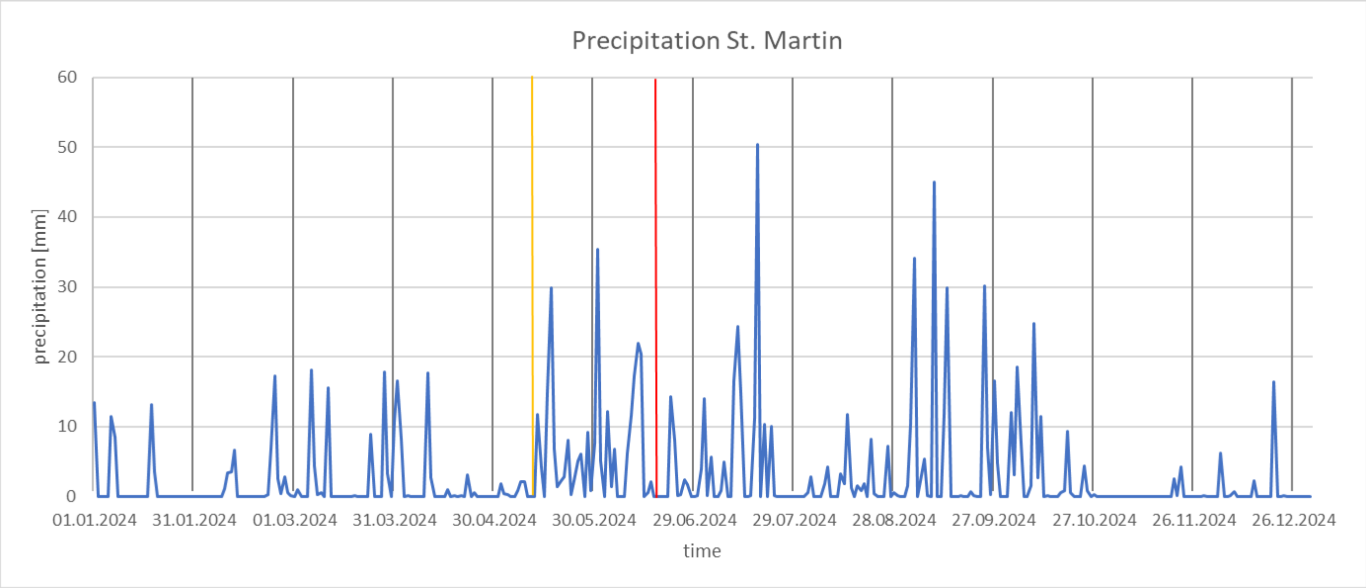

Figure 44: Precipitation record of 2024. The period before the event (between yellow and red line) registered intense precipitation, resulting in the rainiest May since weather recordings in St. Martin.

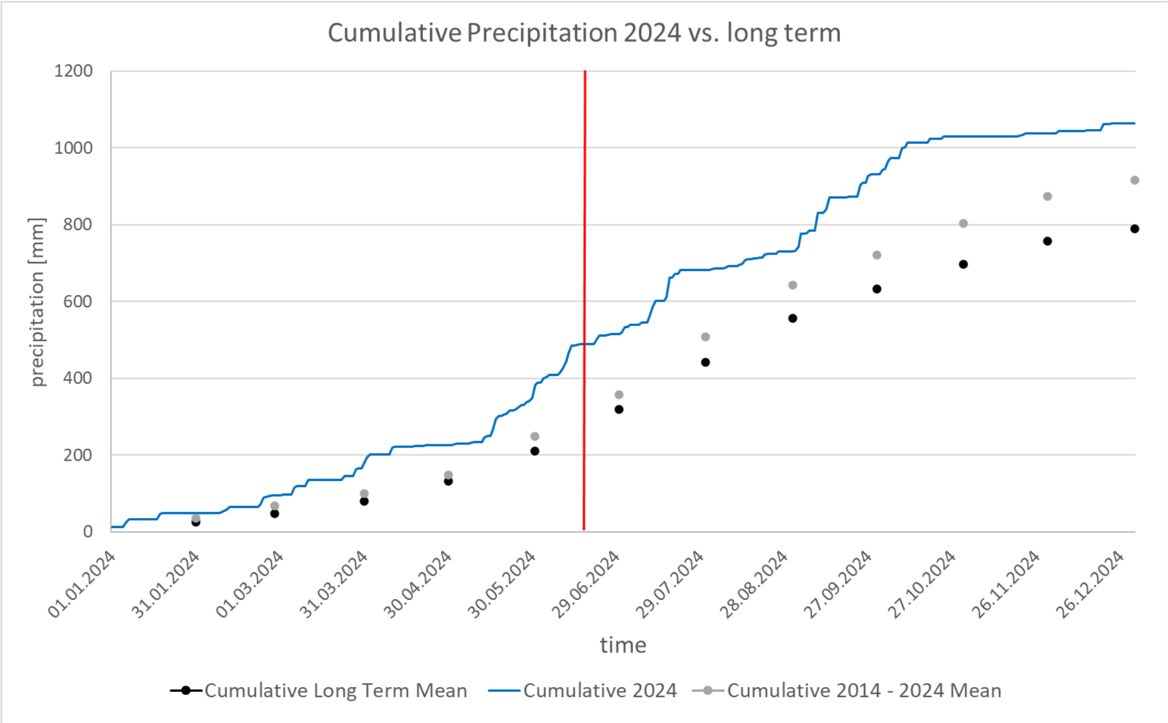

Figure 45: Cumulative precipitation over the year 2024 at St. Martin. 2024 cumulative precipitation vs. long term cumulative mean and last 10 years (2014 - 2024) cumulative mean.

Table 27: precipitation statistics of station St. Martin. Values above 90-Percentile are marked with red font colour and record months have yellow shading.

Months	01	02	03	04	05	06	07	08	…	Sum	March-May	Jan.-June
…												
2023	25,5	3,8	18,3	54,5	155,5	48,2	**285,4**	120,5	…	1013	228	306
2024	50,0	45,9	80,8	50,1	**156,4**	132,5	167,3	48,3	…	1063	287	516
mean	***25,3***	***22,8***	***32,5***	***52,1***	***78,1***	***108,3***	***122,2***	***115,3***	**…**	***790***	**163**	**319**
90_ Percentile	**50,2**	**50,6**	**69,2**	**91,8**	**124,6**	**158,7**	**167,3**	**178,4**	**…**	**1.015**	**286**	**423**
Cum. long term mean	**25,3**	**48,1**	**80,6**	**132,7**	**210,8**	**319,1**	**441,3**	**556,6**	**…**	**789,8**		record month
Cum. 2024	**50,0**	**95,9**	**176,7**	**226,8**	**383,2**	**515,7**	**683,0**	**731,3**	**…**	**1.063**	red	above 90-Percentile

4.4.2 Snow Melt

Snow height timeline of Kreuzkofeljoch station in 2024 indicates when snow melt occurred. From the graph it appears that snow height increased to its maximum value of 140 cm at the beginning of April. During April three snowfall events brought additional 35 cm of snow. The snow melt occurred during April until mid of May (fig. 46), providing water to the system in a period where rainfall was slightly below average. For the accumulated snow depth of 140 cm during winter, an average snow density for typical late-winter snow of 300 kg/m³ was assumed for the Snow Water Equivalent (SWE) calculation. The 35 cm of fresh snow during the snow melt period were added to the SWE with a snow density assumption of typical fresh snow (50 kg/m³). In total 437 mm/m^2 (= L/m^2) resulted from the snow melt. Table 28 shows the combined amounts of precipitation in St. Martin and SWE of Abtei Piz La Ila for the spring period (21.03 - 21.06) of the last 10 years. 2024 resulted as the year with the highest value of combined precipitation and snow melt water of the last 10 years.

As snow height at Kreuzkofeljoch is continuously recorded only from 2023 onwards, snow height records for statistical evaluations have to be analysed from Abtei Piz La Ila station at 1997 m.s.l.. This station shows very good correlation of 0,93 with Kreuzkofeljoch for 2024 as they recorded the same snowfall events with similar values, only the snow melt starts one to two weeks earlier in Abtei Piz La Ila station. Snow height in Abtei Piz La Ila in 2024 showed average values compared to the recorded period of the last 10 years, so probably also at Kreuzkofeljoch snow height was on average.

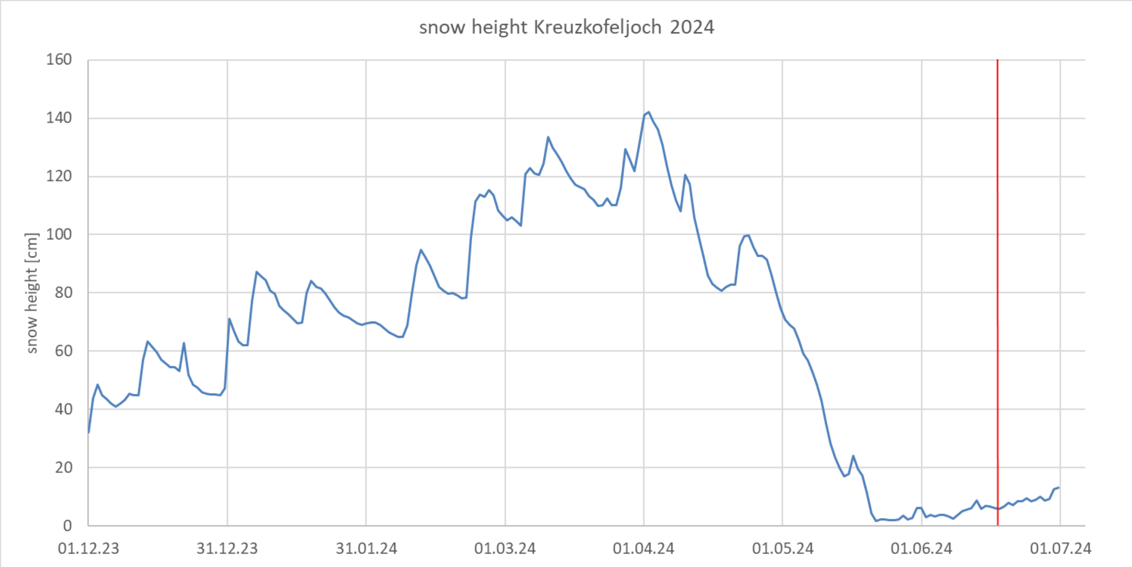

Figure 46: snow height timeline of 2024 from Kreuzkofeljoch meteorological station.

Table 28: Rainfall (St. Martin) and snow melt totals (Abtei Piz La Ila) for the spring period (21.03 - 21.06) from 2015 to 2024, showing that the combination of rainfall and snow melt was significantly high in 2024. For the additional snowfall during the snow melt a snow density for fresh snow of 50 kg/m³ was added in the SWE calculation.

Year	Rainfall [mm]	Snow height [cm]	SWE [mm]	TOT [mm]
2015	248,4	83,7	251,2	499,6
2016	244,6	139,4	425,3	669,9
2017	145,9	70,7	212,1	358,0
2018	201,4	137,5	426,8	628,2
2019	268,4	128,3	409,0	677,4
2020	275,6	157,3	471,9	747,5
2021	181,9	172,8	525,7	707,6
2022	287,4	95,4	300,6	588,0
2023	258,4	77,5	246,9	505,3
2024	352,8	138,6	437,3	790,1

4.4.3 Water as Triggering Factor

A hydrograph is the sum of two flow components, namely the baseflow (groundflow) and the overland flow (surface runoff or storm flow), which itself is subdivided into throughflow (interflow). For a simple qualitative analysis baseflow and overland flow can be roughly estimated by simple observation of the hydrograph. In this case the estimated baseflow below the hydrograph is regarded as a relative estimate for the soil moisture in the catchment area. If the baseflow rises due to snow melt or prolonged precipitation soil moisture is regarded as high. The only available gauging station for this relative estimation is in Montal, at the exit of Val Badia. The catchment of the Badia river (384 km^2 at station of Montal) is much larger than the catchment of the study area (3,9 km^2), thus total numbers would be considerably lower for the Seres creek. But the point here is to look at the baseflow assuming that rainfall conditions are similar throughout the Gader catchment.

The hydrograph shows that baseflow was the highest when the mass movement occurred. This indicates that the soil was well saturated in the Badia catchment and therefore probably also in the study area. Over the last 10 years the baseflow seems to have been the highest in June 2024.

The suspended load concentration shows an extreme peak at the 17th June indicating that the suspended load from the mass movement event reached the measuring station in Montal (about 22 km distance) the same day.

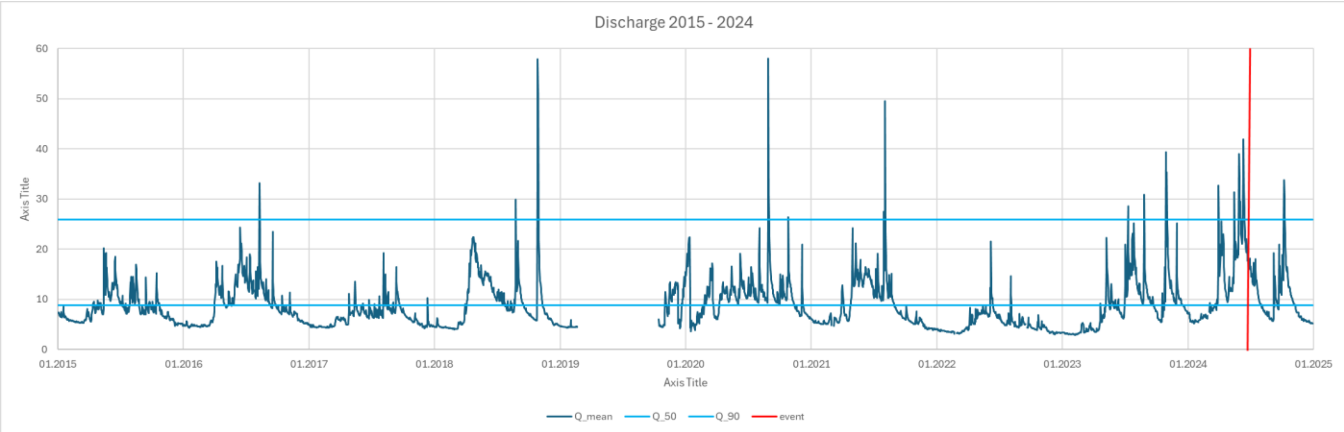

Figure 47: Discharge of the Gader at Montal for the period of 2014 to 2024.

The combined graph with snow melt, discharge and precipitation shows that baseflow is increasing in spring due to snow melt (fig. 48). Together with the precipitation events from mid of May to mid of June not only discharge peaks were recorded but also the baseflow was raised higher. The singular precipitation events alone were high, but as single events probably not significantly high to trigger the mass movement. It was rather the whole period from beginning of the year, especially the month before the event to record extremely precipitation amounts.

These observations leads to the statement that the combination of meltwater between April and May together with the extremely high precipitation amounts from mid of May to mid of June is the probable triggering factor of the mass movement.

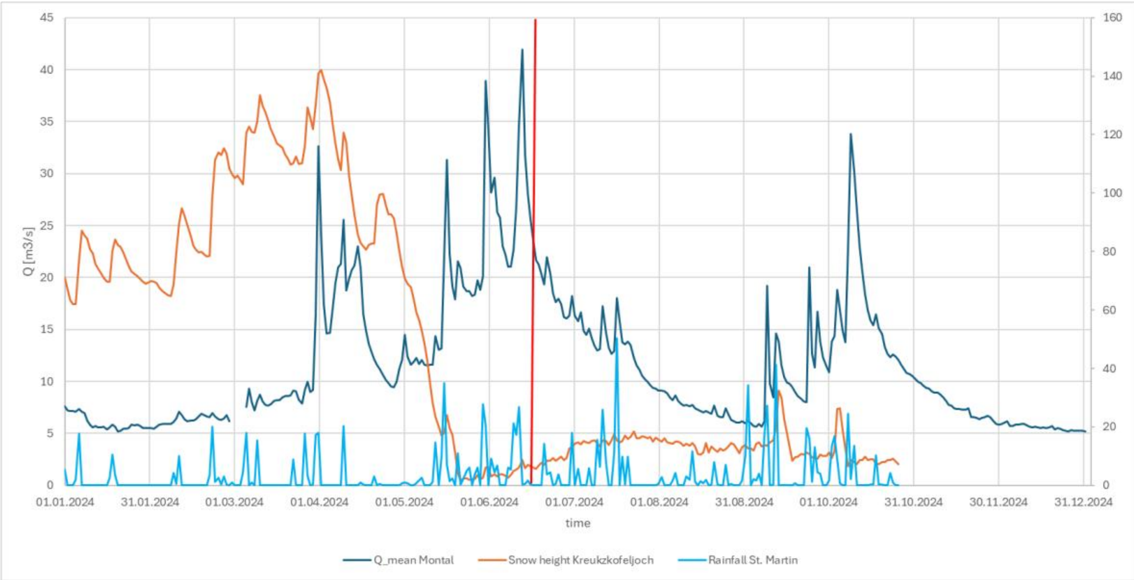

Figure 48: Combined timelines of snow depth (Kreuzkofeljoch), precipitation (St. Martin) and discharge (Montal) indicate significant wet ground conditions as triggering factor for the studied mass movement event. Red line indicates the 17^{th} June (date of the event).

4.5 Conceptual Ground Behaviour Model

4.5.1 Geological and Structural Predisposition

The investigated mass movement in the Seres valley is strongly controlled by the regional structural geological setting of the Dolomites. The slope is located on the **northern limb of an anticline (Bronsara anticline)** formed during Neogene compressional tectonics, resulting in **inclined bedding planes dipping (35 - 45°) unfavourably parallel to the slope**. This structural configuration promotes kinematic instability by facilitating downslope-directed shear along (weakened) bedding surfaces. In fact, the slope surface S of the source area is parallel to the bedding planes, indicating that bedding-parallel sliding must have occurred in the past, as also deposited material at the end of the Ciancidel channel in the pre-event DTM was observed.

A pronounced **competence contrast** exists between the underlying **Schlerndolomite** and the overlying **Zoppé-Formation**. The Schlerndolomite forms a relatively competent, brittle rock mass prone to brittle fracturing and rockfall, whereas the Zoppé Formation consists of **arkosic, fine-grained (peltitic-siltitic) turbidites**, which is **mechanically weak** (testified by folds) and **highly susceptible to weathering**. This lithological contrast promotes stress concentration and differential deformation at the lithological boundary, enhancing slope instability. In addition, the sparse occurrences of coarse grained Zoppé sandstone, could be remnants from the eroded sliding plane between Zoppé and Schlerndolomite, as this sandstone shows medium high SDI. The precedent mass movement at this location (probably of the sliding type), must have been occurred around this lithologic boundary in order to erode the Zoppé-Fm. from the S-slope and limit its occurrence to the gully, while the Schlerndolomite from Col Ciancidel is exposed along the slope and exposed to creeping slope deformation (dormant) expressed in tension cracks, sickle growth and fibrous vein minerals.

4.5.2 Lithological and Weathering Predisposition

The Zoppé Formation plays a key role in controlling slope behaviour. Its siltitic-peltitic grain size and **mineralogical composition**, including feldspar-rich (arkosic) sandstones, promotes **chemical weathering and the formation of clay minerals within** an unconsolidated sedimentary accumulation (colluvium). This process leads to:

- high silt and clay content
- low hydraulic conductivity
- high water retention capacity
- a reduction in shear strength (from bedrock discontinuity controlled shear strength (Barton & Bandis) towards unconsolidated material shear strength (Mohr-Coulomb))

- increased plasticity
- development of low-permeability residual soil horizons

Weathering is further enhanced by the **gully morphology**, which:

- concentrates surface runoff
- promotes infiltration
- accelerates chemical alteration and mechanical degradation
- vegetation free zone (no stabilizing effect by vegetation)

These material properties and site conditions are critical for the mobilization of the unconsolidated colluvium material in the gully.

The morphological connection of the SW - NE trending and with …degrees dipping gully axis of Ciancidel channel with the Seres valley, allows the propagation as a cascading mass movement event (earth-debris flow -> debris flow surges from remobilized material -> mud flow).

4.5.3 Hydro-meteorological Triggering

The hydrogeological regime is dominated by **slow infiltration and progressive saturation**. Due to the low hydraulic conductivity of the fine-grained material, infiltrating water is retained within the colluvium wedge, leading to:

- gradual increase in pore-water pressure
- reduction of effective stress
- progressive weakening of the material

In 2024 water supply was enhanced by:

- **snowmelt during spring (April - mid May)**
- subsequent onset of record-like, **prolonged rainfall** (mid May - mid June)

This combination creates a **compound triggering mechanism**, where antecedent moisture conditions due to snowmelt and additional spring precipitations progressively saturate the colluvium material and increase pore-water pressure within low-permeability layers of silt and clay originated from the weathering of Zoppé-Fm.. As a consequence the reduction of effective stress between grain particles leads to a reduction of shear resistance and has mobilized the colluvium in the gully. In addition, it has to be verified if the small spring like outlets in the Zoppé-Fm. of the source area have its origin from groundwater collecting in the synclinal after prolonged precipitation or snow melt. This could contribute to saturation of the colluvium material from the N flank.

Thus, The failure was likely initiated by a **combination of snowmelt and precipitation**. The delayed response reflects the **hydro-mechanical behaviour of fine-grained materials**, where failure is controlled by cumulative water input rather than short-term rainfall intensity.

The evolution of the mass movement can be described as a **cascade process**:

Phase 1: Preconditioning

- Structurally controlled slope (anticline, unfavourable bedding)
- Competence contrast (Schlerndolomite vs. Zoppé Formation)
- Weathering and clay formation
- Accumulation of colluvial material in gully

Phase 2: Failure Initiation

- Saturation of fine-grained material
- Increase of pore-water pressure
- Mobilization of colluvium material in the gully
- Sliding of the blocky material over the Schlerndolomite surface into the gully
- Initiation of **debris - earth flow-like movement**, which was favoured by sliding along the plane S flank of the Schlerndolomite.

Phase 3: Transfer zone and Remobilization

- The first debris - earth flow reached the upper Seres field around 9:30 am.
- Part of the primarly deposited material at the junction Corëtes channel - Seres valley gets saturated by backwater of Corëtes and Seres creek.
- Remobilization into **muddy debris flow with several surges and characteristic side levees** along Seres valley.

Phase 5: Deposition and mud-flow propagation

- Coarse material deposited where Seres valley channel widened and gradient flattened.
- Fine-grained, water-rich material continued as viscous **mud flow** carrying boulders of max 0,5 x 0,5 size.

5 Discussion

The first part of the discussion explains methodological limitations due to simplifications and assumptions in this thesis. In the second part the Conceptual Ground Behaviour Model is discussed in context of other observed mass movements within the Val Badia region.

5.1 Methodological Discussion

In general, a geological-geotechnical characterization has its limitations due to the complex site conditions of heterogeneous rock and soil materials and limited visibility in the subsurface conditions. When taking samples, it has always to be considered that the resulting lab parameters are always only punctual values of a heterogeneous material. In addition, geotechnical laboratory tests have its own limitations due to the testing of material in the lab without accounting for the in-situ conditions (stresses, saturation, etc.).

Source errors or uncertainties for the different methods are briefly listed as follows:

Grain size distribution: Uncertainties of the debris flow grain size distribution for characterizing the material derives from the fact that it was just one single sample, even if material was taken from many different spots in the deposited mass. The sharp kink of the grain size curve in the coarse silt fraction could derive from the washing away of the finer fractions during the three months between the event and the sampling. Another limitation comes from the exclusion of grain sizes bigger than gravel (> 63 mm). This practice, to account for grain sizes until blocks derives from debris flow literature, stating that flow behaviour (rheology) is controlled by the matrix rather than the blocks (e.g., Bolliger et al., 2024). Here, for the matrix of the debris flow the particle-size distribution was determined on fraction < 63 mm and newly normed without the blocks, according to ASTM D4718. Still the transition towards blocky debris flows has to be accounted, which could be completed by volumetric estimate methods of all grain sizes. A complete grain size could be relevant for exact characterization and debris flow propagation modelling.

Slake Durability Test: The highly weathered siltstones of the Zoppé-Fm. were breaking apart already during sampling and the long transportation distance disintegrated them. So for a better durability characterization SDI should be performed with this material or completed with water immersion test (EN ISO 14689).

Geotechnical Slope stability analyses: The performed slope stability analyses provide a simplified 2D representation of the complex 3D geometrical, geological and hydrogeological conditions in the study area and therefore need to be interpreted qualitatively rather than as exact predictions of slope behaviour. Slope stability analyses were conducted using assumed geotechnical parameters derived through back analysis, where parameters were adjusted until model results matched observed field behaviour. While this approach provides reasonable estimates, it simplifies the in-situ conditions and introduces uncertainties due to: (1) non-uniqueness of parameter combinations due to back-analysed geotechnical parameters. Different parameter sets may lead to comparable FOS values and (2) spatial variability of material properties (heterogeneous material).

Additionally, the use of 2D slope stability models (Janbu method of slices) imposes significant limitations:

- assumes force equilibrium between vertical slices
- simplifies interaction between slices
- inability to represent 3D slope geometry
- neglect of lateral constraints (boundary conditions) and multiple failure surfaces
- inability to account for dynamic changes
- As with all LEM approaches, the sliding mass is treated as a rigid-plastic body and progressive failure processes cannot be represented.
- Assumed constant shear strength along the slip surface, although investigated slope is highly heterogeneous and consists of weathered residual soils, colluvium material and fractured bedrock with strongly variable geomechanical properties.
- simplification of hydrogeological conditions by static groundwater tables. The groundwater regime in the study area is likely highly transient and controlled by snowmelt, prolonged rainfall and preferential flow paths along bedding planes and fractures. In the Janbu analysis, pore-water pressures were approximated using simplified groundwater table assumptions and therefore cannot reproduce the temporal evolution of saturation during the weeks preceding the event. Dynamic hydrological processes such as progressive increase in pore-water pressure within residual soils is difficult to simulate using static LEM calculations.

Therefore, the calculated slope stability results should primarily be interpreted as an indicator of relative instability conditions and possible failure mechanisms rather than as an exact reconstruction of the mass movement failure process.

5.2 Discussion: Conceptual Ground Behaviour Model in regional context

The developed Conceptual Ground Behaviour Model (CGBM) for the Seres valley mass movement is consistent with the general geomorphological framework of the Alta Badia region, where slope instability is primarily controlled by lithological contrasts, post-glacial slope adjustment and hydro-meteorological forcing (Panizza et al., 2011). In Val Badia, mass movements represent the dominant geomorphic process shaping valley slopes since the Last Glacial Maximum, with widespread occurrence of earth flows, debris flows and complex slide–flow movements (Panizza et al., 2011).

The investigated event fits into this regional pattern but also represents a particular case because the source area developed within the Zoppé-Fm. In the consulted literature and inventories of the Alta Badia region (Panizza et al., 2011; Costamoling, 2022; IdroGeo reports; Corsini et al., 2003) numerous mass movements are described in the Wengen and St. Cassian-Formations, whereas no explicitly documented mass movement sourced from the Zoppé-Fm. could be found. However, this is also due to the fact that a) the Zoppé is a thin formation and difficult to identify in the field, and b) does not have as large extension and thicknesses as the Wenge- and St. Cassian-Formation. The Seres valley event therefore represents an important addition to the regional understanding of slope instability in the Dolomites. Nevertheless, the observed process characteristics show strong similarities to mass movements developed within the Wengen and St. Cassian formations, as all three formations consist of relatively weak basinal to turbiditic sedimentary successions with significant fine-grained components and high susceptibility to weathering.

The Wengen and St. Cassian-Fm. are widely associated with large rotatory-translatory slides in Alta Badia, such as the Costa di Pedratsches, Parüs–Runch, Valacia–Murin, San Leonardo and Gianëis–Costalta-Martrara landslides. These landslides commonly affect slopes composed of marls, claystones, volcanoclastic sandstones and calcarenitic interbeds overlain by more or less thick Quaternary colluvial or glacial deposits. Many of these landslides display rotational or translational failure mechanisms in the upper slope sectors that gradually evolve downslope into earth flows or creeping masses.

From a lithological perspective, the Zoppé Formation shares several important characteristics with the Wengen and St. Cassian formations. All three formations contain significant pelitic to marly components, exhibit relatively low rock-mass strength compared to the surrounding dolomitic units and are highly susceptible to weathering and clay-mineral production. Consequently, they favour the development of fine-grained residual soils with low permeability and elevated water retention capacity. These conditions promote prolonged saturation, pore-water pressure build-up and progressive reduction of effective stress during extended wet periods.

However, significant differences also exist between these formations. The Zoppé Formation in the study area is comparatively thin and occurs as a relatively localized turbiditic interval. In contrast, the Wengen and St. Cassian-Fm. in Val Badia reach substantially greater thicknesses, locally several tens to more than one hundred meters, and show pronounced lithological heterogeneity with alternations of marls, volcanoclastic sandstones, calcarenites, limestones and clay-rich intervals.

This difference in thickness and lithological architecture may partly explain the differing failure styles. In the Seres valley, the relatively thin Zoppé-derived weathered material was rapidly mobilized into an earth–debris flow directly within the source gully. In contrast, landslides in the Wengen and St. Cassian formations commonly initiate as larger rotational or translational slides with deeper-seated sliding surface before progressively transforming into earth flows or creeping masses. The larger thickness of weathered and Quaternary-covered Wengen and St. Cassian slopes favours the development of extensive and deep-seated landslide bodies with multiple slip surfaces, as documented for several landslides in Val Badia.

Hydro-meteorological conditions represent another important distinction between finer grained slide–flow movements and coarse debris flow events in the Dolomites. Regional studies indicate that many mass movements within Wengen and St. Cassian-Fm. are linked to prolonged rainfall and snowmelt periods (Costamoling, 2022). Examples such as the reported Seres mass movement, Gianëis or Antersasc landslide show that persistent rainfall combined with snowmelt and groundwater build-up can activate or reactivate mass movements.

In contrast, coarse-grained debris-flow systems such as those occurring in the Bronsara valley are typically associated with short-duration, high-intensity rainfall events. These systems are dominated by coarse colluvium, scree and debris derived from more brittle lithologies and steep slopes where mobilization and connection paths to the channel are short. Due to the high permeability and low cohesion of such deposits, rainfall infiltrates rapidly and runoff becomes quickly concentrated within steep channels, favoring sudden debris-flow initiation. Panizza et al. (2011) report that rainfall events exceeding approximately 50 mm within 1–5 days are frequently associated with debris-flow initiation in the Dolomites, particularly in steep catchments with abundant loose material.

This leads to the conclusion that debris flows in coarse alpine headwaters are primarily controlled by short-duration rainfall intensity thresholds, whereas earth or debris slides and flows in mechanically weak and weathering prone lithologies respond more strongly to cumulative rainfall and antecedent saturation conditions. Panizza et al., 2011 also indicate that debris-flow activity in the Dolomites is often linked to late summer and autumn precipitation peaks, while slower moving slides and flows show a stronger correlation with cumulative rainfall and snowmelt processes (Panizza et al., 2011).

The channel characteristics additionally influence the process behaviour. In Bronsara-type catchments, steep and narrow torrent channels with abundant coarse sediment supply promote rapid runoff concentration and high-energy debris flow transport. In the Seres valley, however, the initial mobilized material contained a high proportion of fine-grained matrix derived from weathered Zoppé sediments. This behaviour reflects the matrix-supported rheology of fine-grained debris flow systems and differs from the clast-supported coarse debris flows typical for many dolomitic torrent systems.

Overall, the CGBM demonstrates that lithology exerts a first-order control on both the failure mechanism and the hydrological response of slopes in Val Badia. Coarse-grained, permeable headwater systems mainly respond to short and intense rainfall by sudden debris flow initiation, whereas fine-grained turbiditic formations such as the Zoppé, Wengen and St. Cassian formations are more susceptible to progressive saturation and delayed failure during prolonged wet periods or snowmelt.

6 Conclusion

This thesis investigated the geological-geotechnical conditions and process evolution of the June 2024 cascading mass movement event in the Seres Valley near Campill, South Tyrol. The results demonstrate that the failure was controlled by the interaction of multiple predisposing factors and hydro-meteorological triggering.

The geological and stratigraphic framework exerted a primary control on instability. The source area developed at the contact between competent Schlerndolomite and the overlying mechanically weak Zoppé-Formation. The fine-grained, thinly stratified turbiditic and pelitic lithologies of the Zoppé-Formation are highly susceptible to weathering and erosion, resulting in the production of fine-grained residual soils. Competence contrasts both at the lithological boundary and within the Zoppé Formation promoted differential deformation and slope weakening.

Structural geological conditions additionally favoured instability. The source area is situated on the northern limb of the Bronsara anticline, where bedding dips parallel to the slope and forms an unfavourable dip-slope geometry. Geomorphological factors such as a colluvium-filled gully below steep rock cliffs, limited vegetation cover and concentrated infiltration further increased susceptibility.

Mineralogical and geotechnical investigations demonstrate strong chemical weathering of feldspar-rich siliciclastic material and the formation of clay minerals including vermiculite, smectite and kaolinite. These minerals increase water retention, reduce permeability and promote progressive strength reduction during saturation. The weathered Zoppé material therefore behaved as a low-permeability horizon favouring pore-water pressure build-up during prolonged wet periods.

Meteorological analyses indicate that the event was triggered by prolonged precipitation combined with antecedent snowmelt during spring 2024. Elevated antecedent saturation conditions led to mobilization of the colluvial and weathered slope material, which subsequently evolved into a cascading earth - debris flow, debris flow and mud flow system.

The developed Conceptual Ground Behaviour Model demonstrates that lithology and weathering behaviour exert first-order controls on mass movement susceptibility in the Dolomites. Fine-grained formations such as the Zoppé-Formation primarily respond to cumulative rainfall and prolonged saturation, whereas coarse dolomitic debris flow systems are more strongly controlled by short-duration rainfall intensity. The results emphasize the importance of integrating geological, geomorphological, geotechnical and hydro-meteorological datasets for hazard assessment and susceptibility analysis in alpine terrain.

7 Bibliography

Allmendinger, R. W., Cardozo, N., & Fisher, D. M. (2011). Structural Geology Algorithms: Vectors and Tensors. Cambridge University Press. https://doi.org/10.1017/CBO9780511920202

ASTM D2487-17. Standard Practice for Classification of Soils for Engineering Purposes (Unified Soil Classification System). (n.d.). Retrieved 21 May 2026, from https://store.astm.org/d2487-17.html

ASTM D4644-16. Standard Test Method for Slake Durability of Shales and Other Similar Weak Rocks (Withdrawn 2025). (n.d.). Retrieved 30 April 2026, from https://store.astm.org/d4644-16.html

Autonomous Province of Bolzano. (2016). RICHTLINIEN ZUR ERSTELLUNG DER GEFAHRENZONENPLÄNE UND ZUR KLASSIFIZIERUNG DES RISIKOS [Beschluss der Landesregierung. Abänderung der Richtlinien zur Erstellung der Gefahrenzonenpläne gemäß Landesraumordnungsgesetz, Landesgesetz vom 11. August 1997, Nr. 13, Artikel 22/bis]. https://assets-eu-01.kc-usercontent.com/f25c3e79-d836-0158-96a2-5418035fd6a5/b9987ae3-f191-4021-8f5f-8349364953de/Direttive%20-%20Richtlinie%202016.pdf

Bailey, P., Wheaton, J., Reimer, M., & Brasington, J. (2020). Geomorphic Change Detection Software [Computer software]. Zenodo. https://doi.org/10.5281/zenodo.7248344

Bargossi, G. M., Kloetzli, U., Mair, V., Marochi, M., & Morelli, C. (2004). The Lower Permian Athesian Volcanic Group (AVG) in the Adige Valley between Meran and Bolzano: A stratigraphic, petrographic and geochronological outline. IGC32, Florence, Italy, 35(15).

Baur, S. (2019, April). Geologie des Peitlerkofel-Gebietes (Dolomiten) mit Schwerpunkt Perm-Trias-Grenze. http://ulb-dok.uibk.ac.at/ulbtirolhs/3591612

Baynes, F., & Parry, S. (2024). Guidelines for the development and application of engineering geological models on projects. International Association for Engineering Geology and the Environment (IAEG), Commission 25 Publication No. 1,(Version 2.0), 81.

Beniston, M. (2006). Mountain weather and climate: A general overview and a focus on climatic change in the Alps. Hydrobiologia, 562(1), 3–16.

Besl, P. J., & McKay, N. D. (1992). A method for registration of 3-D shapes. IEEE Transactions on Pattern Analysis and Machine Intelligence, 14(2), 239–256. https://doi.org/10.1109/34.121791

Bolliger, D., Schlunegger, F., & McArdell, B. W. (2024). Comparison of debris flow observations, including fine-sediment grain size and composition and runout model results, at Illgraben, Swiss Alps. Natural Hazards and Earth System Sciences, 24(3), 1035–1049.

Bosellini, A. (1967). La tematica deposizionale della Dolomia principale (Dolomiti e Prealpi venete). az. tip. eredi dott. G. Bardi.

Bosellini, A. (1968). Paleogeologia pre-anisica delle Dolomiti centro-settentrionali. Accademia Nazionale dei Lincei.

Bosellini, A. (1996). Geologia delle Dolomiti. Athesia.

Bosellini, A., Gianolla, P., & Stefani, M. (2003). Geology of the Dolomites. Episodes Journal of International Geoscience, 26(3), 181–185. https://doi.org/10.18814/epiiugs/2003/v26i3/005

Bovis, M. J., & Jakob, M. (1999). The role of debris supply conditions in predicting debris flow activity. Earth Surface Processes and Landforms, 24(11), 1039–1054. https://doi.org/10.1002/(SICI)1096-9837(199910)24:11%3C1039::AID-ESP29%3E3.0.CO;2-U

Brandner, R., & Gruber, A. (2019a). New Lithostratigraphic terms used in the geological map of the Western Dolomites. Geo.Alp, (16), 47–50.

Brandner, R., & Gruber, A. (2019b). Tectonostratigraphy of the Western Dolomites in the context of the development of the Western Tethys. Geo.Alp, 16, 51–56.

Brandner, R., Gruber, A., & Keim, L. (2007). Geologie der westlichen Dolomiten: Von der Geburt der Neotethys im Perm zu Karbonatplattformen, Becken und Vulkaniten der Trias. Geo.Alp, 4, 95–121.

Brandner, R., Gruber, A., Morelli, C., & Mair, V. (2016). Field trip 1 Pulses of Neotethys-Rifting in the Permomesozoic of the Dolomites. Geo.Alp, 13, 7–70.

Brandner, R., & Keim, L. (2011). A 4-day geological field trip in the western Dolomites. Geo.Alp, 8, 76–118.

Brasington, J., Langham, J., & Rumsby, B. (2003). Methodological sensitivity of morphometric estimates of coarse fluvial sediment transport. Geomorphology, 53(3), 299–316. https://doi.org/10.1016/S0169-555X(02)00320-3

Broglio Loriga, C., Góczán, F., Haas, J., Lenner, K., Neri, C., Oravecz Sheffer, A., Posenato, R., Szabo, I., & Toth Makk, A. (1990). The Lower Triassic sequences of the Dolomites (Italy) and Transdanubian mid-mountains (Hungary) and their correlation. Memorie Di Scienze Geologiche, 42, 41–103.

Bull, W. B. (1964). Alluvial fans and near-surface subsidence in Western Fresno County, California (Professional Paper). U.S. Geological Survey Professional Paper. https://pubs.usgs.gov/pp/0437a/report.pdf

Cardozo, N., & Allmendinger, R. W. (2013). Spherical projections with OSXStereonet. Computers & Geosciences, 51, 193–205. https://doi.org/10.1016/j.cageo.2012.07.021

Cassinis, G., Cortesogno, L., Gaggero, L., Perotti, C. R., & Buzzi, L. (2008). Permian to Triassic geodynamic and magmatic evolution of the Brescian Prealps (eastern Lombardy, Italy). Italian Journal of Geosciences, 127(3), 501–518.

Castellarin, Albert., Selli, L., Picotti, Vincen., & Cantelli, L. (1998). La tettonica delle Dolomiti nel quadro delle Alpi Meridionali Orientali. Mem. Soc. Geol. It, 53, 133–143.

Căţeanu, M., & Ciubotaru, A. (2021). The Effect of LiDAR Sampling Density on DTM Accuracy for Areas with Heavy Forest Cover. Forests, 12(3), 265. https://doi.org/10.3390/f12030265

Cheng, Y., Pang, H., Li, Y., Fan, L., Wei, S., Yuan, Z., & Fang, Y. (2025). Applications and Advancements of Spaceborne InSAR in Landslide Monitoring and Susceptibility Mapping: A Systematic Review. Remote Sensing, 17(6), 999. https://doi.org/10.3390/rs17060999

Costa, J. E. (1984). Physical Geomorphology of Debris Flows. In J. E. Costa & P. J. Fleisher (Eds), Developments and Applications of Geomorphology (pp. 268–317). Springer. https://doi.org/10.1007/978-3-642-69759-3_9

Crozier, M. J. (1989). LANDSLIDES: CAUSES, CONSEQUENCES AND ENVIRONMENT. New Zealand Geographer, 45(2), 93–94. https://doi.org/10.1111/j.1745-7939.1989.tb01143.x

Cruden, D., & Varnes, D. (1996). Landslide types and processes. Transportation Research Board, U.S. National Academy of Sciences, Special Report, 247, 36–75.

Curzi, M., Zuccari, C., Vignaroli, G., Degl'Innocenti, S., & Viola, G. (2023). Alpine transpression in the Passo Rolle area (Dolomites, Italy): New structural and paleostress constraints. Italian Journal of Geosciences. https://doi.org/10.3301/IJG.2023.12

Daly, C., Neilson, R. P., & Phillips, D. L. (1994). A statistical-topographic model for mapping climatological precipitation over mountainous terrain. Journal of Applied Meteorology and Climatology, 33(2), 140–158.

Davies, T. R. H. (1986). Large debris flows: A macro-viscous phenomenon. Acta Mechanica, 63(1), 161–178. https://doi.org/10.1007/BF01182546

De Haas, T., Lau, C.-A., & Ventra, D. (2024). Debris-Flow Watersheds and Fans: Morphology, Sedimentology and Dynamics. In M. Jakob, S. McDougall, & P. Santi (Eds), Advances in Debris-flow Science and Practice (pp. 9–73). Springer International Publishing. https://doi.org/10.1007/978-3-031-48691-3_2

De Zanche, V., Franzin, A., Gianolla, P., & Mietto P, S. C. (1992). The Piz da Peres section (Valdaora-Olang, Pusteria Valley, Italy). A reappraisal of the Anisian stratigraphy in the Dolomites. Eclogae Geologicae Helvetiae, 85(1), 127–143.

Dey, L., Borga, M., Comiti, F., Mergili, M., Pierpaolo, M., Marchi, L., Cavalli, M., Crema, S., Dallan, E., & Mair, V. (2025). Simulating snowmelt-induced muddy debris flows in alpine regions: A case study in the Seres Creek, Dolomites (Nos EGU25-19265). Copernicus Meetings. EGU25. https://doi.org/10.5194/egusphere-egu25-19265

Doglioni, C. (1987). Tectonics of the Dolomites (southern alps, northern Italy). Journal of Structural Geology, 9(2), 181–193. https://doi.org/10.1016/0191-8141(87)90024-1

Doglioni, C. (2007). Tectonics of the Dolomites. Bulletin Für Angewandte Geologie, 12, 11–15.

Doglioni, C., & Bosellini, A. (1987). Eoalpine and mesoalpine tectonics in the Southern Alps. Geologische Rundschau, 76(3), 735–754. https://doi.org/10.1007/BF01821061

Dunham, R. J. (1962). Classification of Carbonate Rocks According to Depositional Texture. In W. E. Ham (Ed.), Classification of Carbonate Rocks—A Symposium (Vol. 1, p. 0). American Association of Petroleum Geologists. https://doi.org/10.1306/M1357

Farabegoli, E., & Viel, G. (1982). Litostratigrafia della formazione di Werfen (Trias Inf.) delle Dolomiti occidentali. Industria Mineraria, 6, 3–14.

Fois, E. (1982). The Sass da Putia Carbonate Buildup (Western Dolomites): Biofacies Succession and Margin Developement during the Ladinian. Riv. Ital. Paleont., 87(4), 565–598.

Froude, M. J., & Petley, D. N. (2018). Global fatal landslide occurrence from 2004 to 2016. Natural Hazards and Earth System Sciences, 18(8), 2161–2181. https://doi.org/10.5194/nhess-18-2161-2018

Gamble, J. C. (1971). Durability—Plasticity Classification of Shales and Other Argillaceous Rocks [Text, University of Illinois at Urbana-Champaign]. https://hdl.handle.net/2142/64715

Genske, D. D. (2014). Ingenieurgeologie: Grundlagen und Anwendung. Springer. https://doi.org/10.1007/978-3-642-55387-5

GeoSphere Austria, Autonome Provinz Bozen, & ARPAV. (2015). DAS KLIMA VON TIROL - SÜDTIROL - BELLUNO.

Gianolla, P., Andreetta, R., Furin, S., S., F., & Riva, A. (2008). Geology of the Dolomites.

Gibson, S., Floyd, I., Sánchez, A., & Heath, R. (2021). Comparing single-phase, non-Newtonian approaches with experimental results: Validating flume-scale mud and debris flow in HEC-RAS. Earth Surface Processes and Landforms, 46(3), 540–553. https://doi.org/10.1002/esp.5044

Giles, D. (2013). The use of ground models for the integration of geomorphological, geoenvironmental and engineering geological data: 8th IAG International Conference on Geomorphology. 82.

Girardeau-Montaut. (n.d.). CloudCompare—3D point cloud and mesh processing software [Computer software]. Open Source Project. Retrieved 22 May 2026, from https://www.cloudcompare.org/

Glade, T., & Dikau, R. (2002). Gefahren und Risiken durch Massenbewegungen. Geographische Rundschau, 54, 38–45.

Glade, T., Mergili, M., & Sattler, K. (Hrsg.). (2020). ExtremA 2019: Aktueller Wissensstand zu Extremereignissen alpiner Naturgefahren in Österreich (1st edn). Vandenhoeck & Ruprecht (V&R unipress). https://austria-forum.org/web-books/en/extremA00de2020isds/000369

Google Maps. (2023). Street view image of Seres valley in 2023. https://www.google.no/maps/@46.6432973,11.8334222

Herzel, P. (2002). Recommendation No. 20 of the commission on Rock Testing of the Deutsche Gesellschaft für Geotechnik e.V. - ‘Slake-durability test’. 79, 101–105.

Highland, L. M., & Bobrowsky, P. (2008). The Landslide Handbook—A Guide to Understanding Landslides. https://pubs.usgs.gov/circ/1325/

Holtz, R. D., & Kovacs, W. D. (1981). An Introduction to Geotechnical Engineering (Vol. 1). Prentice-Hall.

Huggel, C., Salzmann, N., Allen, S., Caplan-Auerbach, J., Fischer, L., Haeberli, W., Larsen, C., Schneider, D., & Wessels, R. (2010). Recent and future warm extreme events and high-mountain slope stability. Philosophical Transactions of the Royal Society A: Mathematical, Physical and Engineering Sciences, 368(1919), 2435–2459. https://doi.org/10.1098/rsta.2010.0078

Hungr, O., Evans, S. G., Bovis, M., & Hutchinson, J. N. (2001). Review of the Classification of Landslides of the Flow Type. Environmental & Engineering Geoscience, 7, 221–238.

Hungr, O., Leroueil, S., & Picarelli, L. (2014). The Varnes classification of landslide types, an update. Landslides, 11. https://doi.org/10.1007/s10346-013-0436-y

Hungr, O., McDougall, S., & Bovis, M. (2005). Entrainment of material by debris flows. In M. Jakob & O. Hungr (Eds), Debris-flow Hazards and Related Phenomena (pp. 135–158). Springer. https://doi.org/10.1007/3-540-27129-5_7

ISPRA (Istituto Superiore per la Protezione e la Ricerca Ambientale). (n.d.). IdroGEO. IdroGEO. The Italian Web Platform on Landslides and Floods. https://idrogeo.isprambiente.it/app/

Iverson, R. M. (1997). The physics of debris flows. Reviews of Geophysics, 35(3), 245–296.

Iverson, R. M. (2000). Landslide triggering by rain infiltration. Water Resources Research, 36(7), 1897–1910. https://doi.org/10.1029/2000WR900090

Jakob, M., & Hungr, O. (2005). Debris-flow Hazards and Related Phenomena. Springer. https://doi.org/10.1007/b138657

Jemec Auflič, M., Bezak, N., Šegina, E., Frantar, P., Gariano, S. L., Medved, A., & Peternel, T. (2023). Climate change increases the number of landslides at the juncture of the Alpine, Pannonian and Mediterranean regions. Scientific Reports, 13(1), 23085. https://doi.org/10.1038/s41598-023-50314-x

Jesacher, M. (1999). Stratigraphische und tektonische Entwicklung des Peitler Kofel-Gebietes (Sas de Pütia) am Nordrand der Dolomiten [Universität Innsbruck]. https://bibsearch.uibk.ac.at/primo-explore/fulldisplay?docid=UIB_alma21181531070003333&context=L&vid=UIB&lang=de_DE&search_scope=Blended&adaptor=Local%20Search%20Engine&tab=default_tab&query=any,contains,Jesacher&facet=searchcreationdate,include,1998%7C,%7C2000&offset=0&pcAvailability=false

Jonas, T., Marty, C., & Magnusson, J. (2009). Estimating the snow water equivalent from snow depth measurements in the Swiss Alps. Journal of Hydrology, 378(1), 161–167. https://doi.org/10.1016/j.jhydrol.2009.09.021

Keim, L. (2008). Geologie im Gebiet Schlern–Seiser Alm: Vom Tethysmeer zum Gebirge. Gredleriana, 8, 25–46.

Keim, L., Brandner, R., & Gruber, A. (2006). Faziesverzahnung in Beckensedimenten der Dolomiten (Ladin-Karn): Vom Aufschluss zur geologischen Karte 1:25.000. Pangeo Austria. https://opac.geologie.ac.at/ais312/dokumente/PANGEO_2006_138_139.pdf

Kohrs, R., Vugt, L. de, Zieher, T., Crespi, A., Rossi, M., Greifeneder, F., Schneider-Muntau, B., Ventura, B., Rutzinger, M., & Steger, S. (2021). Combining static and dynamic environmental factors at various scales to predict shallow landsliding in South Tyrol, Italy – The Proslide project (Nos EGU21-15606). Copernicus Meetings. EGU21. https://doi.org/10.5194/egusphere-egu21-15606

Loriga, C. B., Masetti, D., & Neri, C. (1982). La Formazione di Werfen (Scitico) delle Dolomiti occidentali: Sedimentologia e biostratigrafia. Riv. It. Pal. Strat., 58, 501–598.

Marocchi, M., Morelli, C., Mair, V., Kl, ötzli U., & Bargossi, G. M. (2008). Evolution of Large Silicic Magma Systems: New U-Pb Zircon Data on the NW Permian Athesian Volcanic Group (Southern Alps, Italy). The Journal of Geology, 116(5), 480–498. https://doi.org/10.1086/590135

Masetti, D., & Neri, C. (1980). L'Anisico della Val di Fassa (Dolomiti Occidentali) sedimentologia e paleogeografia.

Massari, F., & Neri, C. (1997). The infill of a supradetachment(?) basin: The continental to shallow-marine Upper Permian succession in the Dolomites and Carnia (Italy). Sedimentary Geology, 110(3), 181–221. https://doi.org/10.1016/S0037-0738(96)00084-X

Maurer, F. (2000). Growth mode of Middle Triassic carbonate platforms in the Western Dolomites (Southern Alps, Italy). Sedimentary Geology, 134, 275–286. https://doi.org/10.1016/S0037-0738(00)00049-X

Maurer, F., & Schlager, W. (2003). Lateral variations in sediment composition and bedding in Middle Triassic interplatform basins (Buchenstein Formation, southern Alps, Italy). Sedimentology, 50(1), 1–22.

Micheletti, S., Marigo, G., & Pelosini, R. (2010). Alpine meteorology. AINEVA.

Mischì, G. (2021). Dizionar: Deutsch—Ladin. Verlag A. Weger. https://woerterbuchnetz.de/?sigle=LDWB2&lemid=A00001

Mojsisovics, E. (1879). Die dolomit-riffe von Südtirol und Venetian: Beträge zur bildungsgeschichte der Alpen. A. Hölder, KK Hof-und Universitatsbuchhandler.

Morelli, C., Marocchi, M., Moretti, A., Bargossi, G. M., Gasparotto, G., De Waele, B., Klotzli, U., & Mair, V. (2012). Volcanic stratigraphy and radiometric age constraints at the northern margin of a mega-caldera system: Athesian Volcanic Group (Southern Alps, Italy). GEOACTA, 11. https://cris.unibo.it/handle/11585/134761

Mutschlechner, G. (1933). Geologie der Peitlerkofelgruppe (Südtiroler Dolomiten). Jahrbuch Der Geologischen Bundesanstalt, 83, 75–112.

Niedrist, G., Zebisch, M., Crespi, A., Iacopino, T., Fritsch, U., Barandun, M., Bertoldi, G., Bottarin, R., Hoffmann, C., Jacob, A., Marin, C., Notarnicola, C., Obojes, N., Premier, V., Renner, K., Sparber, W., Vaccaro, R., & Ventura, B. (2022). Climate Change Monitoring South Tyrol. EURAC Research. https://doi.org/https://doi.org/10.57749/8ZPX-HM12

Nuth, C., & Kääb, A. (2011). Co-registration and bias corrections of satellite elevation data sets for quantifying glacier thickness change. The Cryosphere, 5(1), 271–290. https://doi.org/10.5194/tc-5-271-2011

Petrucci, O. (2022). Landslide Fatality Occurrence: A Systematic Review of Research Published between January 2010 and March 2022. Sustainability, 14(15), 9346. https://doi.org/10.3390/su14159346

Pierson, T. C. (1986). Flow behavior of channelized debris flows, Mount St. Helens, Washington. In Hillslope Processes (pp. 269–296). Routledge.

Pierson, T. C., & Costa, J. E. (1987). A rheologic classification of subaerial sediment-water flows. Geological Society of America, Reviews in Engineering Geology, 7, 1–12. https://doi.org/10.1130/REG7-p1

Pistocchi, A. (2016). Simple estimation of snow density in an Alpine region. Journal of Hydrology: Regional Studies, 6, 82–89. https://doi.org/10.1016/j.ejrh.2016.03.004

Plyer, A., Colin-Koeniguer, E., & Weissgerber, F. (2015). A New Coregistration Algorithm for Recent Applications on Urban SAR Images. IEEE Geoscience and Remote Sensing Letters, 12(11), 2198–2202. https://doi.org/10.1109/LGRS.2015.2455071

Ponziani, M., Pogliotti, P., Stevenin, H., & Ratto, S. M. (2020). Debris-flow Indicator for an early warning system in the Aosta valley region. Natural Hazards, 104(2), 1819–1839. https://doi.org/10.1007/s11069-020-04249-5

Prinz, H., & Strauß, R. (2018). Ingenieurgeologie. Springer. https://doi.org/10.1007/978-3-662-54710-6

QGIS Developement Team. (2024). QGIS (Version Version 3.40.1) [QGIS Geographic Information System]. Open Source Geospatial Foundation (OSGeo Foundation). https://www.qgis.org/

Reiter, F., Freudenthaler, C., Hausmann, H., Ortner, H., Lenhardt, W., & Brandner, R. (2018). Active Seismotectonic Deformation in Front of the Dolomites Indenter, Eastern Alps. Tectonics, 37(12), 4625–4654. https://doi.org/10.1029/2017TC004867

Remondo, J., Sánchez-Díaz, M., & Cuesta-Albertos, J. A. (2026). An Increasing Trend of Landslides as a Consequence of the Global Change. Earth Systems and Environment, 10(2), 1461–1474. https://doi.org/10.1007/s41748-025-00685-0

Rokić, L. J. (2011). Fizička geologija. Ljubomir Rokić, Integraf, Sarajevo.

Scheffler, D., Hollstein, A., Diedrich, H., Segl, K., & Hostert, P. (2017). AROSICS: An Automated and Robust Open-Source Image Co-Registration Software for Multi-Sensor Satellite Data. Remote Sensing, 9(7), 676. https://doi.org/10.3390/rs9070676

Schippa, L. (2021). Yield Stress Model for Natural Debris Flows in Presence of Fine and Coarse–Grained Sediments. Water, 13(13). https://doi.org/10.3390/w13131865

Schlunegger, F., Norton, K., Caduff, R., & Shroder, J. (2013). Hillslope processes in temperate environments. Treatise in Geomorphology, 3, 337–354.

Sevruk, B. (1997). Regional dependency of precipitation-altitude relationship in the Swiss Alps. Climatic Change, 36(3), 355–369.

Siorpaes, C., Morelli, C., Gianolla, P., & Cucato, M. (2018). Note Illustrative della Carta geologica d'Italia alla scala 1:50.000, F. 016 Dobbiaco, Servizio Geologico d'Italia—ISPRA. https://doi.org/10.15161/oar.it/211575

Stingl, V., & Mair, V. (2005). Einführung in die Geologie Südtirols. Kraler Druck.

Strząbała, K., Ćwiąkała, P., & Puniach, E. (2024). Identification of Landslide Precursors for Early Warning of Hazards with Remote Sensing. Remote Sensing, 16(15), 2781. https://doi.org/10.3390/rs16152781

Tabacco. (2024). 07. Alta Badia - Arabba - Marmolada [Topographische Wanderkarte]. Casa Editrice TABACCO Srl.

UNISDR annual report: 2016-17 biennium work programme final report. 2017 (UNISDR Annual Report 2017). (2018). INISDR. https://digitallibrary.un.org/record/3895972

Urumović, K., Borović, S., & Navratil, D. (2020). Validity range and reliability of the United States Bureau of Reclamation (USBR) method in hydrogeological investigations. Hydrogeology Journal, 28(2), 625–636.

Van Husen, D. (1987). Die Ostalpen in den Eiszeiten (pp. 24). Vienna: Veröffentlichung Der Geologischen Bundesanstalt, 2.

Varnes, D. J. (1978). Slope movement types and processes. Landslides, Analysis and Control, Transportation Research Board Special Report, 176, 11–33.

Viel, G. (1979). Litostratigrafia ladinica: Una revisione. Ricostruzione paleogeografica e paleostrutturale dell'area Dolomitica-Cadorina (Alpi Meridionali). Riv. It. Paleont. Strat., 85/1, 85–125.

Wheaton, J. M., Brasington, J., Darby, S. E., & Sear, D. A. (2010). Accounting for uncertainty in DEMs from repeat topographic surveys: Improved sediment budgets. Earth Surface Processes and Landforms, 35(2), 136–156. https://doi.org/10.1002/esp.1886

Winterer, E. L., & Bosellini, A. (1981). Subsidence and sedimentation on Jurassic passive continental margin, Southern Alps, Italy. AAPG Bulletin, 65(3), 394–421.

Zangerl, C., Prager, C., Brandner, R., Brückl, E., Eder, S., Fellin, W., Tentschert, E., Poscher, G., & Schönlaub, H. (2008). Methodischer Leitfaden zur prozess-orientierten Bearbeitung von Massenbewegungen. Geo. Alp, 5, Vol. 5, 1–51.

Zebisch, M., Vaccaro, R., Niedrist, G., Schneiderbauer, S., Streifeneder, T. P., Weiß, M. L., Troi, A., Renner, K., Pedoth, L., & Baumgartner, B. (2018). Klima-report Südtirol 2018. Eurac Research.

Zegers, G., Mendoza, P. A., Garces, A., & Montserrat, S. (2020). Sensitivity and identifiability of rheological parameters in debris flow modeling. Natural Hazards and Earth System Sciences, 20(7), 1919–1930. https://doi.org/10.5194/nhess-20-1919-2020

Appendix: Geotechnical Results

Liquid and Plastic Limits

AUTONOME PROVINZ BOZEN - SÜDTIROL	PROVINCIA AUTONOMA DI BOLZANO - ALTO ADIGE
Abteilung 11 - Hochbau und technischer Dienst	**Ripartizione 11 - Edilizia e servizio tecnico**
Amt 11.6 - Amt für Geologie und Baustoffprüfung	Ufficio 11.6 - Ufficio Geologia e prove materiali

DETERMINAZIONE LIMITI DI ATTERBERG - PUNTA CONICA

LG 01.11 UNI EN ISO 17892-6

Auftragsnummer: 94395
Ordine Nr.:

Prüfkörper: 1
Campione Nr:

Baustelle:
Cantiere:

Ausgeführt durch: Lukas Patscheider
Eseguito da:

am:
data della prova:

Entnahmestelle: Schuttstrom, obere Sereswiesen
Punto di prelievo:

Entnahmetiefe:
Profondità prelievo:

Bodenart: Schuttstrom
Tipo di materiale:

Art der Entnahme: Ablagerungsgebiet, Obere Sereswiesen
Modalità prelievo:

Entnahme am: 25.09.2024 durch: Lukas Patscheider
Prelevato il: da:

LIMITE LIQUIDO

O CAMPIONE INDISTURBATO O CAMPIONE RIMANEGGIATO < 0,42 mm

	1	2	3	4	5		
Numero contenitore	5	38	32	42	50	W_L	34,9
Penetrazione cono (mm)	15,20	17,60	20,40	20,70	22,80	W_p	14,88
Massa umida + contenitore (g) m+mb	59,69	51,25	53,26	53,03	52,96	I_p	20,02
Massa secca + contenitore (g) md+mb	54,55	48,05	49,35	49,11	48,69	W	15
Contenitore (g) mb	38,23	38,23	37,94	38,02	37,18	Ic	0,99
Cantenuto d'acqua (g) m - md = mw	5,14	3,20	3,91	3,92	4,28	IL	0,01
Massa secca netta (g) md	16,32	9,83	11,41	11,09	11,51		
Umidità relativa (%) mw / md * 100	31,48	32,53	34,29	35,34	37,15		

W_L corrisponde al contenuto d'acqua necessario per avere 20 mm di pentrazione della punta conica.

LIMITE PLASTICO

	1	2	3	4	5
Numero contenitore	3	17	18	39	47
Massa umida + contenitore (g) m+mb	42,15	45,86	46,45	48,21	47,90
Massa secca + contenitore (g) md+mb	41,53	44,92	45,32	46,76	46,68
Contenitore (g) mb	37,26	38,58	37,86	37,31	38,30
Cantenuto d'acqua (g) m - md = mw	0,62	0,94	1,13	1,45	1,22
Massa secca netta (g) md	4,26	6,34	7,46	9,46	8,37
Umidità relativa (%) mw / md * 100	14,63	14,76	15,12	15,28	14,60

Data ______ **Il tecnico** ______

Pag. 1 di 2

Annotazioni:

AUTONOME PROVINZ BOZEN - SÜDTIROL	PROVINCIA AUTONOMA DI BOLZANO - ALTO ADIGE
Abteilung 11 - Hochbau und technischer Dienst	**Ripartizione 11 - Edilizia e servizio tecnico**
Amt 11.6 - Amt für Geologie und Baustoffprüfung	Ufficio 11.6 - Ufficio Geologia e prove materiali

DETERMINAZIONE LIMITI DI ATTERBERG

LG 01.10 UNI CEN ISO/TS 17892-12

Auftragsnummer: Ordine Nr.:	Entnahmestelle: Punto di prelievo:
Prüfkörper: Campione Nr:	Entnahmetiefe: Profondità prelievo:
Baustelle: Cantiere:	Bodenart: Tipo di materiale:
Ausgeführt durch: Eseguito da:	Art der Entnahme: Modalità prelievo:
am: data della prova:	Entnahme am: durch: Prelevato il: da:

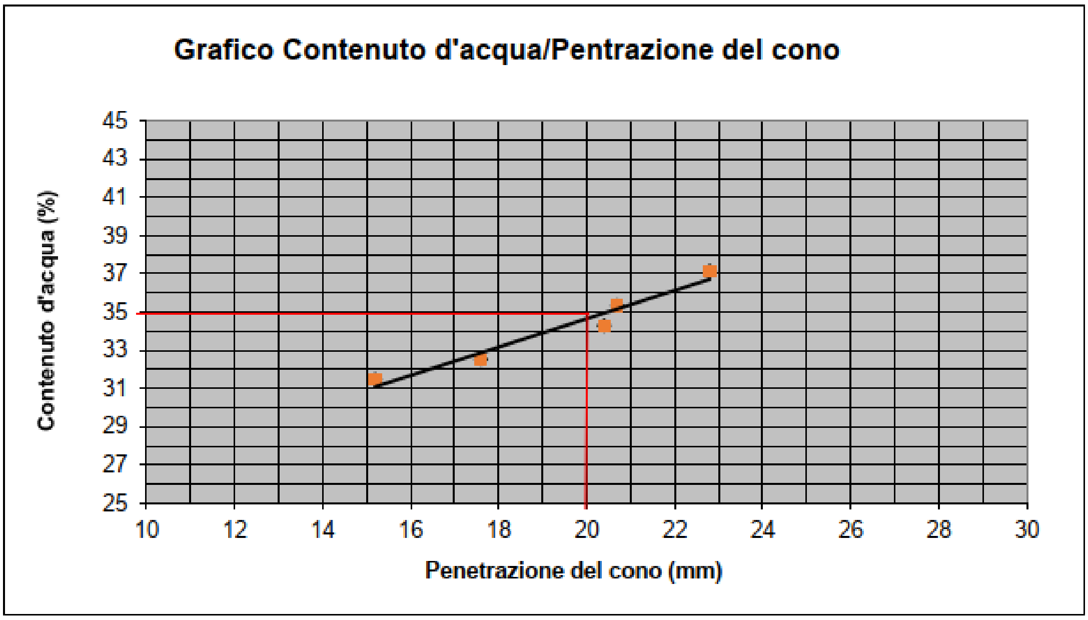

Data ____________________ Il tecnico ____________________

Pag. 2 di 2

Annotazioni: ____________________

AUTONOME PROVINZ BOZEN - SÜDTIROL	PROVINCIA AUTONOMA DI BOLZANO - ALTO ADIGE
Abteilung 11 - Hochbau und technischer Dienst	**Ripartizione 11 - Edilizia e servizio tecnico**
Amt 11.6 - Amt für Geologie und Baustoffprüfung	Ufficio 11.6 - Ufficio Geologia e prove materiali

DETERMINAZIONE LIMITI DI ATTERBERG - PUNTA CONICA

LG 01.11 UNI EN ISO 17892-6

Auftragsnummer: 94395
Ordine Nr.:

Prüfkörper: 2.2
Campione Nr:

Baustelle:
Cantiere:

Ausgeführt durch: Lukas Patscheider
Eseguito da:

am: Oktober 2025
data della prova:

Entnahmestelle: Abbruchgebiet
Punto di prelievo:

Entnahmetiefe:
Profondità prelievo:

Bodenart:
Tipo di materiale:

Art der Entnahme:
Modalità prelievo:

Entnahme am: 20.09.2024 durch: Lukas Patscheider
Prelevato il: da:

LIMITE LIQUIDO

O CAMPIONE INDISTURBATO O CAMPIONE RIMANEGGIATO < 0,42 mm

	1	2	3	4	5		
Numero contenitore	7	12	21	23	36	W_L	38,4
Penetrazione cono (mm)	15,10	17,00	19,60	22,20	24,10	W_P	12,81
Massa umida + contenitore (g) m+mb	49,57	48,21	50,36	53,55	53,72	I_P	25,59
Massa secca + contenitore (g) md+mb	46,40	45,44	46,79	49,06	49,23	W	15
Contenitore (g) mb	37,24	37,72	37,36	37,85	38,46	Ic	0,91
Cantenuto d'acqua (g) m - md = mw	3,17	2,77	3,57	4,49	4,49	IL	0,09
Massa secca netta (g) md	9,16	7,72	9,43	11,21	10,77		
Umidità relativa (%) mw / md * 100	34,67	35,88	37,83	40,03	41,68		

W_L corrisponde al contenuto d'acqua necessario per avere 20 mm di pentrazione della punta conica.

LIMITE PLASTICO

	1	2	3	4	5
Numero contenitore	2	16	25	26	37
Massa umida + contenitore (g) m+mb	43,909	44,722	46,476	46,565	44,864
Massa secca + contenitore (g) md+mb	42,917	43,816	45,429	45,670	44,104
Contenitore (g) mb	35,724	36,765	37,101	38,510	37,932
Cantenuto d'acqua (g) m - md = mw	0,99	0,91	1,05	0,89	0,76
Massa secca netta (g) md	7,19	7,05	8,33	7,16	6,17
Umidità relativa (%) mw / md * 100	13,79	12,85	12,57	12,50	12,31

Data ____________ Il tecnico ____________

Pag. 1 di 2

Annotazioni: ____________

AUTONOME PROVINZ BOZEN - SÜDTIROL	PROVINCIA AUTONOMA DI BOLZANO - ALTO ADIGE
Abteilung 11 - Hochbau und technischer Dienst	**Ripartizione 11 - Edilizia e servizio tecnico**
Amt 11.6 - Amt für Geologie und Baustoffprüfung	Ufficio 11.6 - Ufficio Geologia e prove materiali

DETERMINAZIONE LIMITI DI ATTERBERG

LG 01.10 UNI CEN ISO/TS 17892-12

Auftragsnummer:
Ordine Nr.:

Entnahmestelle:
Punto di prelievo:

Prüfkörper:
Campione Nr:

Baustelle:
Cantiere:

Ausgeführt durch:
Eseguito da:

am:
data della prova:

Entnahmetiefe:
Profondità prelievo:

Bodenart:
Tipo di materiale:

Art der Entnahme:
Modalitá prelievo:

Entnahme am: durch:
Prelevato il: da:

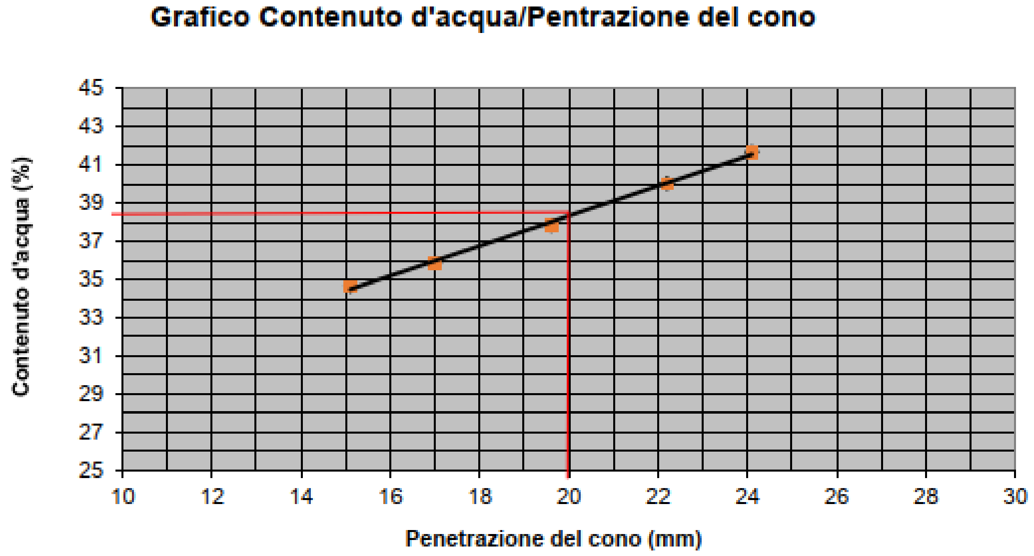

Data ______ Il tecnico ______

Annotazioni:

AUTONOME PROVINZ BOZEN - SÜDTIROL		PROVINCIA AUTONOMA DI BOLZANO - ALTO ADIGE
Abteilung 11 - Hochbau und technischer Dienst		**Ripartizione 11 - Edilizia e servizio tecnico**
Amt 11.6 - Amt für Geologie und Baustoffprüfung		Ufficio 11.6 - Ufficio Geologia e prove materiali

DETERMINAZIONE LIMITI DI ATTERBERG - PUNTA CONICA

LG 01.11 UNI EN ISO 17892-6

Auftragsnummer: 94395 Ordine Nr.:	Entnahmestelle: Abbruchgebiet Punto di prelievo:
Prüfkörper: 3 Campione Nr:	Entnahmetiefe: Profondità prelievo:
Baustelle: Cantiere:	Bodenart: Schuttstrom Tipo di materiale:
Ausgeführt durch: Lukas Patscheider Eseguito da:	Art der Entnahme: Modalità prelievo:
am: Oktober 2025 data della prova:	Entnahme am: 25.09.2024 durch: Lukas Patscheider Prelevato il: da:

LIMITE LIQUIDO O CAMPIONE INDISTURBATO O CAMPIONE RIMANEGGIATO < 0,42 mm

	1	2	3	4	5		
Numero contenitore	28	1	24	31	34	W_L	42
Penetrazione cono (mm)	15,50	16,70	17,60	21,00	22,90	W_p	17,80
Massa umida + contenitore (g) m+mb	49,73	46,32	58,07	54,03	57,51	I_p	24,20
Massa secca + contenitore (g) md+mb	46,43	42,98	52,39	49,11	51,68	W	19,2
Contenitore (g) mb	37,82	34,75	38,90	37,33	38,40	Ic	0,94
Cantenuto d'acqua (g) m - md = mw	3,30	3,34	5,68	4,91	5,83	IL	0,06
Massa secca netta (g) md	8,61	8,23	13,48	11,78	13,28		
Umidità relativa (%) mw / md * 100	38,32	40,65	42,14	41,68	43,86		

W_L corrisponde al contenuto d'acqua necessario per avere 20 mm di pentrazione della punta conica.

LIMITE PLASTICO

	1	2	3	4	5
Numero contenitore	18	30	20	35	46
Massa umida + contenitore (g) m+mb	43,991	41,693	41,944	42,345	43,879
Massa secca + contenitore (g) md+mb	42,986	41,037	41,300	41,502	43,082
Contenitore (g) mb	38,649	36,907	37,276	36,619	38,304
Cantenuto d'acqua (g) m - md = mw	1,01	0,66	0,64	0,84	0,80
Massa secca netta (g) md	4,34	4,13	4,02	4,88	4,78
Umidità relativa (%) mw / md * 100	23,17	15,88	16,00	17,26	16,68

Data ____________ **Il tecnico** ____________

Pag. 1 di 2

Annotazioni: ____________

AUTONOME PROVINZ BOZEN - SÜDTIROL		PROVINCIA AUTONOMA DI BOLZANO - ALTO ADIGE
Abteilung 11 - Hochbau und technischer Dienst		**Ripartizione 11 - Edilizia e servizio tecnico**
Amt 11.6 - Amt für Geologie und Baustoffprüfung		Ufficio 11.6 - Ufficio Geologia e prove materiali

DETERMINAZIONE LIMITI DI ATTERBERG

LG 01.10 UNI CEN ISO/TS 17892-12

Auftragsnummer: Ordine Nr.:	Entnahmestelle: Punto di prelievo:

Prüfkörper: Campione Nr:	Entnahmetiefe: Profonditá prelievo:
Baustelle: Cantiere:	Bodenart: Tipo di materiale:
Ausgeführt durch: Eseguito da:	Art der Entnahme: Modalitá prelievo:
am: data della prova:	Entnahme am: durch: Prelevato il: da:

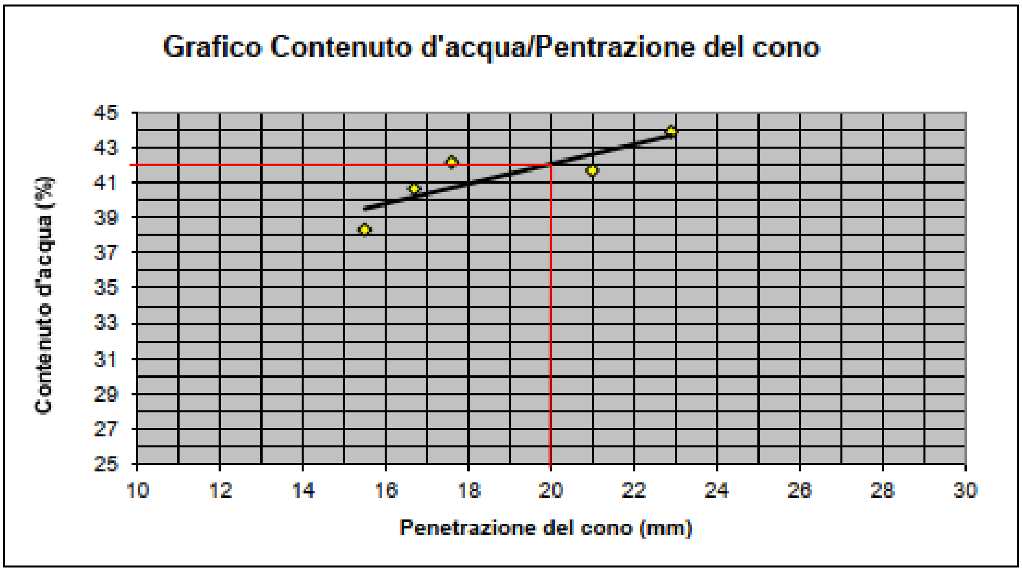

Data ______________________ Il tecnico ______________________

Pag. 2 di 2

Annotazioni: ______________________

Slak Durability Test

Slake Durability Test | ASTM 4644-16

Auftraggeber	
Projekt/Auftragsnummer	

Probenbezeichnung		
Lithologie		Lab. Nr 2
Slake Durability Index I_d [%] nach dem 2. Zyklus	98,2	
Klassifizierung der Zerfallsbeständigkeit	zerfallsresistent	
Wassergehalt der Probe [%]	-0,5	

Visuelle Beurteilung der nach dem Versuch in der Trommel verbliebenen Gesteinsstücke (ASTM 4644-16)

I		Gesteinsstücke unverär	III		nur kleine Gesteinsstücke
II	x	große und kleine			

Datum	Probe feucht + Trommel [g]	Probe trocken + Trommel [g]	Trommel [g]	Probe trocken [g]	Wassergehalt [%]
26.05.2026	1697,59	1699,94	1196,7	503,24	-0,5

		Probe trocken + Trommel [g]	Probe trocken [g]	Trommel [g]	Wasser-temperatur [°C]	Zerfalls-beständigkeit I_d [%]	Klassifizierung (DGGT 2002; Gamble 1971)
1. Zyl	vor	1699,94	503,24	1196,7	22		
	nach	1698,72	502,02	1196,7	22	99,8	zerfallsresistent
2. Zyl	vor	1698,72	502,02	1196,7	22		
	nach	1690,64	493,94	1196,7	22	98,2	zerfallsresistent
3. Zyl	vor	1690,64	493,94	1196,7	22		
	nach	1696,07	499,37	1196,7	22	99,2	zerfallsresistent
4. Zyl	vor	1696,07	499,37	1196,7	22		
	nach	1682,17	485,47	1196,7	22	96,5	sehr hoch
5. Zyl	vor	1682,17	485,47	1196,7	22		
	nach	1676,31	479,61	1196,7	22	95,3	sehr hoch
6. Zyl	vor	1676,31	479,61	1196,7	22		
	nach	1694,39	497,69	1196,7	22	98,9	zerfallsresistent

Slake Durability Index (Zerfallsbeständigkeit)

Probenbezeichnung	0	
Lithologie	0	Lab. Nr. 2

Probe vor Versuchsbeginn

Probe nach dem letzten Zyklus

Slake Durability Test | ASTM 4644-16

Auftraggeber	
Projekt/Auftragsnummer	

Probenbezeichnung		
Lithologie		Lab. Nr 3
Slake Durability Index I_d [%] nach dem 2. Zyklus	90,2	
Klassifizierung der Zerfallsbeständigkeit	hoch	
Wassergehalt der Probe [%]	1,2	

Visuelle Beurteilung der nach dem Versuch in der Trommel verbliebenen Gesteinsstücke (ASTM 4644-16)

I		Gesteinsstücke unverändert	III		nur kleine Gesteinsstücke
II	x	große und kleine			

Datum	Probe feucht + Trommel [g]	Probe trocken + Trommel [g]	Trommel [g]	Probe trocken [g]	Wassergehalt [%]
26.05.2026	1754,49	1748,16	1199,6	548,56	1,2

		Probe trocken + Trommel [g]	Probe trocken [g]	Trommel [g]	Wasser-temperatur [°C]	Zerfalls-beständigkeit I_d [%]	Klassifizierung (DGGT 2002; Gamble 1971)
1. Zy	vor	1748,16	548,56	1199,6	22		
	nach	1712,62	513,02	1199,6	22	93,5	hoch
2. Zy	vor	1712,62	513,02	1199,6	22		
	nach	1694,56	494,96	1199,6	22	90,2	hoch
3. Zy	vor	1694,56	494,96	1199,6	22		
	nach	1672,30	472,7	1199,6	22	86,2	hoch
4. Zy	vor	1672,30	472,7	1199,6	22		
	nach	1651,30	451,7	1199,6	22	82,3	mittel
5. Zy	vor	1651,30	451,7	1199,6	22		
	nach	1634,02	434,42	1199,6	22	79,2	mittel
6. Zy	vor	1634,02	434,42	1199,6	22		
	nach	1618,42	418,82	1199,6	22	76,3	mittel

Slake Durability Index (Zerfallsbeständigkeit)

Probenbezeichnung	0	
Lithologie	0	Lab. Nr. 3

Probe vor Versuchsbeginn

Probe nach dem letzten Zyklus

Slake Durability Test | ASTM 4644-16

Auftraggeber	
Projekt/Auftragsnummer	

Probenbezeichnung		
Lithologie		Lab. Nr **4.3**
Slake Durability Index I_d [%] nach dem 2. Zyklus	**98,2**	
Klassifizierung der Zerfallsbeständigkeit	**zerfallsresistent**	
Wassergehalt der Probe [%]	**0,1**	

Visuelle Beurteilung der nach dem Versuch in der Trommel verbliebenen Gesteinsstücke (ASTM 4644-16)

I		Gesteinsstücke unverändert	III		nur kleine Gesteinsstücke
II	**x**	große und kleine Gesteinsstücke			

Datum	Probe feucht + Trommel [g]	Probe trocken + Trommel [g]	Trommel [g]	Probe trocken [g]	Wassergehalt [%]
26.05.2026	1706,47	1705,91	1196,34	509,57	0,1

		Probe trocken + Trommel [g]	Probe trocken [g]	Trommel [g]	Wasser-temperatur [°C]	Zerfalls-beständigkeit I_d [%]	Klassifizierung (DGGT 2002; Gamble 1971)
1. Zy	vor	1705,91	509,57	1196,34	22		
	nach	1702,47	506,13	1196,34	22	99,3	zerfallsresistent
2. Zy	vor	1702,47	506,13	1196,34	22		
	nach	1696,72	500,38	1196,34	22	98,2	zerfallsresistent
3. Zy	vor	1696,72	500,38	1196,34	22		
	nach	1698,99	502,65	1196,34	22	98,6	zerfallsresistent
4. Zy	vor	1698,99	502,65	1196,34	22		
	nach	1702,63	506,29	1196,34	22	99,4	zerfallsresistent
5. Zy	vor	1702,63	506,29	1196,34	22		
	nach	1690,01	493,67	1196,34	22	96,9	sehr hoch
6. Zy	vor	1690,01	493,67	1196,34	22		
	nach	1618,42	422,08	1196,34	22	82,8	mittel

Slake Durability Index (Zerfallsbeständigkeit)

Probenbezeichnung	**0**	
Lithologie	**0**	Lab. Nr. **4.3**

Probe vor Versuchsbeginn

Probe nach dem letzten Zyklus

Slake Durability Test | ASTM 4644-16

Auftraggeber	
Projekt/Auftragsnummer	

Probenbezeichnung		
Lithologie		Lab. Nr 7
Slake Durability Index I_d [%] nach dem 2. Zyklus	**96,8**	
Klassifizierung der Zerfallsbeständigkeit	**sehr hoch**	
Wassergehalt der Probe [%]	**0,8**	

Visuelle Beurteilung der nach dem Versuch in der Trommel verbliebenen Gesteinsstücke (ASTM 4644-16)

I		Gesteinsstücke unverändert	III		nur kleine Gesteinsstücke
II	x	große und kleine Gesteinsstücke			

Datum	Probe feucht + Trommel [g]	Probe trocken + Trommel [g]	Trommel [g]	Probe trocken [g]	Wassergehalt [%]
26.05.2026	1696,79	1692,91	1198,67	494,24	0,8

		Probe trocken + Trommel [g]	Probe trocken [g]	Trommel [g]	Wasser-temperatur [°C]	Zerfalls-beständigkeit I_d [%]	Klassifizierung (DGGT 2002; Gamble 1971)
1. Zy	vor	1692,91	494,24	1198,67	22		
	nach	1682,68	484,01	1198,67	22	97,9	sehr hoch
2. Zy	vor	1682,68	484,01	1198,67	22		
	nach	1677,10	478,43	1198,67	22	96,8	sehr hoch
3. Zy	vor	1677,10	478,43	1198,67	22		
	nach	1670,54	471,87	1198,67	22	95,5	sehr hoch
4. Zy	vor	1670,54	471,87	1198,67	22		
	nach	1664,81	466,14	1198,67	22	94,3	hoch
5. Zy	vor	1664,81	466,14	1198,67	22		
	nach	1655,55	456,88	1198,67	22	92,4	hoch
6. Zy	vor	1655,55	456,88	1198,67	22		
	nach	1662,83	464,16	1198,67	22	93,9	hoch

Slake Durability Index (Zerfallsbeständigkeit)

Probenbezeichnung	**0**	
Lithologie	**0**	Lab. Nr. **7**

Probe vor Versuchsbeginn

Probe nach dem letzten Zyklus